

**DESIGN AND FABRICATION OF SILICONE-BASED COMPOSITE  
TISSUE-MIMICKING PHANTOMS FOR MEDICAL TRAINING**

by

BURÇİN GÜL

Submitted to the Graduate School of Engineering and Natural Sciences  
in partial fulfilment of the requirements for the degree of  
Doctor of Philosophy

Sabanci University

February 2018

**DESIGN AND FABRICATION OF SILICONE-BASED COMPOSITE  
TISSUE-MIMICKING PHANTOMS FOR MEDICAL TRAINING**

APPROVED BY:

Asst. Prof. Dr. Özge Akbulut  
(Thesis Supervisor)



Prof. Dr. Mustafa Erkin Arbal



Prof. Dr. Nilhan Kayaman Apohan



Assoc. Prof. Dr. Ayhan Bozkurt



Assoc. Prof. Dr. Selmiye Alkan Gürsel



DATE OF APPROVAL: 10/01/2018

© Burçin Gül 2018

All Rights Reserved

*To my father, my family,  
and my beloved half Emre ...*

# DESIGN AND FABRICATION OF SILICONE-BASED COMPOSITE TISSUE-MIMICKING PHANTOMS FOR MEDICAL TRAINING

BURÇİN GÜL

MAT, Doctor of Philosophy, 2018

Thesis Supervisor: Asst. Prof. Dr. Özge AKBULUT

**Keywords:** Silicone-based composites; Surgical simulations; Tissue-mimicking; Peripheral nerve microsurgery model; Oncoplasty models; Breast ultrasonography phantom; Mammography; Microsurgical simulations; Medical training; Synthetic cadavers

## ABSTRACT

Silicone-based composite phantoms were fabricated to be used as an education model in medical training. A matrix of silicone formulations was tracked to mimic the ultrasonography, mammography, surgical, and microsurgical responses of different human tissue and organs. The performance of two different additives: i) silicone oil and ii) vinyl-terminated poly (dimethylsiloxane) (PDMS) were monitored with the acoustic setup and evaluated by the surgeons. Breast cancer is one of the most common types of cancer among women, and early diagnosis significantly improves the patient outcomes. The surgeons-in-training necessitate the vast amount of practice to facilitate a noteworthy contribution to this outcome. Therefore, breast simulation models that contain skin layer, inner breast tissue, and tumor structures which allow the collection of samples with biopsy needle were fabricated to be used in ultrasonography, as well as mammography models to be used in tumor diagnostics, and breast oncoplasty models for surgeons to practice their suturing skills.

Development of microsurgical techniques signifies a foremost advance in the intervention of the injured peripheral nerves and with the aid of the operating microscopes; it is possible to evaluate the severity of the neural trauma. The advanced microsurgical skills of surgeons are essential for the success of the microsurgery, and in turn for the preservation of the nerve continuity. With this motive, a peripheral nerve phantom that contains skin layer, fascia tissue, epineurium, connective tissue, the fascicles, and the muscle layer has been designed. Herein, we highlight the fabrication of a realistic, durable, accessible, and cost-effective training platform that contains breast ultrasonography, mammography, and oncoplasty models, as well as peripheral nerve with complex hierarchical layers. For training purposes, closest media to reality, fresh cadavers, are hard to obtain due to their price and/or unavailability. Hence, a variety of synthetic tissues were also designed through the optimization of formulations of silicone. Surgical simulation models that mimic various human tissue and organs such as i) multi layers of skin, ii) axilla and axillary lymph nodes, iii) veins, iv) isthmus of the thyroid gland, cricoid cartilage, tongue, larynx, esophagus, tracheal rings, and bronchial tree for the tracheostomy and bronchoscopy models were fabricated.

**İNSAN DOKUSUNU TAKLİT EDEN SİLİKON-BAZLI KOMPOZİT  
FANTOMLARIN TIP EĞİTİMİNDE KULLANILMA AMAÇLI DİZAYN VE  
FABRİKASYONU**

BURÇİN GÜL

MAT, Doktora Tezi, 2018

Tez Danışmanı: Yrd. Doç. Dr. Özge AKBULUT

**Anahtar kelimeler:** Silikon esaslı kompozitler; Cerrahi Simülasyonlar; Doku taklit eden; Periferik sinir mikrocerrahi modeli; Onkoplasti modelleri; Meme ultrasonografi fantomu; Mamografi; Mikrocerrahi simülasyonları; Tıp eğitimi; Sentetik kadavralar

## ÖZET

Silikon-bazlı kompozit fantomlar, tıp eğitiminde model olarak kullanılmak üzere üretilmiştir. Farklı insan doku ve organlarının ultrasonografi, mamografi, cerrahi ve mikro cerrahi tepkilerini taklit etmek için bir silikon formülasyonları matrisi yapılmıştır. İki farklı katkı maddesinin performansı: i) silikon yağı ve ii) vinil ile sonlandırılmış poli (dimetilsiloksan) (PDMS) akustik deney kurulumu ile incelenerek, cerrahlar tarafından değerlendirildi. Meme kanseri, kadınlarda en sık görülen kanser türlerinden biridir ve erken teşhis, hastaların iyileşme süreçlerini belirgin şekilde etkiler. Eğitim dönemindeki cerrahların, bu sonuca kayda değer bir katkı sağlamaları için yüksek miktarda pratik yapmaları gereklidir. Bu nedenle, meme simülasyon modelleri, cilt katmanı, meme iç dokusu ve biyopsi iğnesi ile numune toplanmasına izin veren tümör yapılarını içeren şekilde, ultrasonografide kullanılmak üzere tasarlanmıştır. Bunun yanı sıra tümör teşhisinde

kullanılmak üzere mamografi modelleri ve aynı zamanda cerrahların dikiş becerilerini geliştirebilecekleri meme onkoplasti modelleri de üretilmiştir.

Mikrocerrahi tekniklerin geliştirilmesi, hasarlı periferik sinirlerin müdahalesindeki gelişmelere öncü olmuştur. Ayrıca operasyon mikroskoplarının yardımıyla; sinir travmasının ciddiyetini değerlendirmek mümkündür. Cerrahların gelişmiş mikrocerrahi becerileri, mikrocerrahi müdahalenin başarısı için ve ayrıca sinir sürekliliğinin korunması için de gereklidir. Bu motivasyonla, deri, fasya dokusu, epinöryum, bağ dokusu, fasiküller, ve kas dokusunu içeren bir periferik sinir modeli tasarlanmıştır. Bu tez çalışmasında, meme ultrasonografisi, mamografi, onkoplasti modelleri ve karmaşık hiyerarşik katmanlara sahip periferik siniri içeren, gerçekçi, dayanıklı, erişilebilir ve düşük maliyetli bir eğitim platformunun üretilmesini vurgulanmaktadır. Eğitim amaçlı olarak, gerçekliğe en yakın ortam olan kadvraların yüksek fiyatlı ve/veya kısıtlı tedariki nedeniyle elde edilmesi güçtür. Bu sebeple, silikon formülasyonlarının optimizasyonu ile çeşitli sentetik dokular tasarlanmıştır. Cerrahi simülasyon modeli olarak kullanılmak üzere, i) çok katmanlı cilt, ii) aksilla ve aksiller lenf düğümleri, iii) damarlar, iv) tiroid bezi isthmusu, krikoid kıkırdak, dil, gırtlak, yemek borusu, trakeal halkalar ve bronş ağacı trakeostomi ve bronkoskopi modellerinde kullanılmak üzere üretilmiştir.

## ACKNOWLEDGEMENTS

Firstly, I would like to express my sincere gratitude to my supervisor Asst. Prof. Dr. Özge Akbulut for her continuous support of my PhD study and related research, for her patience, motivation, and immense knowledge. Her guidance and understanding helped me in all the phases of my research and writing of this thesis. I could not have imagined having a better advisor and mentor for my PhD study.

Besides my advisor, I would like to thank Prof. Dr. Mustafa Erkin Arıbal, for his help, guidance, encouragement and constructive critics throughout this study. I would also like to thank Assoc. Prof. Dr. Ayhan Bozkurt for enlightening me, guiding through the complicated phases of my research, for his help, and enthusiasm. I would like to thank the rest of my thesis committee Prof. Dr. Nilhan Kayaman Apohan and Assoc. Prof. Dr. Selmiye Alkan Gürsel for their insightful comments and encouragement, detailed review, excellent advice and helpful attitude which incited me to widen my research from various perspectives. Without their precious support, it would not have been possible to conduct this research.

I also would like to thank most helpful professors of our faculty: Prof. Dr. Yusuf Menciloğlu, Prof. Dr. Yuda Yürüm, Prof. Dr. Mehmet Yıldız, Prof. Dr. Mehmet Ali Gülgün, Prof. Dr. Melih Papila, Prof. Dr. Cleva Ow-Yang, Prof. Dr. Canan Atılgan, Assoc. Prof. Dr. Burç Mısırlıoğlu, Assoc. Prof. Dr. Gözde İnce, and Assoc. Prof. Dr. Fevzi Çakmak Cebeci. They always listen and approach with the most excellent solutions when you're entering a dead end.

I thank my fellow labmates Gökay Avcı, Zekiye Pelin Güven, Deniz Kılıç Yanılmaz, Omid Akhlaghi Baghoojari, and Onur Zırhlı for the stimulating discussions, and the sleepless nights we were working together before deadlines, and for all the fun we have had in these challenging years of PhD.

Also I would like to thank my precious MAT-GRAD and BIO-GRAD family: Canhan Ően, Leila Haghghi Poudeh, İpek-Kaan Bilge, Senem-Utku Seven, Deniz-Serkan Sırlı, Onur Özensoy, GökŐin Liu, Deniz Köken, Efe Armaĝan, Yelda Yorulmaz, Farzin Javanshour, Aysu YurduŐen, Billur-Murat Özbulut, Kadriye Kahraman, Tuĝdem Muslu, Omid Mohammad Mouradi, Tuĝçe AkkaŐ, Buket-Erdinç TaŐ, Çaĝatay Yılmaz, and countless many others.

Last but not the least, I would like to thank my family, İdil-Ömer Irmak, my cousin Selin GünüŐen who has been a sister to me, Nükhet-Ufuk GünüŐen, Aslı Atilla Bozdaĝ-Ergün Bozdaĝ, Suat ÜstbaŐ, Piyale İstep, my brother Serhat ÜstbaŐ, and my husband Emre for loving, listening, and supporting me spiritually throughout my life. They are the reason for the person I have become today and the builders of my future.

## TABLE OF CONTENTS

ABSTRACT.....	iv
ÖZET .....	vi
ACKNOWLEDGEMENTS.....	viii
TABLE OF CONTENTS.....	x
LIST OF FIGURES .....	xiii
LIST OF TABLES.....	xvii
LIST OF SCHEMES .....	xviii
LIST OF SYMBOLS AND ABBREVIATIONS .....	xix
<b>Chapter 1</b> Introduction .....	1
<b>Chapter 2</b> Breast Phantoms for Surgical, Ultrasonography, and Mammography Training .....	.5
2.1 Introduction.....	5
2.2 Materials and Methods .....	8
2.2.1 Formulation of the Tissue-mimicking Materials .....	8
2.2.2 Preparation of the Inner Breast Tissue and the Skin.....	9
2.2.3 Chemical Characterization of the Inner Breast Tissue Formulation.....	10
2.2.4 Preparation of the Tumor Structures.....	11
2.2.5 Fabrication of the Breast Phantom.....	11
2.2.6 Acquisition of Ultrasonography Images .....	12
2.3 Results and Discussion.....	14
2.3.1 Design and Fabrication of the Breast Ultrasonography Phantom.....	14
2.3.2 Acoustical Characterization.....	15
2.3.3 Acquisition of Ultrasonography Images of Inner Breast Tissue.....	16
2.3.4 Ultrasonography of Tumar Structures .....	20
2.3.5 Ultrasonography Images of the Muscle and Rib Bones Simulation Models .....	23

2.3.6	Ultrasonography Images of Skin Model .....	24
2.3.7	Fabrication of the Mammography Phantoms.....	25
2.3.8	Fabrication of Breast Phantoms for Surgical Training .....	27
2.4	Conclusions .....	28
<b>Chapter 3</b>	<b>Fabrication of the Peripheral Nerve Model .....</b>	<b>30</b>
3.1	Introduction .....	30
3.2	Materials and Methods .....	32
3.2.1	Tissue-Mimicking Materials.....	32
3.2.2	Design of the Peripheral Nerve Model .....	33
3.2.3	Preparation of the Nerve Structures.....	33
3.2.4	Mechanical Characterization .....	34
3.2.5	Scanning Electron Microscopy .....	34
3.2.6	Visible Light Microscopy .....	34
3.2.7	Assessment of Microsuturing in the Tissue-mimicking Phantom .....	34
3.3	Results and Discussion.....	35
3.3.1	Selection of materials for the nerve model .....	325
3.3.2	Evaluation of Microsuture on Nerve Phantoms.....	327
3.3.3	Microsurgical Assesment of Peripheral Nerve Phantom.....	40
3.4	Conclusion.....	43
<b>Chapter 4</b>	<b>Skin, Axilla, Axillary Lymph Nodes, Tracheostomy, Bronchoscopy, and Vascular Models for Surgical Training .....</b>	<b>45</b>
4.1	Introduction .....	45
4.1.1	Significance of Surgical Education Materials .....	47
4.1.2	Assessment of the Medical Applications and Determination of Organs to Fabricate.....	52
4.2	Materials and Methods .....	55

4.2.1	Design of the Skin Model .....	55
4.2.2	Axilla and Axillary Lymph Nodes.....	55
4.2.3	Fabrication of the Vascular Model .....	56
4.2.4	Material Selection and Design of Tracheostomy and Bronchoscopy Model ..	56
4.3	Results and Discussions .....	57
4.3.1	Surgical Skin Model .....	57
4.3.2	Axilla and Axillary Lymph Nodes.....	59
4.3.3	Vascular Model with Blood Flow Mechanism .....	61
4.3.4	Tracheostomy and Bronchoscopy Model .....	66
4.4	Conclusion.....	75
<b>Chapter 5</b>	<b>Conclusion and Future Aspects .....</b>	<b>77</b>
<b>BIBLIOGRAPHY</b>	<b>.....</b>	<b>81</b>
<b>CV</b>	<b>.....</b>	<b>96</b>

## LIST OF FIGURES

<b>Figure 1</b> The anatomy of human breast that illustrates the skin, subcutaneous fat tissue, inner breast tissue, mammary glands, the muscle layer, and the rib bones (from outer to inner) [64].	8
<b>Figure 2</b> The wt % of A and B components and the additives (i.e., silicone oil or thinning agent)	9
<b>Figure 3</b> The beam pattern of the transducer for $f=4$ MHz and $a=16$ mm.	13
<b>Figure 4</b> FTIR spectra of two-component silicone elastomer, with 50 wt % vinyl-terminated PDMS additive.	14
<b>Figure 5</b> Ultrasonography of the inner breast tissue performed by layered application of two-component silicone elastomers with different elasticity.	16
<b>Figure 6</b> Comparison of the ultrasonography images of cured two-component silicone elastomers, with increasing amounts of a) 10 wt %, b) 20 wt %, and c) 30 wt % carbon black powder added samples.	17
<b>Figure 7</b> Ultrasonography images obtained by the placement of a water-immersed water-absorbing additive onto the pre-cured two-component silicone elastomer.	17
<b>Figure 8</b> Ultrasonography image of heterogeneous breast tissue resulting from the mixture of two different oil content silicone elastomers with different colors.	18
<b>Figure 9</b> Acoustic parameters of thinning agent-added silicone phantom with increasing frequency between 1–5 MHz.	19
<b>Figure 10</b> Comparison of the ultrasonography images of inner breast tissue simulation with different amounts of vinyl-terminated PDMS (thinning agent) content; image acquisition with 12 MHz ultrasound probe, scale bar represents 1 cm.	19
<b>Figure 11</b> Comparison of ultrasonography images of inner breast tissue simulation with different amounts of silicone oil content; image acquisition with 12 MHz ultrasound probe, scale bar represents 1 cm.	20
<b>Figure 12</b> Ultrasonography of two-component silicone elastomer inner breast tissue with a) pristine and b) alumina added PAA gel tumor models	21
<b>Figure 13</b> Acoustic parameters of different breast tumor-mimicking phantom materials measured with 5 MHz transducer.	22

<b>Figure 14</b> Simulation of the tumor structure with 35 wt % alumina added silicone. a) Ultrasonography of tumor structure, the arrows indicate the entry and exit of the biopsy needle from the tumor. Scale bar represents 1.5 cm. b) Images of biopsy needle entry to the breast and the collected tumor piece. Scale bar represents 0.5 cm. ....	23
<b>Figure 15</b> Ultrasonography of two-component silicone elastomer inner breast tissue, and different sizes and shapes a) fabric and b) paper addition for the muscle layer imitation....	23
<b>Figure 16</b> Ultrasonography images of (a) two-component silicone elastomer inner breast tissue, and (b) imitated rib bones layer. ....	24
<b>Figure 17</b> a) The skin model that consists of cured two-component silicone elastomers, b) Ultrasonography of human muscle tissue (arm). ....	24
<b>Figure 18</b> Mammography image of inner breast tissue that contains two-component silicone elastomer with 66.6 wt % silicone oil and 30 wt % expancel additive. ....	25
<b>Figure 19</b> Comparison of mammography images of inner breast tissue that contain two-component silicone elastomer with a) 10 wt % expancel, and b) 50 wt % expancel. ....	26
<b>Figure 20</b> Comparison of additives (10 wt %) in two-component silicone elastomer inner breast tissue that mimic calcification in breast mammography images, a) alumina ( $\mu\text{m}$ scale), b) egg shell (mm scale).....	26
<b>Figure 21</b> Sequential photography of Batwing Mammoplasty technique .....	27
<b>Figure 22</b> Sequential photography of Rezai technique .....	28
<b>Figure 23</b> The representation of the ulnar nerve in hand upon decompression of the branch [94].....	31
<b>Figure 24</b> Different layers of the designed phantom .....	33
<b>Figure 25</b> Comparison of elastic modulus of formulations with increasing wt % silicone oil .....	35
<b>Figure 26</b> Tensile test with dog-bone shaped specimens, a) plastic deformation of the sample during the test, and b) after fracture .....	36
<b>Figure 27</b> Comparison of elastic modulus of two highest wt % silicone oil containing specimens with increasing wt % cotton content .....	37
<b>Figure 28</b> The VLM images of 8/0 microsuture and 0.1 wt % cotton fibers in epineurium model. a-b) BF (a) and DF (b) images of the microsuture, c-d) BF (c) and DF (d) images of	

the microsuture with arrows indicating the needle entry sites, e-f) Cotton fibers in the epineurium structure. All the scale bars represent 200  $\mu\text{m}$  (e–50  $\mu\text{m}$ ).....38

**Figure 29** a-b) Epineurium model pristine, c-d) Epineurium model with 0.1 wt % cotton fibers, e-f) Fascicle model with 0.1 wt % cotton fibers. 10/0 sutures were used. Entry sites of the needle were focused on the smaller scale bars. ....39

**Figure 30** a-b) Epineurium model pristine, c) Fascicle model with 0.1 wt % cotton fibers, d-f) Epineurium model with 0.1 wt % cotton fibers. 8-0 sutures were utilized.....40

**Figure 31** Nerve model pristine. a-c) Removal of fascia part to release the nerve, d-f) A cut on epineurium, and beneath outer epineurium layer, connective tissues and fascicles viewed, g-h) Microsutures on fascicles, i) Microsutures on epineurium.....41

**Figure 32** Nerve model with 0.1 wt % cotton fibers. a-f) Systematic assessment of a nerve cut, and microsuturing of the epineurium layer. ....42

The images of designed pristine epineurium of the peripheral nerve model can be seen in Fig. 33. A cut was made and a microsuture with 10/0 sutures were achieved on the model. ....42

**Figure 33** Sutures (10/0) on the epineurium part of the peripheral nerve model.....42

**Figure 34** ‘Adult Cric Trainer’ cricothyrotomy model produced by SynDaver [177]. .....50

**Figure 35** IMOLA larynx model for laser microsurgery simulation [178].....51

**Figure 36** A transverse and vertical incision of trachea for the tracheostomy application [184].....52

**Figure 37** Oral tracheal intubation with the aid of laryngoscope [189].....53

**Figure 38** The views of bronchi during bronchoscopy. a) left and right main bronchus, b) branches of right main bronchus, c) left main bronchus, d) right upper lobe, e) left upper lobe, f) right basal segments, g) right middle lobe, h) left basal segments [190].....54

**Figure 39** The skin model with different layers: Skin, subcutaneous fat and the muscle layers from top to bottom.....57

**Figure 40** Different suture techniques were applied on the designed skin model with subcutaneous fat layer and the textile in between those two layers.....58

**Figure 41** The cast and clay molds prepared for the axilla model. ....59

**Figure 42** Axilla model that consists of the breast and arm pit. ....60

**Figure 43** The second design of axilla model with the stretched skin layer. ....61

<b>Figure 44</b> Different size and diameter branched vessels for the aneurism simulation model. .....	62
<b>Figure 45</b> Endovascular imaging of the aneurism model. ....	62
<b>Figure 46</b> The mechanism that contain fabricated veins with different diameters and a blood flow system through a water pump.....	64
<b>Figure 47</b> The anatomy of the neck indicating the structures to be mimicked for the model [184].....	67
<b>Figure 48</b> The anatomy of the trachea and surrounding structures [198].....	70
<b>Figure 49</b> The anatomy of esophagus monitored including epiglottis, and cartilages that were designed within the model [190].....	70
<b>Figure 50</b> The anatomy of the strap muscles [199].....	71
<b>Figure 51</b> The anatomical models that were utilized as a mold in the fabrication of the tracheostomy and the bronchoscopy models. ....	72
<b>Figure 52</b> Clay molds that were used in the production of the model. ....	72
<b>Figure 53</b> Thyroid gland with inferior veins.....	73
<b>Figure 54</b> a) Bronchial tree, and b) The trachea with bronchial tree and the modular parts	74
<b>Figure 55</b> a) Tongue, b) Tongue with the sheath that contain vallecula fold that allows the epiglottis movement.....	74
<b>Figure 56</b> Modular parts of the thyroid cartilage, cricoids cartilage, arytenoids cartilage, and tracheal rings, and their assembled imaged. ....	75
<b>Figure 57</b> The prototype of the knee model, a) meniscus structures with different colors representing the accumulation of the blood vessels, b) the knee model with the meniscus cartilages and bursa sacs combined into a single model.....	80

## LIST OF TABLES

<b>Table 1</b> List of measured acoustic parameters of silicone formulations and human breast tissue as reported in literature. ....	16
<b>Table 2</b> The heart pulses and the time elapsed between the two pulses .....	65

## LIST OF SCHEMES

<b>Scheme 1</b> Fabrication steps of the breast phantom .....	12
<b>Scheme 2</b> Experimental setup of the acoustical measurements .....	13
<b>Scheme 3</b> Chemical formulations of a) Vinyl-terminated PDMS, b) Poly(dimethylsiloxane- <i>co</i> -methylhydrosiloxane), trimethylsilyl-terminated, c) Silicone dioxide .....	14
<b>Scheme 4</b> Schematic of the vascular model with blood flow mechanism .....	63
<b>Scheme 5</b> The schematic of the electrical circuit of the vascular mode.....	66

## LIST OF SYMBOLS AND ABBREVIATIONS

PDMS	: Poly (dimethylsiloxane)
PVA	: Poly (vinyl) alcohol
PA	: Polyacrylamide
PLA	: Poly(lactide)
BWM	: Batwing Mammoplasty
BF	: Bright Field
DF	: Dark field
VLM	: Visible light microscope
FTIR	: Fourier Transformed Infrared Spectroscopy
ATR	: Attenuated-Total Reflection
SEM	: Scanning electron microscope
SEI	: Secondary Electron Image
UV-Vis	: Ultraviolet-Visible
ASTM	: American Society for Testing and Materials
UTM	: Universal Testing Machine
LSR	: Liquid Silicone Rubber
RTV	: Room Temperature Vulcanizing

# Chapter 1

## Introduction

In this thesis, the design and fabrication of realistic, durable, reliable, cost-effective, and hence, accessible silicone-based composite human tissue-like models are proposed. The thesis consists of six chapters that include an array of synthetic models which can be utilized in medical education. The first chapter provides an introduction and brief explanation of the proposed models; and the main findings of each chapter of the thesis.

In the second chapter, the design and fabrication of silicone-based composite breast ultrasonography, mammography, and surgical simulation models, with a significant focus on their applications are elucidated in line with the given literature review. These fabricated breast phantoms include a multi-layered skin, inner breast tissue, and different sizes and shapes of malign/benign tumors that were prepared separately and combined into a single model afterward. A matrix of silicone formulations was investigated in order to mimic the ultrasonography, mammography, and surgical responses, and significant resemblance to acoustic, cosmetic, and tactile properties of the human breast tissue was achieved [1]. In the design of the ultrasonography model, the acoustic performance of two different additives: i) silicone oil and ii) vinyl-terminated PDMS were assessed by a home-made acoustic setup. One of the main challenges in the design of such ultrasonography model was to reach the acoustic similarity to human tissues.

Through the use of 75 wt % vinyl-terminated PDMS in two-component silicone elastomer mixture,  $1.43\text{--}1.57\times 10^3$  m/s and attenuation coefficient of 9.5–12.6 dB/cm, as reported in the literature for human breast tissue was reached with 7 MHz ultrasound probes [1]. The optimized formulations exhibited a sound velocity of  $1.29\pm 0.09\times 10^3$  m/s and an attenuation coefficient of  $12.99\pm 0.08$  dB/cm—values those match closely to the human breast tissue—that were measured with 5–7 MHz probe. This model can also be used for ultrasound-guided needle biopsy applications as well as for self-examination trainings. The mechanical properties of these phantoms were also investigated and the design parameters were optimized respectively. These models were also evaluated by radiologists and surgeons who are experts in their fields, and the validity of the models was approved.

Surgeons-in-training necessitates practice to improve their skill sets and the shift towards simulation-based trainings enables trainees to learn at their own pace and experience custom-based cases rather than responding to the immediate needs of the patients. Oncoplasty for breast cancer encompasses tumor removal and subsequent breast reconstruction; and there are several oncoplastic techniques to ensure suitable treatment of the patients [2, 3]. Silicone-based composite models can be designed and manufactured to fulfill the necessities of breast surgery such as precise incision, epidermal undermining, suturing, and resisting suture tension after excision of a considerable mass [4]. In Chapter 2, the performance of breast model for two oncoplastic techniques, “Batwing Mammoplasty” and “Modified Inferior Flap Rezaei” have shown. This phantom can be used in settings where it is difficult and/or expensive to find fresh cadavers. In addition, the model is also suitable to be used in self-diagnosis trainings, and contributes to communication platforms between surgeons and patients.

Chapter three provides useful information about the development of peripheral nerve phantoms. The advancements in microsurgery techniques signify foremost intervention to treat the injured peripheral nerves. The employment of the operating microscopes and the interoperative electrodiagnosis in these surgeries paved the way to evaluate the severity of the degree of the neural trauma. The advanced microsurgical skills of surgeons are essential for the success of the microsurgery, and in turn for the preservation of the nerve continuity [5].

The competence of the microsurgical skills requires excellent dexterity, and the microsurgeons require medical education platforms that contain plenty of practices to advance their suturing skills. With this motive, a peripheral nerve microsurgery phantom that contains skin layer, fascia tissue, epineurium, connective tissue, the fascicles, and the muscle layers has been designed. This model can be utilized as an assessment tool for the improvements of technical skills of surgeons and how these techniques have been applied to the peripheral nerve microsurgery [6].

In chapter four, the production of phantoms for surgical training was overviewed. The main aim was to fabricate a prototype of cost-effective, sustainable, and reliable synthetic surgical systems with blood and air flow that provide realistic responses to surgical interventions. Unlike digital simulation and virtual reality systems, the suggested tactile systems work based on imitation of the incision and suturing responses that are obtained from real tissue and organs; and the intra- and inter-blood and/or air flow in these systems ensures a traditional learning platform. Surgical trainees can receive training on a fresh cadaver and animal models that are tactile, suturable, cuttable [7]. However, the cost of fresh cadavers and complications in proper protection of these cadavers; the anatomical differences in animal models, the difficulty of obtaining animal models and accompanying ethical concerns prevent the spread of high-quality education among an ever-mounting number of medical students [8].

In recent years, synthetic surgical models are utilized for the education of interventions that involve especially needles and tubes. These models are designed to be used for several times. They are closer to anatomical models in terms of durability; thus, their high prices are legitimized. The surgical models that can enable complex operations are very costly since they are damaged in every operation and their price prevents their use except in a few institutions in developed countries [9]. In the framework of this chapter, surgical simulations models: i) multi layers of skin, ii) axilla and axillary lymph nodes, iii) vascular models, iv) isthmus of the thyroid gland, cricoid cartilage, tongue, larynx, esophagus, tracheal rings, and bronchial tree for the tracheostomy and bronchoscopy models were fabricated.

And finally, chapter five concludes the thesis with future aspects, including proposed traumatic torax and abdomen, and the knee models. There is a need for a sustainable, reliable, and affordable platform to diffuse simulation-based trainings to medical curricula and provide trainings even in resource-limited settings. Through cost-effective design and fabrication, it is possible to produce training models in any non-chemistry setup. This practical solution also eliminates the need for chemical/cold storage and risk of infections/molding, thus making it a preferable tool for teaching hospitals and also for individual practice. These models, which can generate realistic responses, will contribute to the level of medical education and in turn the global economy.

# Chapter 2

## Breast Phantoms for Surgical, Ultrasonography, and Mammography Training

### 2.1 Introduction

Breast cancer is the most common type of cancer and foremost cause of death from cancer among women [10-12]. The frequency of women diagnosed with breast cancer increases rapidly due to the advances in technology [13, 14]. Ultrasonography and mammography are widely-used screening tools for the detection of breast cancer [15, 16] and their use in routine screening have been reported to reduce the mortality rates [17-22]. These techniques can differentiate the stages of breast carcinoma [23, 24] and segregate cystic lesions and benign/malign tumors based on their size, shape, and echo feedback with high precision [25, 26]. In addition, compared to the other imaging methods, such as magnetic resonance imaging and computed tomography, all of which produce ionizing radiation, ultrasonography utilizes high-frequency sound waves; thus, is not harmful to the patient [27-30]. Hence, in this study, special attention was paid on the design of the breast ultrasonography, mammography, and oncoplasty phantoms.

Surgical training models were studied since it is essential to preserve the physical appearance to facilitate the well-being of the patient upon breast surgeries [31, 32]. Medically and aesthetically successful oncoplastic surgeries assure the health of women and return of these women to their pre-cancer lives [33-35]. Therefore, the conflict of removing the carcinoma whilst preserving the breast tissue became a challenge for the specialists over the past few decades [36]. In recent years, the breast-conservation surgery along with the radiotherapy treatment is more favored over mastectomy, which results in the loss of higher mass breast tissues. In addition, where possible, the reconstruction of the breast through plastic surgery was preferred following mastectomy and breast-conserving therapy [37]. Oncoplastic surgery, an emerging branch in breast surgeries, combines oncological and aesthetic procedure such that it allows patients to circumvent a secondary reconstruction. Through oncoplastic surgery, the patients can avoid breast deformities caused by the post-plastic surgeries and encounter reduced treatment costs [38]. Immediate reconstruction facilitates the creation of more symmetric and well-positioned breast shape with fewer scars [39, 40]. Compared to breast conservation and mastectomy techniques, oncoplastic surgery was reported to have higher patient satisfaction, higher survival rates, reduced reoperation rates; and, hence ease of patient recovery after the treatment [41].

Proficiency of surgeons on oncoplastic techniques, and the success of radiologists in diagnostic accuracy depend on the level of experience and practice they get [42, 43]. Simulation in the training of doctors has improved patient outcomes [44-46]. Availability of realistic ultrasonography, mammography, and surgical phantoms are, thus, crucial for effective trainings—phantoms with a cosmetic, acoustic, and tactile resemblance to human breast tissue have the potential to enhance skill sets of medical doctors [47]. However, in general, commercially available models are not affordable; hence, not accessible by many, and laboratory scale models are either too simple or not durable. There is a need for realistic and easy-to-access models to realize the true impact of simulation in medical education.

Materials selection is the most critical step in simulating the complex structure of the breast. Hydrogels, such as polyvinyl alcohol (PVA) [48], gelatin [49], agar [50], and polyacrylamide (PA) [1], are reported as tissue-mimicking materials. The phantoms that

utilize agar and gelatin are easy-to-produce, cost-effective, and non-toxic; but, they do not have long shelf lives and are prone to bacterial and yeast infection. These models necessitate an anti-bacterial treatment and refrigeration for prolonged durability [51]. PA cross-linked polymer matrices require a chemical setup and safety measures since toxic chemicals are utilized during the synthesis [52]. In PVA cryogel formation, chemical agents and experimental steps such as freeze-thawing cycles are also involved. These factors limit the fabrication of PA- and PVA-based phantoms to more advanced laboratories [53].

Silicone is extensively used as a tissue mimicking material in various fields from the film industry to prosthetics [54, 55]. The ease of shaping, coloring, and durability make silicone a noteworthy possibility for surgical, ultrasonography and mammography phantoms [56]. Silicone-based materials can be tailored to provide realistic responses to incision, dissection, and suturing; thus, enable tactile simulations in surgical skills laboratories and there are several companies that provide silicone-based models and materials for modeling purposes [57]. However, studies that utilize silicone as a tissue mimicking material for ultrasonography training reported lower attenuation coefficients in comparison to the human breast tissue [1, 58]. On the other hand, in several patents on silicone-based breast phantoms, although detailed production process and ultrasonography images are revealed, systematic studies on acoustical properties are not demonstrated [59-63]. Here we report, the design of such training phantoms by tracking the formulation of silicone layers to imitate tactile and acoustic responses of human breast tissue, as well as malign tumors. Skin, inner breast tissue, tumor structures, and muscle layer were fabricated according to the human anatomy (Fig. 1) [64]. These models can be fabricated in a simple setup (e.g., in a non-chemistry lab) that contain only a scale and an oven.

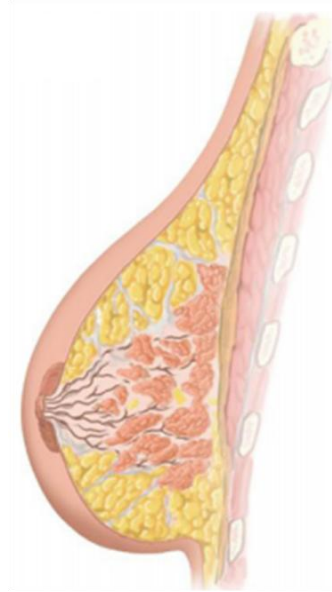


**Figure 1** The anatomy of the human breast that illustrates the skin, subcutaneous fat tissue, inner breast tissue, mammary glands, the muscle layer, and the rib bones (from outer to inner) [64].

These models have the potential to overcome the limitations that other materials pose with their simplicity in fabrication, cosmetic similarity to the human tissue, and reusability. Therefore, the designed ultrasonography model reveal similar attenuation coefficient to that of biological tissues as well as matching the speed of sound, the mammography model mimic the breast calcifications successfully, and the oncoplasty training phantom poses an adequate imitation of surgical sutures and significant tactile similarity.

## **2.2 Materials and Methods**

### **2.2.1 Formulation of the Tissue-mimicking Materials**

Two-component liquid silicone rubber; component A (SL-3358A) and B (SL-3358B), and vinyl-terminated PDMS were obtained from KCC Corporation, Korea. Silicone oil was purchased from Sapar, Turkey (PMX200-350 CST). Carbon black, graphite flakes and PVA were purchased from Sigma-Aldrich, alumina nanopowder was obtained from AKP-50 Sumitomo Chemicals, Japan, and gypsum was received from local providers. For the

cosmetic resemblance, a coloring agent (Wacker Chemie AG) in the skin color was added to the formulation. Fabrics that were supplied from local providers applied between two different skin layers (skin and subcutaneous fat layer) in surgical models and also utilized for simulation of the rib bone in ultrasonography phantoms.

### 2.2.2 Preparation of the Inner Breast Tissue and the Skin

Component A and B were mixed in equal weight, while the additives were utilized at different amounts for the inner breast tissue. The amount of additives (i.e., silicone oil and thinning agent) spanned a range of 50–83.3 wt% of the total mixture, and the remaining weight was equally split between components A and B, and silicone oil (Fig. 2).

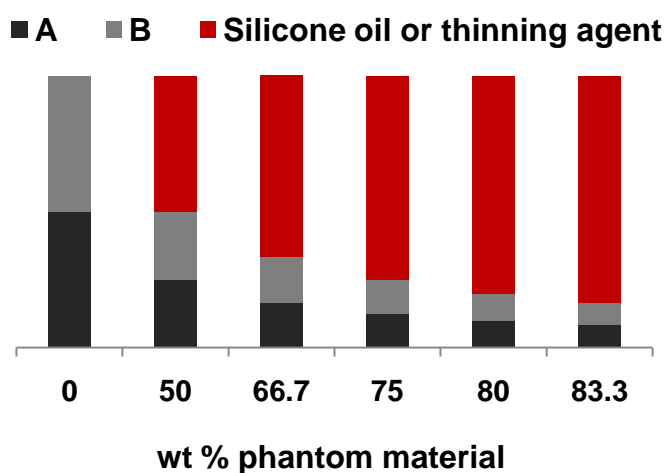


**Figure 2** The wt % of A and B components and the additives (i.e., silicone oil or thinning agent)

These formulations were prepared by mixing the components with a hand mixer and kept under vacuum for 30 min and then cured at 110 °C for 1 h. The reaction was addition curing with a platinum catalyst and no by-product was observed. Although curing step can be carried out at room temperature, higher temperatures were utilized to speed up the process. In addition, the vacuuming step can also be eliminated by waiting for 2–3 hours for possible air bubbles to leave the system. The formulation of the skin layer was prepared with the same method by mixing equal amounts of component A and B with 50 wt % silicone oil. Inner breast tissue and lesions were combined into a single model during

molding. The areola was prepared through the molding of dye-colored silicone elastomers and after curing, attached to the breast. Although there are various areola-related diseases that require imaging, the areola region was mainly included in the model to offer a reference point for the needle biopsy and provide a breast-like appearance [65, 66]. All silicone formulations were cured in an aluminum mold that was designed as a tear-drop shape in order to mimic the anatomy of the human breast and provide dimensional stability. However, any mold (e.g., made out of gypsum) that can withstand temperatures around 110 °C without deformation can be used to prepare the inner breast tissue.

Various materials were studied for tissue-mimicking and added to the silicone formulations for the imitation of the inner breast tissue. Carbon black powder, which is an organic material, and formed by the combustion of hydrocarbons, and water absorbent poly (sodium acrylate) gel particles (10 wt %) were utilized to obtain information about the reflection of ultrasonic sound waves. Expancel (30 wt %) was used as an additive in the silicone formulations for the fabrication of mammography and surgical models. PAA gel was also utilized for the imitation of inner breast tissue and tumor structures in the ultrasonography model. 600 mL of distilled water, 120 mL of acrylic acid, 0.96 g of reaction initiator ammonium persulfate, and 600 mL of cross-linker ethylene glycol dimethacrylate, all purchased from Sigma Aldrich were added to the reaction vessel respectively, and the mixture was stirred at room temperature for 5 minutes using a magnetic stirrer to form the inner breast tissue. After that, it was kept in a zipped bag in the oven at 60 °C for 4 hours. The reaction was subjected to deoxygenation with nitrogen gas, which is an important step for the successful completion of the polymerization and for the absence of air bubbles in the model that will adversely affect the ultrasonic measurements.

### **2.2.3 Chemical Characterization of the Inner Breast Tissue Formulation**

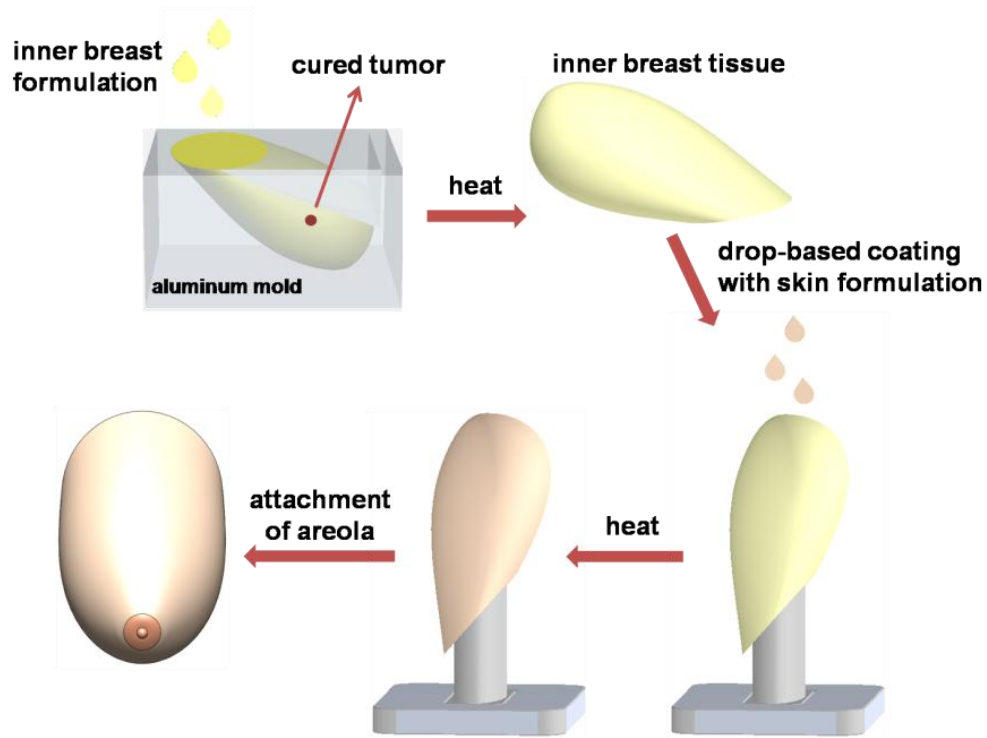
FTIR spectra of the inner breast tissue formulation that contains two-component silicone elastomer with 50 wt % vinyl-terminated PDMS was recorded on Thermo Scientific Nicolet IS10 ATR-FTIR Spectrometer equipped with diamond Smart ATR Attenuated Total Reflectance sampling accessory. The minimum and maximum range limits were 550 to 4000  $\text{cm}^{-1}$  with a resolution of 0.5  $\text{cm}^{-1}$ .

#### **2.2.4 Preparation of the Tumor Structures**

The preparation of different masses within the breast tissue was achieved with the formulation of two-component silicone elastomer, 50 wt % silicone oil, and 35 wt % different additives. Carbon black, graphite flakes, PVA, alumina nanopowder, and gypsum were screened to simulate acoustic properties of human breast tumor. Calcium-rich egg shells and alumina particles that simulate tumor tissue-specific calcifications have been used for the mammography model. In order to attain a heterogeneous structure in ultrasonography images and increase the density, 35 wt % alumina was added to PAA gel during the reaction within a 1.5 mL eppendorf tube. Non-spherical shapes without any distinctive contours (1–2 cm) were prepared by curing silicone elastomers. These tumor-simulators placed into the uncured formulation of the inner breast tissue at different locations (close to the nipple or to the lymph nodes, upper outer and central quadrants) during molding, and the inner breast tissue was cured afterward. We specifically focused on the upper outer quadrant since the occurrence rate in this region was reported to be higher than that of upper inner, lower outer, or central quadrants [67].

#### **2.2.5 Fabrication of the Breast Phantom**

The fabrication process (Scheme 1) was composed of four steps: i) preparation and curing of the tumor/lesions, ii) preparation of the inner breast tissue formulation, iii) combination of the cured tumor/lesions and inner breast tissue; curing the inner breast, and iv) application of the skin. Here, for the breast models, we used tear-drop shaped aluminum molds. Silicone-based or gypsum molds did not produce models with well-defined contours and dimensional stability. We, first, cured the inner breast tissue, employed a textile layer, and then, applied the outer silicone layer that simulates dermis and epidermis. The Young's Modulus of the inner breast tissue was adjusted through the addition of silicone oil. The areola was molded and colored separately, and attached to the breast after curing the outer layer. The back of the models was capped with Velcro to be attached to a wooden plane that provides four different angles of inclination. Anatomical landmarks like the clavicles and jugular notch can be marked on this plane for training purposes.



**Scheme 1** Fabrication steps of the breast phantom

### 2.2.6 Acquisition of Ultrasonography Images

Measurements were performed using a 16 mm diameter PZT-5A sheet of thickness 0.508 mm ( $f_0=4.28$  MHz). The transducer element was glued on a plastic rod of identical radius, and the front surface was covered with a 1 mm thick epoxy layer for electrical insulation. The sample was placed within the Fraunhofer region of the acoustic beam for which  $1 < S < 3$  was satisfied so that radial field variations did not have an effect on the measurement, where  $S$  is the Fresnel parameter given as  $S = z\lambda/a^2$ , with  $\lambda$  the wavelength (nm),  $a$ , the transducer radius (mm), and  $z$ , the axial distance (cm) [68]. For  $f=4$  MHz this corresponds to a range of  $171 \text{ mm} < z < 512 \text{ mm}$  (Fig. 3). To avoid possible errors caused by transients, the transducer was driven by a tone burst of at least 10 RF-cycles, as to mimic a continuous-wave measurement. The beam propagating in the specimen would have a length of 15 mm in the case of  $V_a=1500$  m/s, where  $V_a$  is the acoustic propagation velocity (m/s) so that multiple reflections were avoided in a sample thickness of 20 mm. Measurement results later indicated that  $V_a < 1500$  m/s, so that the requirement was met. An Onda HGL-0200 hydrophone (Onda Corporation, Sunnyvale, CA) was used in the measurements.

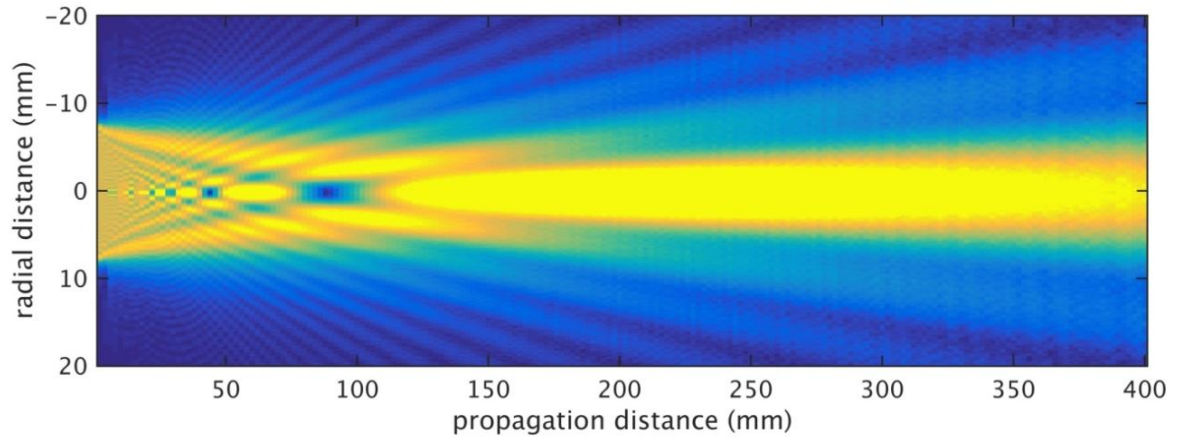
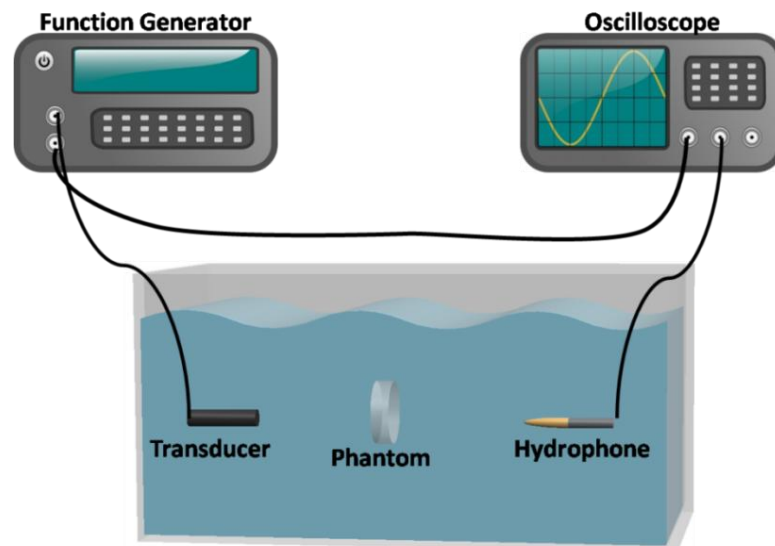


**Figure 3** The beam pattern of the transducer for  $f=4$  MHz and  $a=16$  mm

The samples were placed into a setup shown in Scheme 2, for tracking the acoustical properties. A transducer that was connected to a function generator was located 180 mm away from the sample and used as an ultrasound source to form longitudinal ultrasonic waves. Measurements were completed in an aqueous environment in the presence of a hydrophone and an oscilloscope for the acquisition of the signal. The transducer, phantom, and hydrophone were aligned coaxially in a water bath. The ultrasonography imaging of the phantoms was performed with a 9–15 MHz ultrasound probe (Aplio 400, Toshiba, Tokyo, Japan) by an expert radiologist in the field.

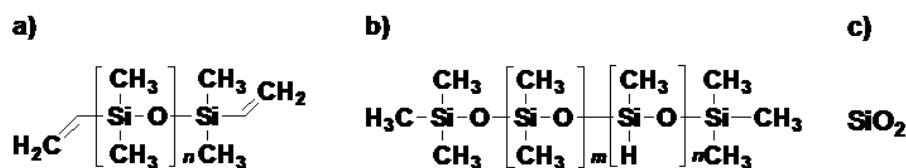


**Scheme 2** Experimental setup of the acoustical measurements

## 2.3 Results and Discussion

### 2.3.1 Design and Fabrication of the Breast Ultrasonography Phantoms

Various formulations of silicone with different additives (i.e., silicone oil and thinning agent) were tested for acoustical properties. The chemical formulations of these materials that were utilized in the design of the breast phantom can be seen in Scheme 3. Chemical characterization of the two-component silicone elastomer and vinyl-terminated PDMS additive formulation was also revealed in Fig. 4 via FTIR measurements. In addition to the inner breast tissue; the tumor structures, skin, muscle, and ribs were also simulated to be used in ultrasonography training. Materials selection was followed by the optimization of the formulations of two-component silicone elastomers with different additives.



**Scheme 3** Chemical formulations of a) Vinyl-terminated PDMS, b) Poly(dimethylsiloxane-co-methylhydrosiloxane), trimethylsilyl-terminated, c) Silicone dioxide

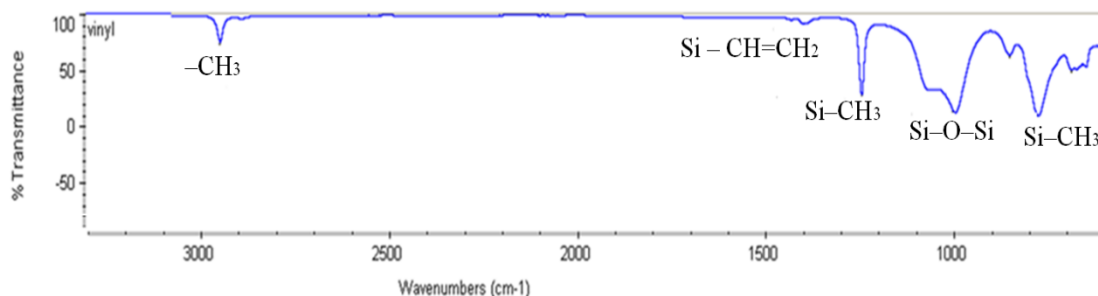


**Figure 4** FTIR spectra of two-component silicone elastomer, with 50 wt % vinyl-terminated PDMS additive.

### 2.3.2 Acoustical Characterization

Design parameters of the breast ultrasonography phantom were determined with respect to the acoustical characterization results. Sound velocity and attenuation coefficient were tracked to assess the capacity of the formulations to imitate the breast tissue. The ultrasound signal was transmitted through the sample or water (as a control) and using the temporal shift  $\Delta t$  (s) between the sample and the control, sound velocity was calculated as:

$$c_p = \left( \frac{1}{c_w} - \frac{\Delta t}{\Delta x} \right)^{-1} \quad (1)$$

where  $c_p$  is the sound velocity of the phantom (m/s),  $c_w$  is sound velocity of water (m/s) and  $\Delta x$  is the thickness of the sample (m). Attenuation coefficient of the sample material  $\alpha_p$  (Np/m) was calculated as in Eq. (2):

$$\alpha_p = \alpha_w - [\ln(A_p/A_w) - \ln(T_{wp} \cdot T_{pw})]/\Delta x \quad (2)$$

where  $\alpha_w$  is the attenuation coefficient of water (Np/m),  $A_p$  and  $A_w$  are the amplitude of the received ultrasound signal with and without the presence of the phantom (Pa),  $T_{wp}$  and  $T_{pw}$  are the pressure transmission coefficients (Pa/Pa) at the water-phantom and phantom-water interfaces, respectively. The transmission coefficients were given by:

$$T_{wp} = \frac{2Z_p}{(Z_w + Z_p)}, \quad T_{pw} = \frac{2Z_w}{(Z_w + Z_p)} \quad (3)$$

$$Z_p = \rho_p V_{a,p}, \quad Z_w = \rho_w V_{a,w} \quad (4)$$

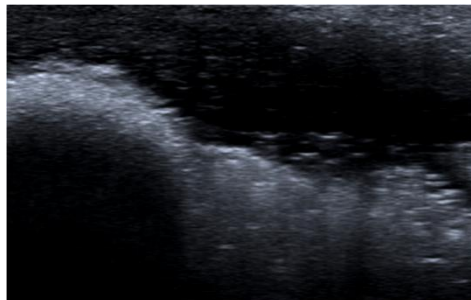
where  $\rho_p$  and  $\rho_w$  are the mass densities ( $\text{kg/m}^3$ ),  $V_{a,p}$  and  $V_{a,w}$  are acoustic propagation velocities (m/s), and,  $Z_p$  and  $Z_w$  are specific acoustic impedances ( $\text{Pa}\cdot\text{s/m}$ ) of the respective medium [1, 69]. A transducer was prepared to generate frequencies up to 5 MHz and an average of triplicate measurements with the standard deviations was reported. Table 1 lists the acoustical properties (sound velocity and attenuation coefficient) of the silicone formulations as well as human breast tissue as reported in literature [1, 70].

**Table 1** List of measured acoustic parameters of silicone formulations and human breast tissue as reported in literature

Material	wt%	Sound Velocity $\times 10^3$ (m/s)	Attenuation coefficient(dB/cm)
Human breast tissue [1]	0	1.43–1.57	9.5–12.6
No additive	0	0.98 $\pm$ 0.1	5.84 $\pm$ 0.08
Breast model-oil	50	1.025 $\pm$ 0.02	2.79 $\pm$ 0.1
	66.6	1.036 $\pm$ 0.04	2.65 $\pm$ 0.04
	75	1.046 $\pm$ 0.01	2.83 $\pm$ 0.1
	80	1.08 $\pm$ 0.09	2.10 $\pm$ 0.09
	83.3	1.08 $\pm$ 0.01	2.16 $\pm$ 0.06
Breast model-thinning agent	50	0.98 $\pm$ 0.08	7.48 $\pm$ 0.09
	66.6	0.99 $\pm$ 0.12	9.69 $\pm$ 0.09
	75	1.29 $\pm$ 0.09	12.99 $\pm$ 0.08

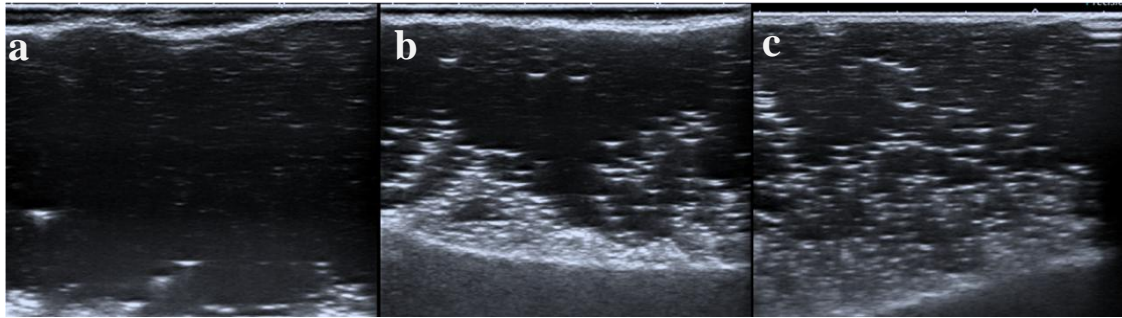
### 2.3.3 Acquisition of Ultrasonography Images of Inner Breast Tissue

Two-component silicone elastomers dyed with different color and elasticity were prepared, from the outside to the inside in a consecutively layered manner, to achieve the heterogeneous structure of the breast tissue. Each layer was cured separately, with the elimination of air bubbles between the layers. In Fig. 5, this heterogeneous layers and the image difference resulting from a change of depth in the model can be observed.



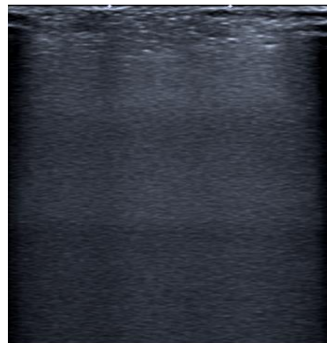
**Figure 5** Ultrasonography of the inner breast tissue performed by layered application of two-component silicone elastomers with different elasticity.

The feedback of the sound waves has been studied in samples where carbon black was added between the silicone layers. In Fig. 6, the comparison of the ultrasonography images with the increasing amount of carbon black addition can be seen. As the amount of carbon black increased, a similar to the feedback from the air bubbles in the image was generated. With these conclusions, it was decided not to use carbon black in the models.



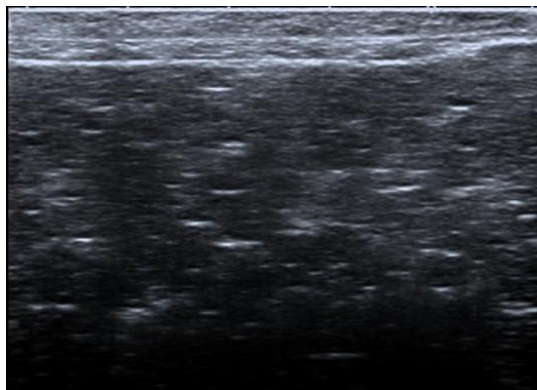
**Figure 6** Comparison of the ultrasonography images of cured two-component silicone elastomers, with increasing amounts of a) 10 wt %, b) 20 wt %, and c) 30 wt % carbon black powder added samples.

Ultrasonography was performed with poly (sodium acrylate) gel which is a water-absorbing material. The resulting image quality indicates that this material was suitable to be utilized for the inner breast tissue (Fig. 7). However, during the curing process onto a two-component silicone elastomer layer in the oven; reflections in the form of air bubbles were generated. Therefore; although gel particles were thought to be appropriate for applications that involve curing in the room temperature. However, this method was not a cost-effective and easy-to-produce fabrication as proposed in this study.



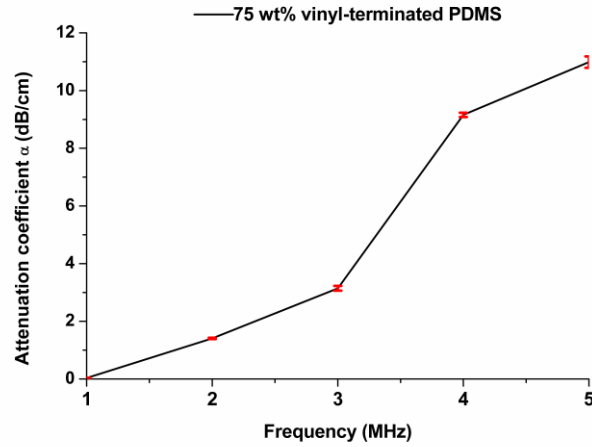
**Figure 7** Ultrasonography images obtained by the placement of a water-immersed water-absorbing additive onto the pre-cured two-component silicone elastomer.

Fig. 8 reveals the ultrasonography image of two-component silicone elastomers with different oil ratios (50 and 66.6 wt % silicone oil) that mixed with each other just before curing in the oven. Different oil ratios in the composition allowed the system to form a heterogeneous structure from these two silicone formulations with different densities.



**Figure 8** Ultrasonography image of heterogeneous breast tissue resulting from the mixture of two different oil content silicone elastomers with different colors.

The sample that contains 75 wt % thinning agent as an additive exhibited a considerable increase in the sound velocity in comparison to the samples with silicone oil, and approximating the values of human breast (Table 1). Expectedly, this sample generated better images in ultrasonography, based on the feedback provided by the radiologists. Although samples with silicone oil also produced acceptable images, the attenuation coefficients in the thinning agent-added samples were much larger than those with silicone oil-added samples; thus, we concluded the superiority of the formulation with 75 wt % thinning agent. We have, then, monitored the attenuation coefficient and sound velocity of this formulation as a function of frequency between 1 to 5 MHz (Fig. 9). The increasing frequency resulted in the enhancement of the attenuation values [49, 68, 71].



**Figure 9** Acoustic parameters of thinning agent-added silicone phantom with increasing frequency between 1–5 MHz.

The obtained ultrasonography images reveal the effects of additives in the inner breast tissue design. Experimentally measured acoustic parameters—sound velocity and attenuation coefficient of the phantoms—were correlated with the ultrasonography results of a series of phantoms. Fig. 10 and Fig. 11, show the direct comparison of the ultrasonography images of 50, 66.6, and 75 wt % thinning agent-added, and 50, 66.6, 75, 80, and 83.3 wt % silicone oil-added samples. The use of silicone oil and thinning agent with different wt % resulted in the change of inner breast tissue ultrasonography in parallel with acoustic measurements.

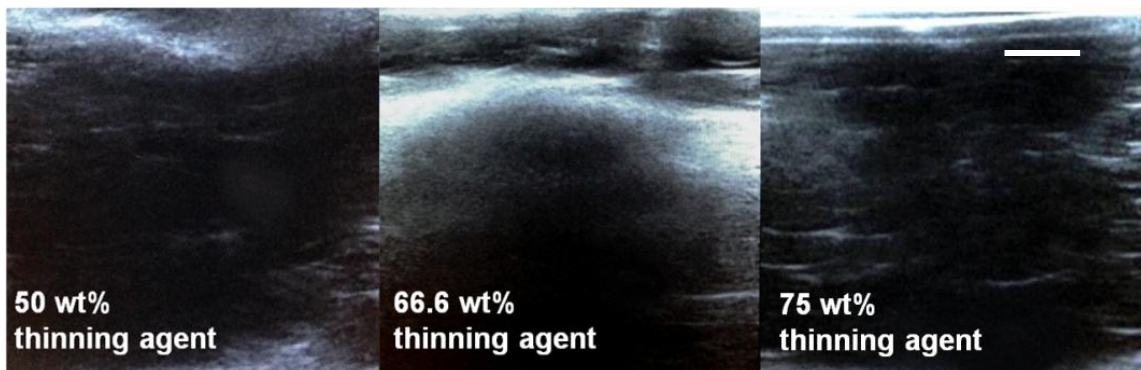


**Figure 10** Comparison of the ultrasonography images of inner breast tissue simulation with different amounts of vinyl-terminated PDMS (thinning agent) content; image acquisition with 12 MHz ultrasound probe, scale bar represents 1 cm.

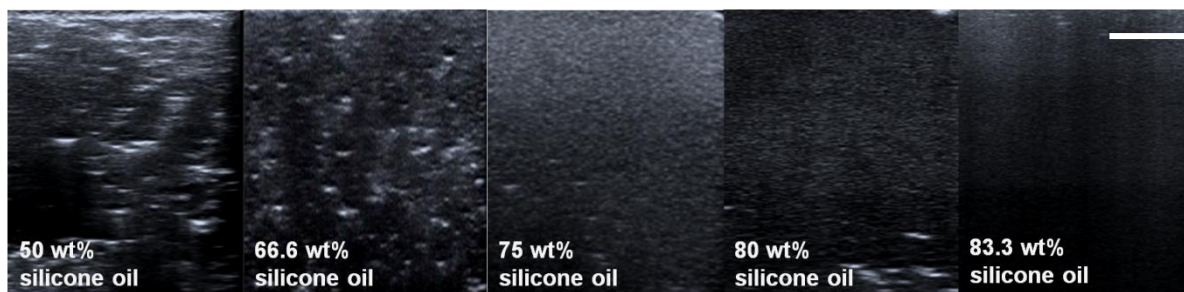


**Figure 11** Comparison of ultrasonography images of inner breast tissue simulation with different amounts of silicone oil content; image acquisition with 12 MHz ultrasound probe, scale bar represents 1 cm.

### 2.3.4 Ultrasonography of Tumor Structures

The material selection for the inner breast tissue was followed by the design of tumor structures within the breast with various sizes and shapes. It has been concluded that the ratio obtained in the experiments using different amounts of alumina was the limiting ratio that will not prevent the polymerization of the liquid reaction to solid-state gel. Another important parameter was to prevent the formation of air bubbles; hence two-component silicone elastomer mixtures in different formulations were kept under vacuum for 1–2 h. To mimic the acoustic response of tumor structures within the breast tissue, 10 wt % carbon black, alumina, gypsum, graphite flakes, and PVA were separately added to the silicone formulations. In addition, although PAA hydrogel was not preferred as an appropriate material for the fabrication of breast phantom due to its homogeneous appearance in ultrasonography, which was highly similar to water, the role of PAA hydrogels for the demonstration of tumor masses (benign or malign, fibroadenoma, or fibrocystic changes) were investigated. The lack of inhomogeneity of real breast tissues such as muscle, fat, tumor, and milk glands and the complexity during the polymerization process were the main reasons for eliminating PAA in the design. Figure 12a indicates the 10 wt % alumina added-PAA gel tumor model located in two-component silicone elastomer inner breast tissue. The PAA gel used in this model has not shown any significant difference in density despite the alumina addition; hence PAA gel has not been utilized in the fabrication of both inner breast and tumor structures. Two-component silicone elastomers were chosen to be the most favorable material to be used as an inner breast.

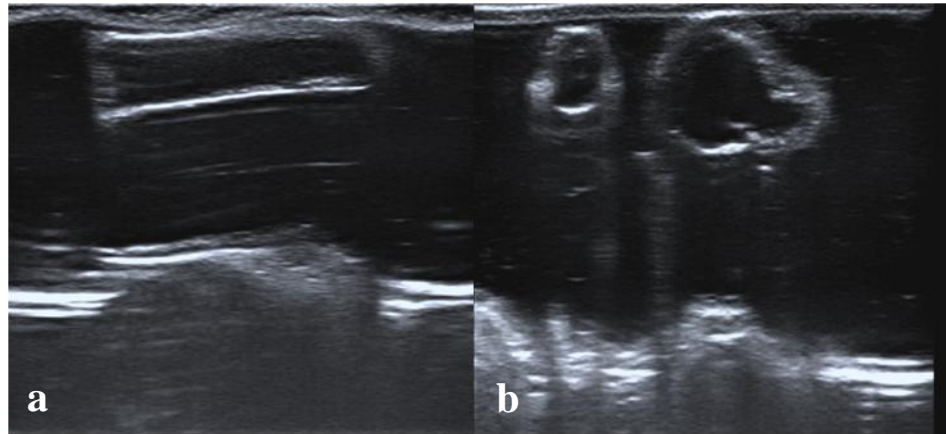


**Figure 12** Ultrasonography of two-component silicone elastomer inner breast tissue with a) pristine and b) alumina added PAA gel tumor models

Two-component silicone elastomer formulations without silicone oil provided comparable structures with breast tumors; however, the addition of silicone oil was found to be necessary for the successful entry of the biopsy needle and for the ease of tissue collection during the biopsy. 50 wt % silicone oil was qualitatively found to be the minimum amount to enable pinching of the material. The graph in Fig. 13 demonstrates the acoustic parameters of these tumor simulations measured with 5 MHz transducer. Both alumina and carbon black addition increased the attenuation coefficient; however, alumina was selected due to its higher sound velocity. 35 wt % alumina was the highest-possible amount that could be incorporated into the silicone mixture without forming clumps; therefore, we utilized this amount to simulate malign tumor structures.

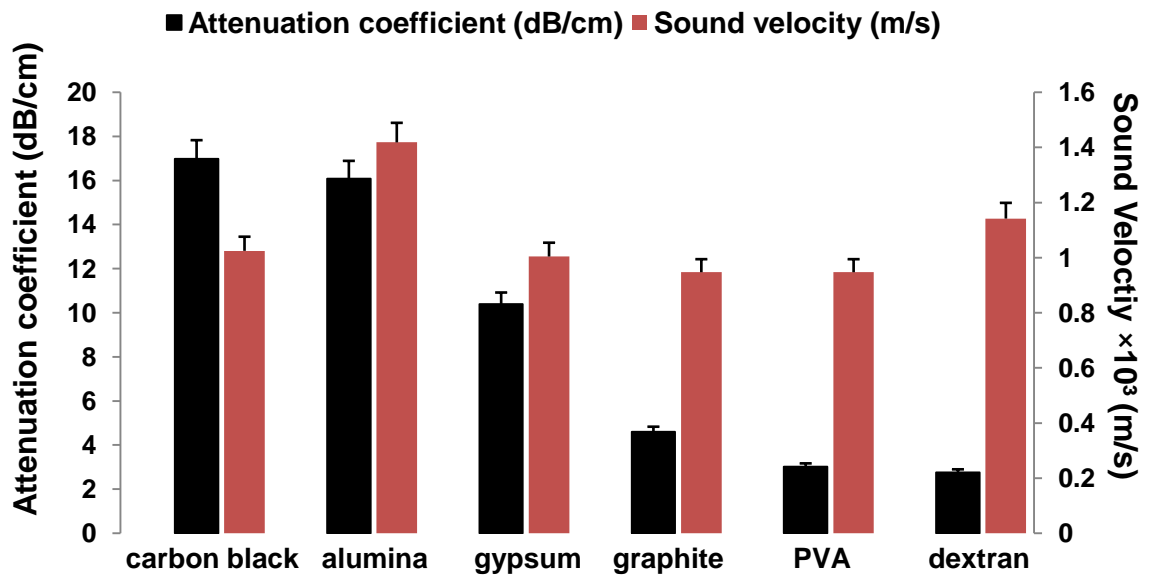


**Figure 13** Acoustic parameters of different breast tumor-mimicking phantom materials measured with 5 MHz transducer.

In Fig. 14a, the ultrasonography images of the tumor tissue with 35 wt % alumina added two-component silicone elastomer formulations were demonstrated. A size of 1.5 cm was chosen since 51.3 % of the invasive lobular carcinomas are reported to be  $\leq 2$  cm [72]. An ultrasound-guided needle biopsy was achieved with a 12 MHz probe through locating the mass within the breast using an ultrasound transducer and taking a piece of the mass with a biopsy needle simultaneously. The arrows in Fig. 14a shows the biopsy needle moving inside the inner breast tissue, entering into the tumor structure, and leaving the phantom with the collected tumor sample. Fig. 14b shows the image of the entry of the biopsy needle and the collected piece of tumor. Tumor structures were designed in a different color (beige) than the inner breast tissue (white) to confirm the successful collection of the tumor sample.

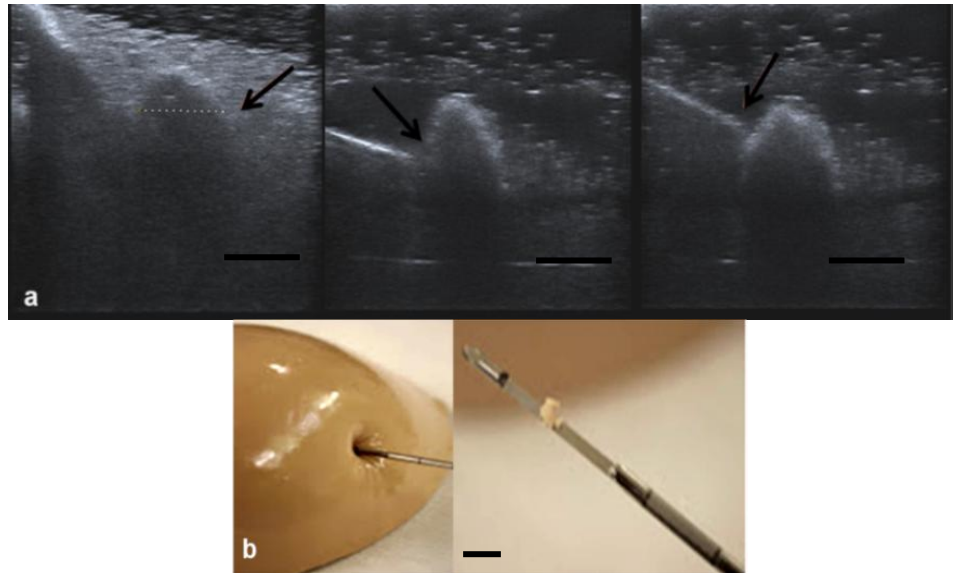


**Figure 14** Simulation of the tumor structure with 35 wt % alumina added silicone. a) Ultrasonography of tumor structure, the arrows indicate the entry and exit of the biopsy needle from the tumor. Scale bar represents 1.5 cm. b) Images of biopsy needle entry to the breast and the collected tumor piece. Scale bar represents 0.5 cm.

### 2.3.5 Ultrasonography Images of the Muscle and Rib bones Simulation Models

Another important component of the breast phantom is the muscle layer that supports the breast tissue and provides an anatomical separation between the rib bones and the breast. Since muscle tissue has a highly fibrillated structure, a variety of papers with different thickness and shapes have been used due to their fabrics and cellulose contents for the successful design. As seen in Figure 15, since these fabrics provided an image with high contrast in ultrasonography images, it has been deemed appropriate to use them by pre-curing with silicone material instead of a direct addition to the breast formulations.

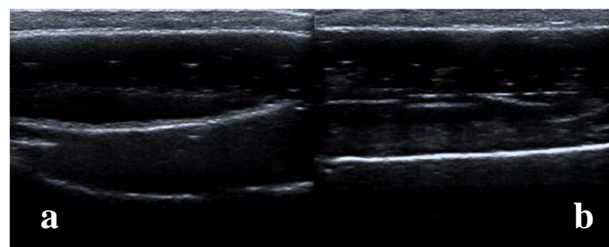


**Figure 15** Ultrasonography of two-component silicone elastomer inner breast tissue, and different sizes and shapes a) fabric and b) paper addition for the muscle layer imitation.

In order to design the muscle layer and rib bones that are similar to human tissues, models were produced inside a mold with a specific pattern, and fabrics and fibrils were applied into this silicone layer in repetitive patterns. Fibrous fabrics were placed into the silicone as a thin layer repeatedly to imitate the ultrasonography response of the rib bones. In Fig. 16, attention is drawn to these repetitive structures integrated with the breast tissue.

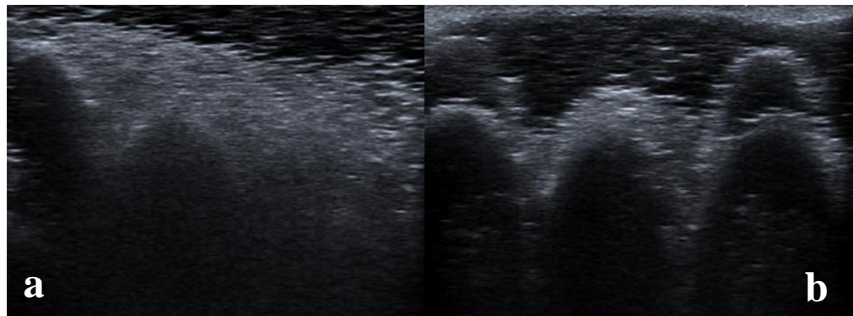


**Figure 16** Ultrasonography images of (a) two-component silicone elastomer inner breast tissue, and (b) imitated rib bones layer.

### 2.3.6 Ultrasonography Images of the Skin Model

The ultrasonography images of the skin model formed through the utilization of two-component silicone elastomers (Fig. 17a) emphasizes the similarity to the human skin and subcutaneous muscle tissue (Fig. 17 b). However, the fabric between the muscle layer and the skin layer presented an exceedingly sharp feedback, hence it was decided that no fabric should be applied between these layers in the following models.

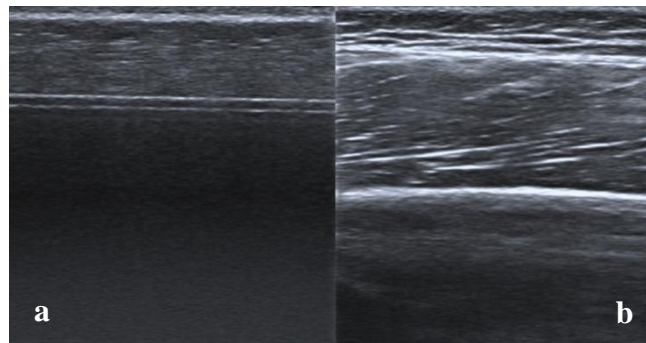


**Figure 17** a) The skin model that consists of cured two-component silicone elastomers, b) Ultrasonography of human muscle tissue (arm).

### 2.3.7 Fabrication of the Mammography Phantoms

Silicone formulation with 66.6 wt % silicone oil is utilized for the mammography model with the addition of 30 wt % expancel additive for the inner breast tissue. Expancel that composed of ultra light microspheres has the potential to expand upon curing with higher temperatures, due to its thermoplastic nature. Although incorporation of these microspheres has shown absorption of the ultrasound waves, it has appeared that expancel can be used as an additive to the silicone formulation as a tissue-mimicking material for the breast mammography model which is another important imaging and diagnostic technique. Fig. 18 shows the mammography image of this model.

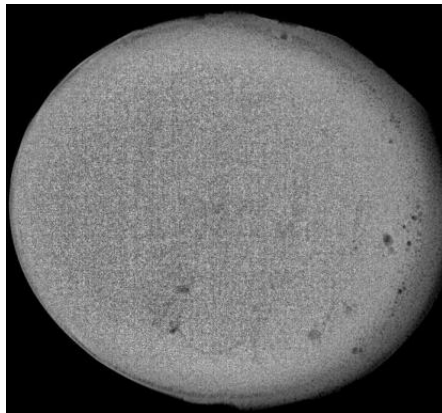


**Figure 18** Mammography image of inner breast tissue that contains two-component silicone elastomer with 66.6 wt % silicone oil and 30 wt % expancel additive.

In mammography models, the diagnostic effects of the low dose x-ray on the breast model were examined by the comparison of the elasticity that was adjusted by varying silicone oil and the additive content. In this view, the addition of expancel to silicone formulations with different densities has allowed the diagnostic screening of the breast tissue in mammography imaging. The model aimed to simulate human breast with lower (10 wt % silicone oil added) and higher (50 wt % silicone oil) elasticity and the differences were observed in mammography images in Fig. 19.

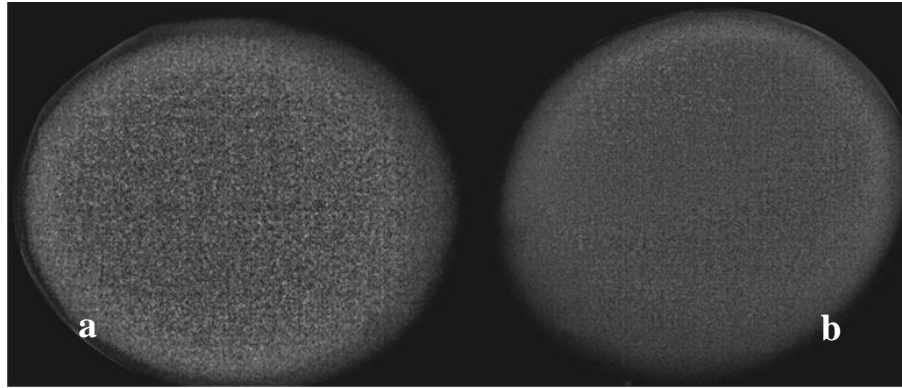


**Figure 19** Comparison of mammography images of inner breast tissue that contains two-component silicone elastomer with a) 10 wt % expancel, and b) 50 wt % expancel.

Alumina particles and egg shells were utilized in order to simulate tumor calcification, which is an important parameter for the diagnosis of the breast tumor in mammography. The aim was to capture the mammography images of these materials in the form of calcification, which is a result of deposits near the ducts of the milk glands, or their transformation into a tumoral structure (Fig. 20).

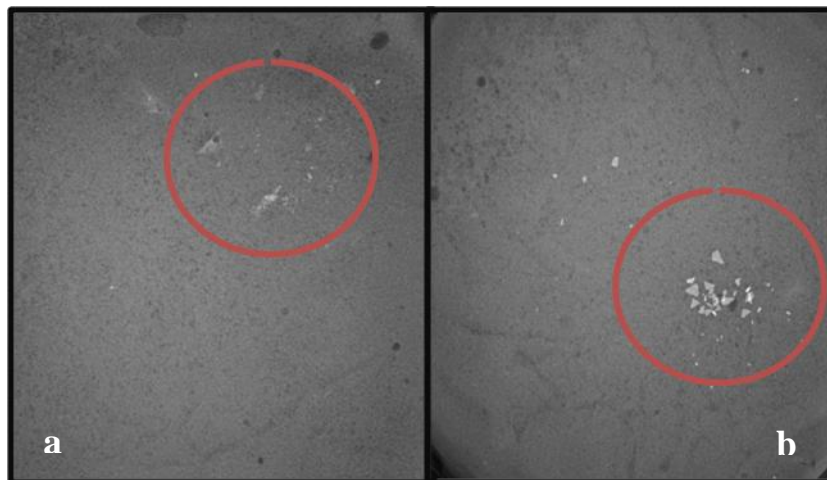


**Figure 20** Comparison of additives (10 wt %) in two-component silicone elastomer inner breast tissue that mimics calcification in breast mammography images, a) alumina ( $\mu\text{m}$  scale), b) egg shell (mm scale).

### 2.3.8 Fabrication of Breast Phantoms for Surgical Training

Two different techniques to underline the performance of surgical breast models have been selected. In Fig. 21, Batwing Mammoplasty (BWM) technique was demonstrated [73, 74]. BWM is an effortless and easy-to-learn technique that is mostly targeted for periareolar cancers that are located in the upper quadrant of the breast. In this technique, the positioning of the nipple-areola complex was not necessary and the patients report positive cosmetic outcomes upon the surgery [74]. After marking and measuring the landmarks, the tumor site above the nipple site was resected until deep fascia of pectoralis major muscle. Then, the operation site was repaired with the neighboring breast tissue.

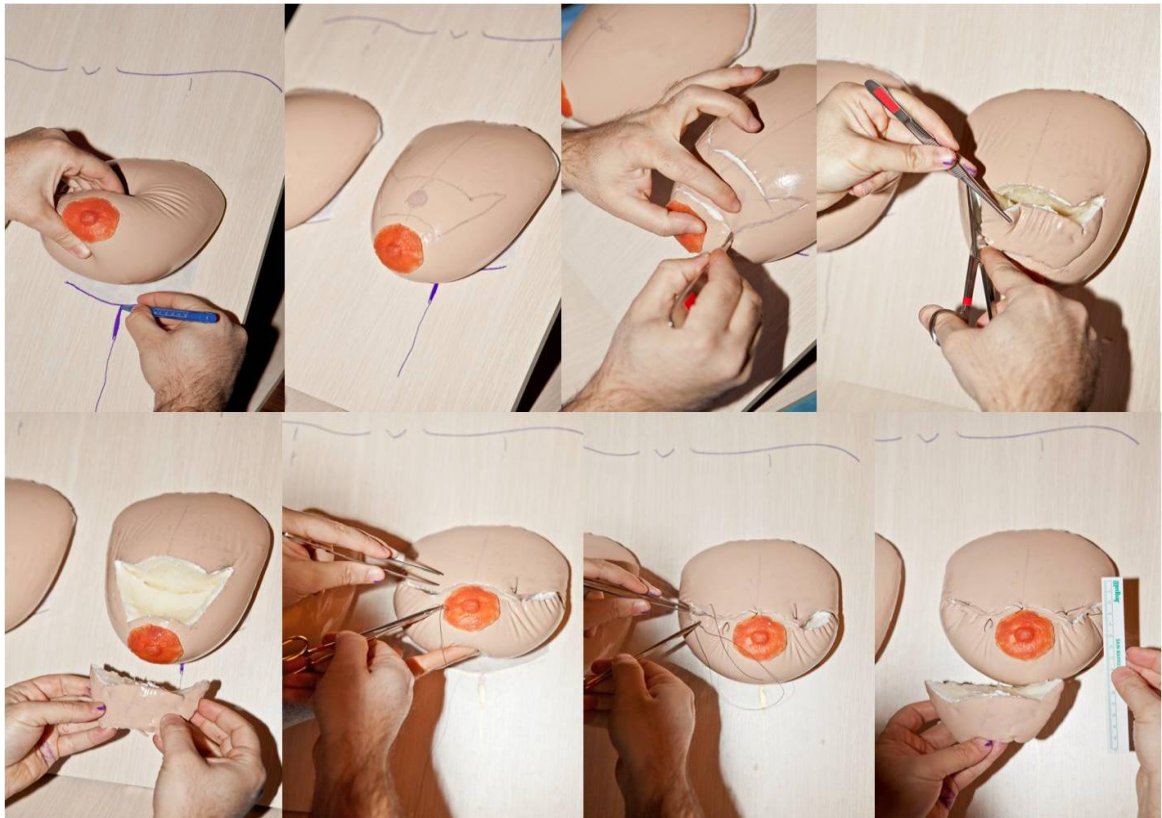


**Figure 21** Sequential photography of Batwing Mammoplasty technique

In Fig. 22, Rezai technique is presented. It is one of the oncoplastic techniques that can offer a high level of local control along with the aesthetic outcome [75]. After planning the Wise Pattern which was modified by Dr. Mahdi Rezai [76], the surgeon can resect the

tumor in any portion of the breast. After resection, the site was reconstructed with the remaining breast tissue.

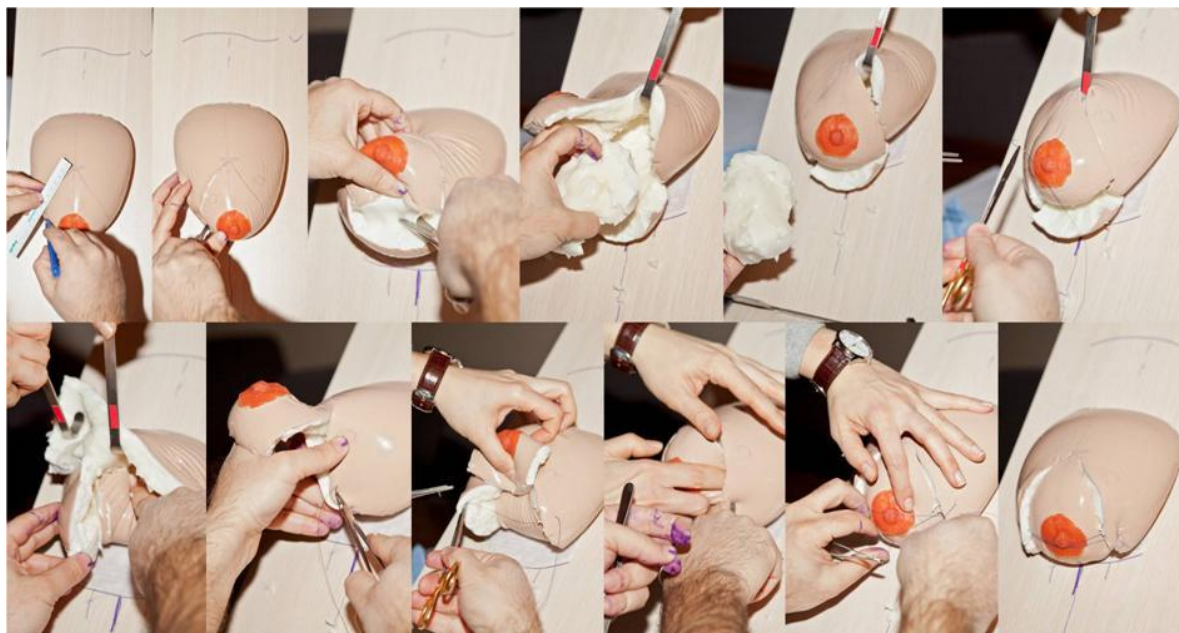


**Figure 22** Sequential photography of Rezai technique

Moreover, these models can also be used in public education as “self-diagnosis” models. These models were designed to contain masses that simulate malign tumors of different sizes at different locations such that self-examination can be learned. During the molding process, pieces of cured silicone from the used models were added to the uncured silicone mix, and then the entire system was cured to ensure the attachment of individual recycled pieces. These models can also be employed as anatomical models in clinical practice as decision-making tools for surgeons to determine proper operation techniques for complicated cases and as a platform for communication between surgeons and patients.

## 2.4 Conclusions

The formulations of two-component silicone elastomers were tuned with two different additives (i.e., silicone oil and vinyl-terminated PDMS) in order to approximate the acoustical, tactile, and mammography properties of human breast tissue (skin, subcutaneous fat, muscle, and rib bones) as well as malign tumors. The sample that contains 75 wt %

thinning agent exhibited the highest similarity to acoustical properties of human breast, while the utilization of alumina to the silicone formulation simulated malign masses effectively in the ultrasonography phantom.

In addition, the designed surgical models offer a cost-effective, easy-to-handle, and sustainable alternatives to human tissues. A key milestone for global impact on medical education is to design and fabricate affordable models such that medical schools and even individual physicians can afford these models. Depending on the utility of the model, the target groups can also be expanded to nursing students, medical staff, and healthcare professionals. Considering new laws restraining cadaver use outside of anatomy laboratories and European Union regulations limiting training hours of medical interns, demand for this type models is expected to increase. In addition, affordable “self-diagnosis” models will facilitate the training of healthcare workers and the public; and are expected to potentially enable earlier diagnosis of breast cancer. For early diagnosis, self-exam is crucial; however, surveys from resource-limited settings clearly demonstrate the lack of education for self-diagnosis in public and most strikingly even among healthcare workers. Countries that lack proper infrastructure rely especially on non-governmental organizations or healthcare workers to visit rural areas [77, 78]. Portable education-enabling tools, such as the “self-diagnosis” model that is described here, are expected to improve breast cancer awareness and detection. Cost-effective fabrication of realistic self-diagnosis models will potentially allow access to these models by a higher number of agents that provide such trainings; hence, increase the number of beneficiaries.

The fabrication process was specifically designed to enable the production of this type of models in a non-laboratory setup in order to spread the utilization of phantoms in medical trainings and educating women and medical personnel for palpation. We believe with cost-controlled production and utilizing silicone, which can mimic the human breast tissue much better than other materials; it is possible to fabricate cost-effective, thus accessible models, with good quality. Hence, through effective collaboration between medical doctors and engineers, best possible training platforms can be designed for the betterment of the medical education.

# Chapter 3

## Fabrication of the Peripheral Nerve Model

### 3.1 Introduction

In the last several decades, great advances have been made in the microsurgery of peripheral nerves. The return of the developments in technology has been significant for the enhancements of the microsurgery techniques [79]. Peripheral nerve disorders occur either due to the entrapment of structural tunnels, compression of anomalous structures or severe external injuries [80]. In addition, heavy sports activities [81], traumas associated with accidents [82], or stress accumulation due to the repetitive physical movements of joints, muscles, or ligaments [83, 84] can be classified as several reasons of serious peripheral nerve damage. The presence of nerve injuries in the lives of patients leads to significant limitations on the physical activity of the patients and most of the time also has psychological implications [85-87].

Microsurgery became an integral part of several branches of surgery, such as plastic surgery, neurosurgery, and orthopaedic surgery as well as other surgical disciplines to ensure improved clinical outcomes [88, 89]. Long-term assessment of recovery on nerve injuries that are repaired through microsurgery indicates a faster healing process and

retrieval of sensory and motor functions [90]. The correct assessment of the treatment plan can be achieved upon the accurate classification of the nerve injury [91] which was introduced by Seddon [92], and further divided into five sub-groups by Sunderland [93]. Injuries of peripheral nerves can be debilitating, in particular the injuries of the nerves in hands may cause the weakness of the arm, wrist, and hand, and once these injuries severely affect the nerve continuity, by creating a fifth-degree nerve injury, the surgical intervention is necessary to restore the hand functions (Fig. 23) [94].

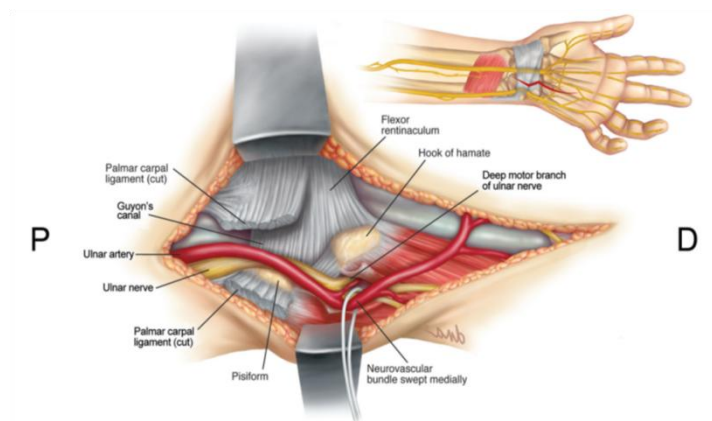


**Figure 23** The representation of the ulnar nerve in hand upon decompression of the branch [94].

Microsurgeons-in-training necessitates intense practice to augment their surgical competence, proficiency, and dexterity [95]. Current education system relies on the Halstedian apprenticeship model [96], where a senior surgeon evaluates competence and technical skills of trainees [97]. Working with animal models and cadavers along with living patients is considered as the gold standard in medical education [98]. In addition, fresh tissues such as pig legs [99], human placenta [100], and avulsed skin [101] are utilized as practice media; while surgical gloves and medical grade tubes [98, 102] are also employed as primitive alternatives. However, i) access to cadavers and live humans/animals is not constantly available [98], ii) there are ethical concerns related to working on live patients and animal models [103], iii) fresh tissues require either refrigeration or contain high risk of transmissible diseases, hence can be classified as biohazard, and vast amount of effort is needed for self-protection [104], and iv) synthetic materials latex [105], polyethylene [106], Gore-Tex [107] and parafilm [108] cannot offer

the necessary fragility, complexity, and hierarchical outlook of real tissues. Unrealistic materials such as latex strips, latex tubes, or natural tissues (chicken wings) are utilized as injured nerves for the training models in nerve microsurgery simulations [109, 110]. The survey in 38 training center in the U. S. confirms that only 3 % of the students could receive neuromicrosurgical training [111]. There is a need for a realistic, standardized—hence reliable, and accessible platform for microsurgical trainings.

Here we report, the design of a silicone-based, composite peripheral nerve microsurgery phantom. We have optimized the formulations of silicone to imitate tactile, cosmetic, and mechanical responses of human peripheral nerve tissues. These models can also be fabricated in a simple setup (e.g., in a non-chemistry lab) that contain a scale and an oven. The phantom consists of i) a skin layer (i.e., epidermis and subcutaneous fat), ii) fascia layer, iii) peripheral nerves, (i.e., epineurium, connective tissue, and fascicles), and iv) a muscle layer. These components were prepared separately and combined into a single model afterward. The layers were designed out of two-component silicone elastomers that were formulated to simulate tactile and cosmetic properties of peripheral nerves. We tracked a matrix of silicone formulations to reach the reported elastic modulus of 3–10 MPa for live tissues [112-114]. Visible light microscopy (VLM) and scanning electron microscopy (SEM) indicated no damage upon the entry of the needle while still offering fragility towards microsurgical suturing. This model provides a durable and realistic tactile medium for surgical simulations where surgeons-in-training can learn at their own pace as well as be examined on a standardized platform.

## **3.2 Materials and Methods**

### **3.2.1 Tissue-Mimicking Materials**

Two-component liquid silicone elastomer; component A (SL-3358A) and B (SL-3358B), were obtained from KCC Corporation, Korea. Silicone oil was purchased from Sapar, Turkey (PMX200-350 CST). Cotton fibers were received from local providers. Dyes that were used in coloring were obtained from Wacker Chemie, AG.

### 3.2.2 Design of the Peripheral Nerve Model

The phantom was prepared according to the human anatomy of the peripheral nerve tissues [115]. The model aimed at mimicking ulnar, median or radial nerves in the upper extremity. Fig. 24 demonstrates different layers of the phantom, which consists of i) a skin layer, ii) fascia (the connective tissue layers between the skin, nerves, and the muscle layers), and iii) peripheral nerves (epineurium and fascicles). The epineurium has an inner diameter of 3 mm with a wall thickness of 1 mm. It holds three fascicles which were 1 mm-thick composite structures that contain 0.1 wt % cotton fiber in their formulation.

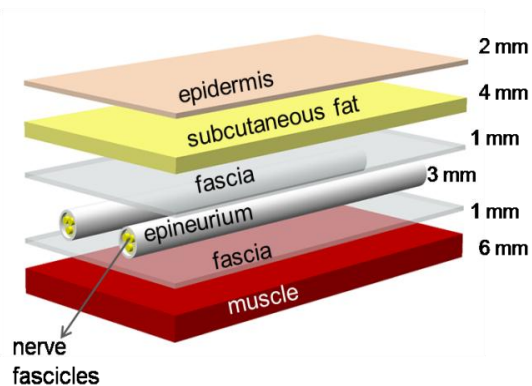


**Figure 24** Different layers of the designed phantom

### 3.2.3 Preparation of the Nerve Structures

Same curing method of the breast model with two-component silicone elastomers was used in the fabrication of microsurgery phantom (refer to section 2.2.2). The formulation of the skin layer was prepared by mixing equal amounts of component A and B with 50 wt % silicone oil. A single red line of silicone in sinusoidal shape was deposited on epineurium to enable the confirmation of successful joining of the broken ends of the nerves. Cotton or wool natural fibers were further added to the formulations of silicone between 0.1–1 wt % to tune the elastic modulus of the epineurium and fascicles. Consecutive curing of the muscle layer, fascia layer (before and after the attachment of pre-cured fascicles), subcutaneous fat layer and the epidermis layer was achieved in a 14x7 cm sized mold. The fascicles were cured in a 3D-printed poly lactic acid (PLA) mold for the precise size and shape match.

### **3.2.4 Mechanical Characterization**

Different formulations of silicone, either pristine specimens or those that contain natural fibers, were prepared in dog-bone shape according to the ASTM (American Society for Testing and Materials International) standards. The specimens were tested with 200 kN force in the Universal testing machine (UTM), and an average of 4 tests was reported as the test result.

### **3.2.5 Scanning Electron Microscopy**

The microsutures of epineurium and the nerve fascicles containing cotton fibers or pristine formulations were sputter coated with a thin layer of carbon by Cressington carbon coater and mounted onto the carbon tape. Images were acquired by scanning electron microscope JSM6010-LV, with in-lens secondary electron (SEI) detector, using an electron gun voltage of 5 kV.

### **3.2.6 Visible Light Microscopy**

The 8/0 microsuture on the epineurium that contains cotton fibers were cut longitudinally and the suture part was placed between the microscope slides. The entry sites of the suture needle, the suture knots, and the fibers within the two-component silicone elastomer structure were observed with visible light microscope (VLM) Nikon Eclipse ME 600, both in the bright field (BF) and the dark field (DF).

### **3.2.7 Assessment of Microsuturing in the Tissue-mimicking Phantom**

The suturing properties of the designed nerve samples were assessed by one of the surgeons (M.B.) who is an expert in his field. Samples were tested by 8/0 and 10/0 non-absorbable polypropylene sutures (Prolene) with BV 175–7 and BV 100–4 needle and 11/0 polyester fiber (Mersilene) with TG 160/4 Plus needle (Ethicon Inc., New Jersey, USA), with the aid of an operating microscope (OPMI Vario 700, Carl Zeiss Meditech AG, Germany).

### 3.3 Results and Discussion

#### 3.3.1 Selection of materials for the nerve model

For the design of this model, we have surveyed a matrix of formulations of silicone that is commonly used as a tissue-mimicking material in prosthetics [54, 55], film industry, and soft robotics [57]. The ease of fabrication, molding, and coloring have made silicone a remarkable option for the simulation models [116]; for instance, there are numerous commercially available phantoms (e.g., skin pads) for suturing practice [117]. Likewise, silicone tubes are utilized for microsurgical models [118, 119].

The suturing strength of epineurium, perineurium or fascicles demonstrate differing values of elastic modulus [120]. Hierarchical structure of the model was designed to match the elastic modulus of these nerves. The elastic modulus of the samples decreased with increasing silicone oil content (Fig. 25). The sample with 83.3 wt % silicone oil exhibited highest similarity to nerve tissues in terms of elastic modulus (3–10 MPa [112, 121]) and thus was chosen as the material to form fascicles. The sample that contains 66.6 wt % silicone oil was preferred for the epineurium, since it has higher elastic modulus than the inner connective tissues. UTM results also showed plastic deformation before fracture in all specimens (Fig. 26).

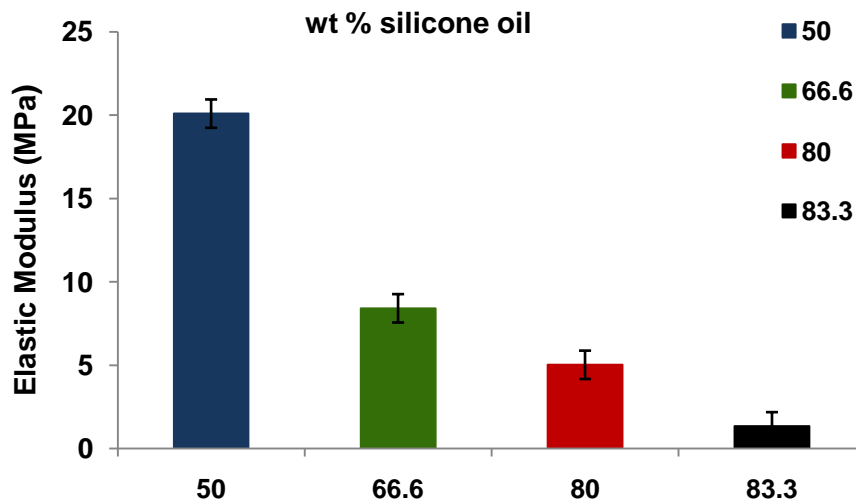


**Figure 25** Comparison of elastic modulus of formulations with increasing wt % silicone oil

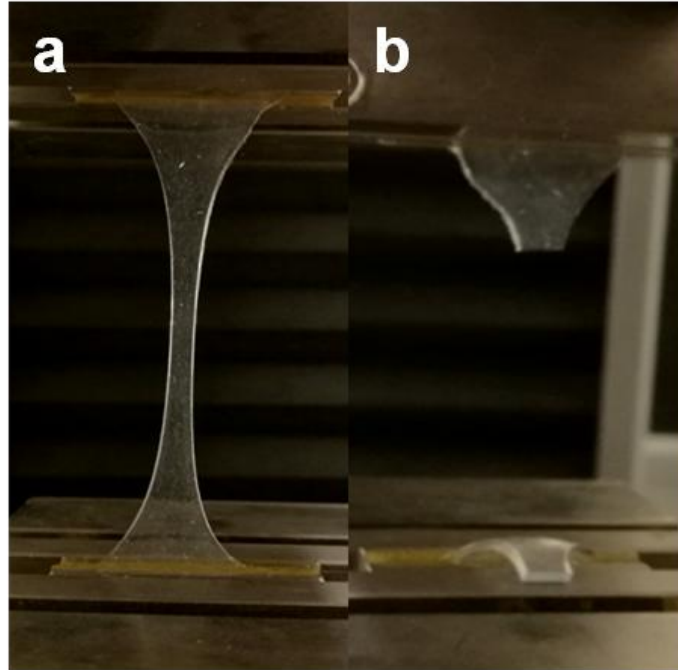


**Figure 26** Tensile test with dog-bone shaped specimens, a) plastic deformation of the sample during the test, and b) after fracture

For the design of epineurium, we have added wool or cotton fibers (0.1 wt %) to the sample that contains 80 and 83.3 wt % silicone oil to further tune the elastic modulus and imitate microsuturing of the nerve tissue. These fibers facilitate realistic suturing of the epineurium since they strengthen the medium against tensile forces. Wool and cotton were chosen as reinforcing fibers due to their accessibility at a low-cost [122, 123]

We focused on the elastic modulus at the range of 3–10 MPa [124-128]. The aim is to sustain the fragility of the fibers; thus having a low elastic moduli while asserting attraction force on the needle during suturing. Since, cotton fiber-added samples exhibited relatively smaller values than the wool-added ones, we tracked the change in elastic modulus at cotton-added samples in formulations with 80 and 83.3 wt % silicone oil. The higher silicone oil content assured lower values of elastic modulus (Fig.27).

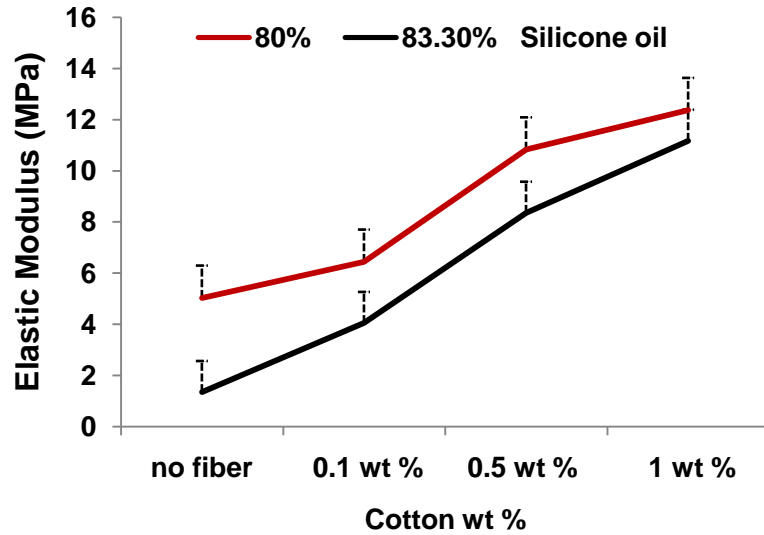


**Figure 27** Comparison of elastic modulus of two highest wt % silicone oil containing specimens with increasing wt % cotton content

The sample with 83.3 wt % silicone oil that contains 0.1 wt % cotton fiber was chosen to be used as the nerve fascicles mimicking part of the phantom. Having fibers in the model allowed the microsuture to remain intact on the nerves. It can be concluded that utilizing either 83.3 wt % with cotton fibers or 66.6 wt % without fibers can both give microsuturing response similar to epineurium at the wall thickness of 1 mm, while the cotton-added sample provides a form of traction. Hence, our model has both the elastic modulus and the suture response resemblance to the nerve tissues.

### 3.3.2 Evaluation of Microsuture on Nerve Phantom

One of the main obstacles during microsurgery is the damage imposed by the entry of needle to the tissues where bleeding is possible. This bleeding, in turn, may result in the disruption of the area of surgery, and hence obstruct the vision of surgeon during the operation. Having smaller damage can also provide a faster healing process after the surgery. The mechanical properties of the suggested model allow entry of the needle without introducing a significant hole that may cause leakage. In order to evaluate the damage around the entry sites of the needle, we have monitored the sutures by VLM (Fig. 28) and SEM. Two different sizes of sutures were utilized for the evaluation of the damage. The suture ends (entry sites) and the contribution of the fibers was focused.

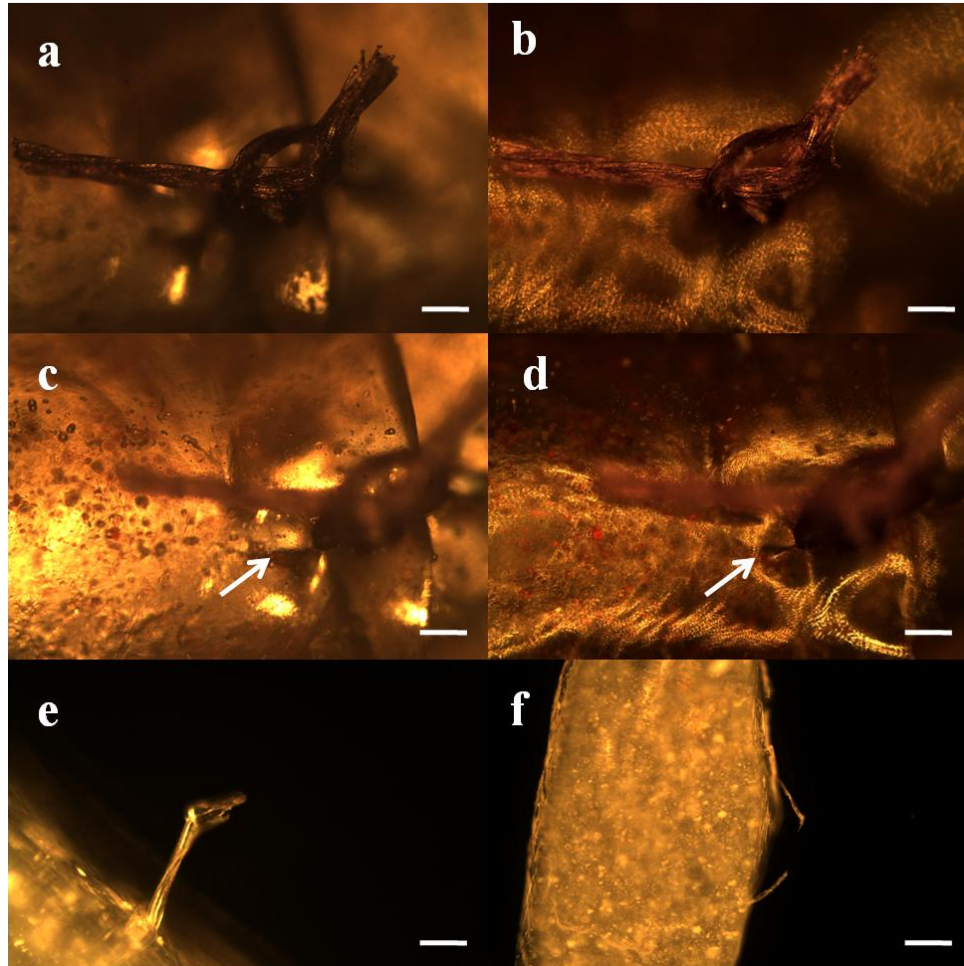


**Figure 28** The VLM images of 8/0 microsuture and 0.1 wt % cotton fibers in epineurium model. a-b) BF (a) and DF (b) images of the microsuture, c-d) BF (c) and DF (d) images of the microsuture with arrows indicating the needle entry sites, e-f) Cotton fibers in the epineurium structure. All the scale bars represent 200  $\mu\text{m}$  (e-50  $\mu\text{m}$ ).

In Fig. 29, 10/0 sutures were used on the formulations of silicone with i) pristine epineurium models, ii) 0.1 wt % cotton fiber-added epineurium, and iii) 0.1 wt % cotton fiber-added fascicles. SEM micrographs confirm that the sutures inflicted no significant damage on the entry sites of the needle and adequately joined two sides of the epineurium and the fascicles. The traumatized peripheral nerves were cut in order to simulate the fifth-degree nerve injury. Despite the overlap of two sides of the nerves, the placement of 10/0 sutures resulted in the successful entry of the needle, hence a knot was tied effectively even on the pristine models. The addition of the cotton fibers allows the peripheral nerve model to hold the sutures securely.

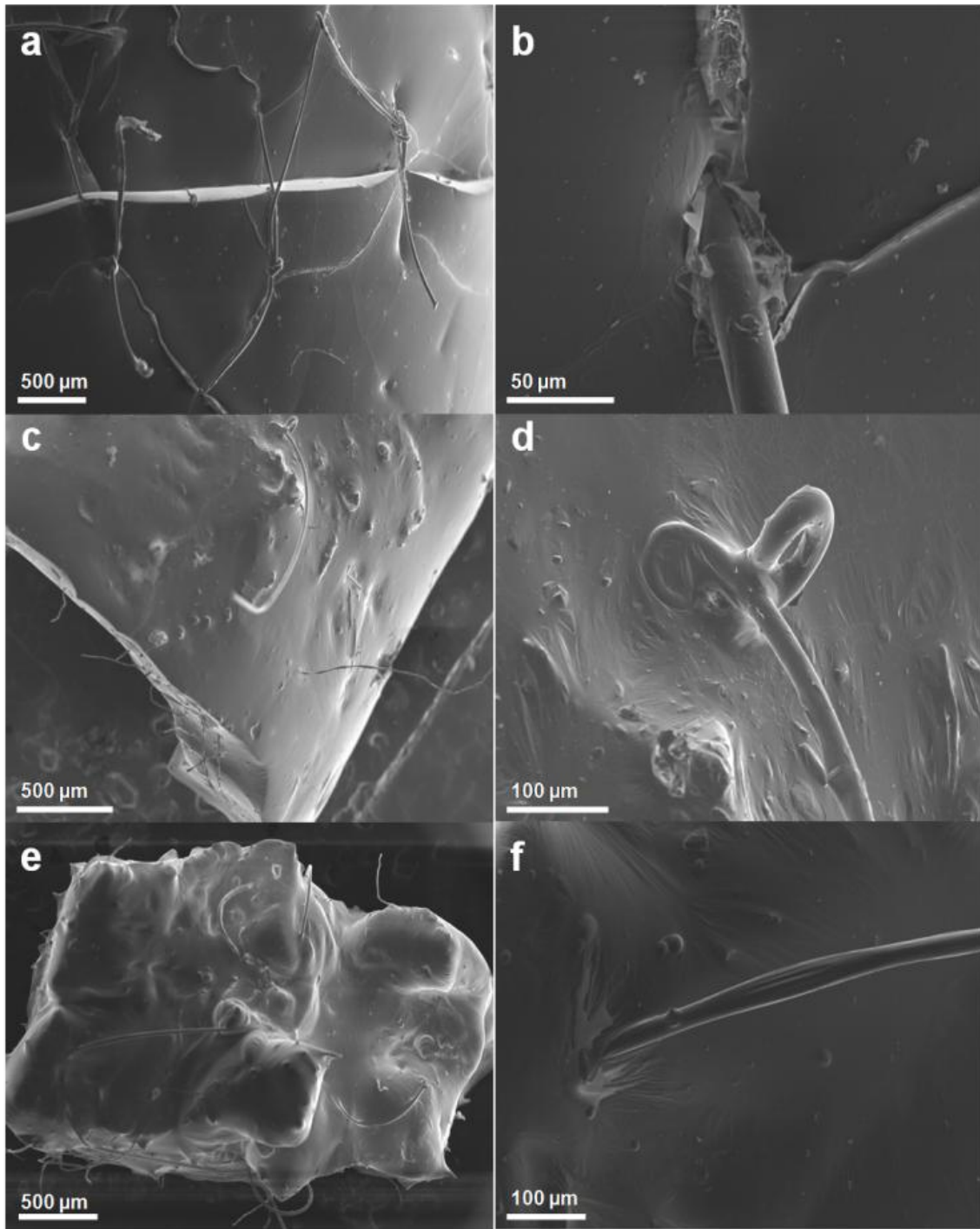


**Figure 29** a-b) Epineurium model pristine, c-d) Epineurium model with 0.1 wt % cotton fibers, e-f) Fascicle model with 0.1 wt % cotton fibers. 10/0 sutures were used. Entry sites of the needle were focused on the smaller scale bars.

In Fig. 30, the silicone formulations with pristine (a-b), and 0.1 wt % cotton fiber-added (d-f) epineurium models, and the 0.1 wt % cotton fiber-added fascicles (c) were tested, and the repair of peripheral nerves with 8/0 sutures applied on the phantom showed no substantial damage at the entry sites of the needle.

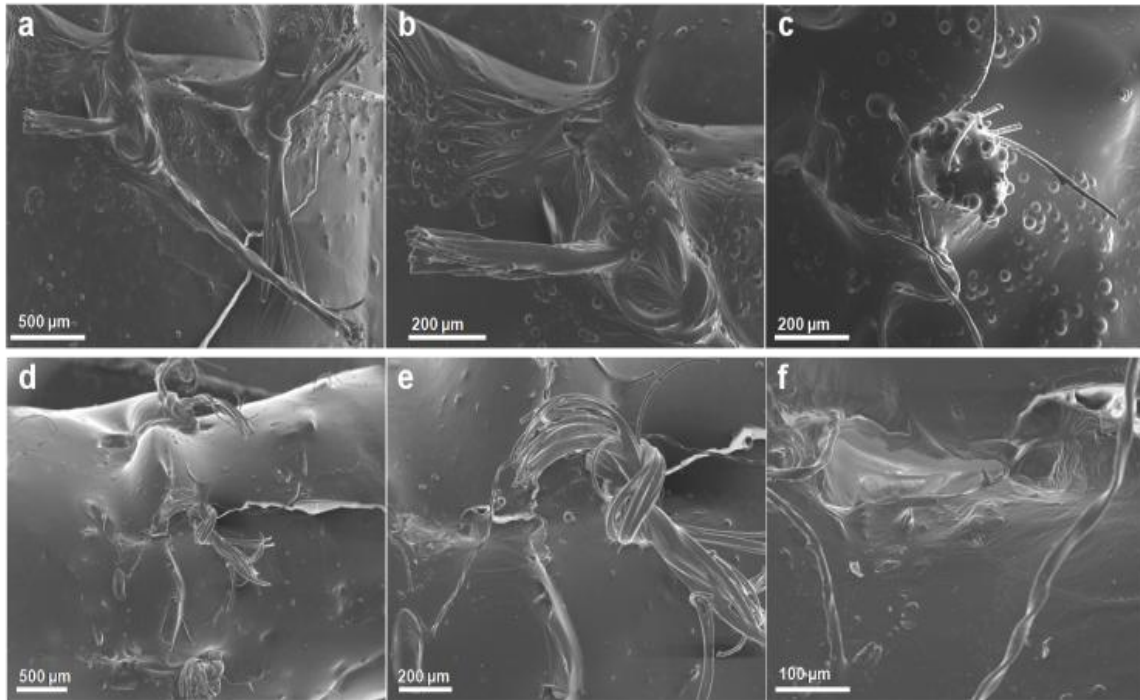


**Figure 30** a-b) Epineurium model pristine, c) Fascicle model with 0.1 wt % cotton fibers, d-f) Epineurium model with 0.1 wt % cotton fibers. 8-0 sutures were utilized.

### 3.3.3 Microsurgical Assessment of Peripheral Nerve Phantom

A fifth-degree severe peripheral nerve injury has been simulated with the fabricated peripheral nerve model. The anatomy of these nerves is mimicked including the fascia tissue, vasa nervorum, epineurium, connective tissue, and the fascicles. In Fig. 31, the microsurgery on the nerve model without the addition of cotton fibers can be seen. The fascia tissue on the nerves was removed gently (a-c), and a cut on the peripheral nerve was achieved, and the fascicles and connective tissue were observed. The blue tissue paper was placed below the area of procedure for the ease of visualization (d-f). Vasa nervorum was aligned on both sides of the nerve and the fascicles were sutured with 8/0 suture. The needle was inserted with 45° angle and removed with circular movements to prevent

generating the excess needle hole. Then, the same application with reverse order was achieved to complete the nerve repair. The model has considerable resemblance to peripheral nerve tissues with similar resistance to the sutures.

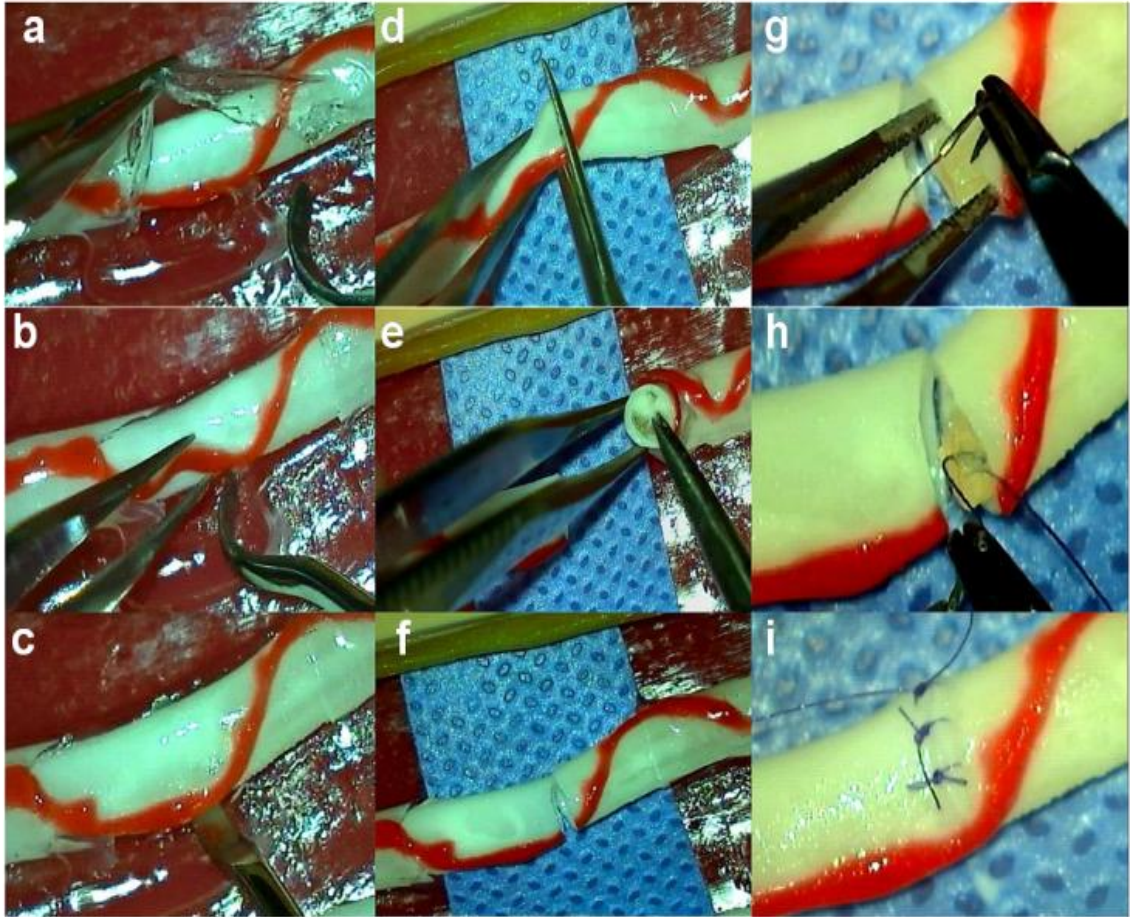


**Figure 31** Nerve model pristine. a-c) Removal of fascia part to release the nerve, d-f) A cut on epineurium, and beneath outer epineurium layer, connective tissues and fascicles viewed, g-h) Microsutures on fascicles, i) Microsutures on epineurium.

The significant part of the epineural repair was the correct alignment of the nerve ends to be sutured. The size of the suture must comply with the topology of interest. In Fig. 32, a cut on the peripheral nerve model with 0.1 wt % cotton fiber can be seen. The alignment of both ends was followed by the suturing of these sides with 8/0 suture. The addition of cotton fibers has improved the suture resistance of the epineurium, while facilitated the successful alignment since the sutures of epineurium should be loose to avoid the overlapping of the fascicles within the structure.

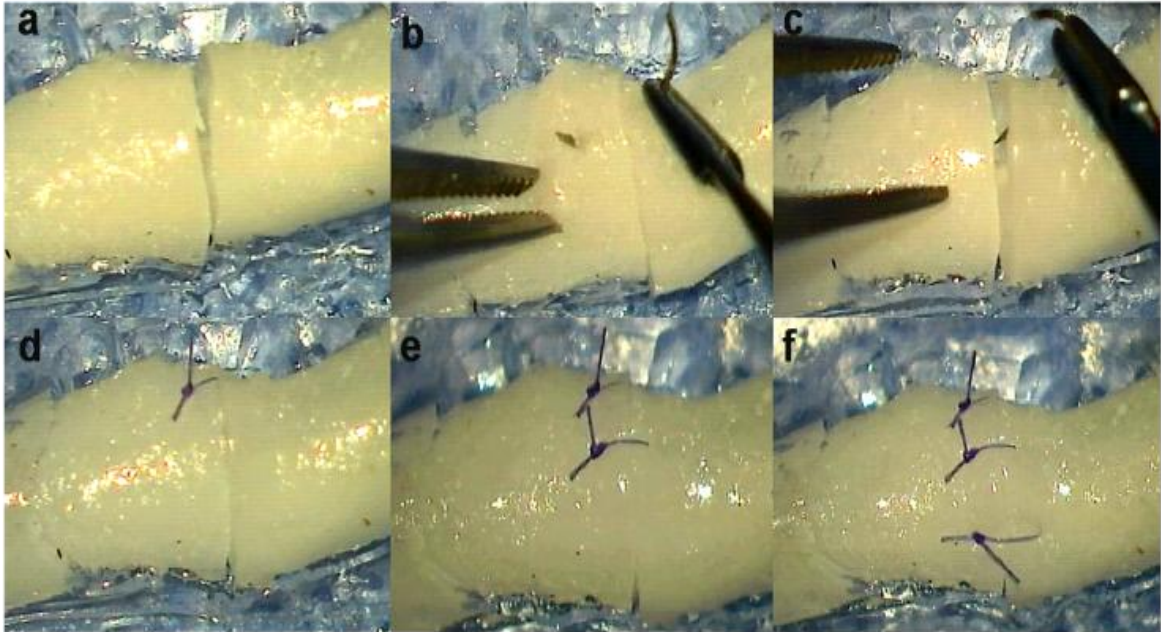


**Figure 32** Nerve model with 0.1 wt % cotton fibers. a-f) Systematic assessment of a nerve cut, and microsuturing of the epineurium layer.

The images of designed pristine epineurium of the peripheral nerve model can be seen in Fig. 33. A cut was made and a microsuture with 10/0 sutures were achieved on the model.

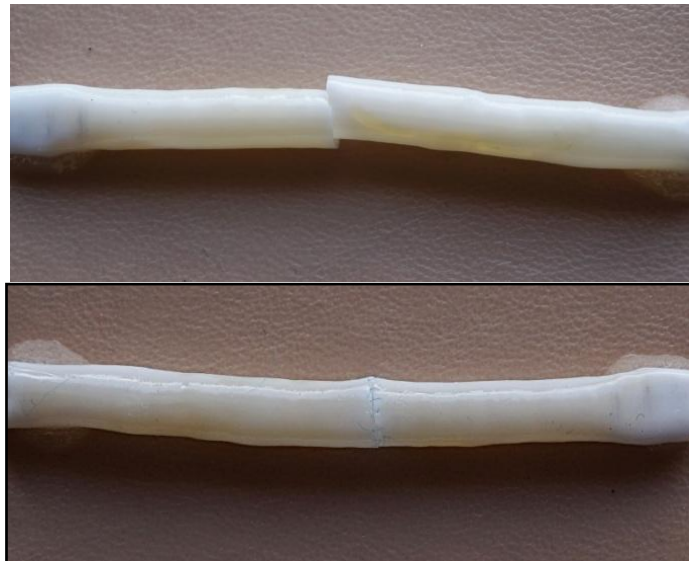


**Figure 33** Sutures (10/0) on the epineurium part of the peripheral nerve model.

### 3.4 Conclusions

Peripheral nerve injuries commonly occur in radial, ulnar and median nerves [129-131]. However, treatment of these nerves has been a challenge for surgeons due to the lack of advancements in technology [132, 133], e.g., development of higher magnification operating microscopes [134], instrumentation and suturing materials [135]. Although technological aids in reconstructive processes facilitate significant enhancement in peripheral nerve surgery, due to the complex nature of these structures, this field still remains grueling for the microsurgions [136, 137]. The most severe type of these peripheral nerve injuries is the fifth-degree (Seddon's neurotmesis) [138, 139] injuries, where a local response to the rigorous trauma arises. Proximal and distal changes in peripheral nerves can be reckoned as an evidence of the injuries [140]. The electrodiagnostic studies can determine the degree and the localization of the injury at early stages. The anatomical structures that peripheral nerves composed of—endoneurium, the fascicles, Schwann cells, axons, and the epineurium are completely ruptured at this level of injury. In addition, the activated morphology of the fibroblasts at the severed areas of epineurium, Schwann cells, perineurium, and endoneurium can be observed [141, 142]. The overall response of the peripheral nerve tissue components and the surrounding tissues correlates with the asperity of the experienced trauma and the scar formation [142].

The uttermost importance of the microsurgical techniques in the successful restoration of the injured peripheral nerve tissues has been recognized with the aid of advancements in technology [143]. According to the anatomical part of the nerve that has been injured, a pertinent microsuturing technique shall be achieved. As an instance, coaptation of the fascicular tissue which is the most significant repair technique of the peripheral nerve tissues is achieved upon the injury [144].

Silicone-based simulation models were repaired through the alignments of the epineurium and the fascicles by utilizing 10/0 and 8/0 sutures. Precise alignment in fascicular level with the shorter operation, dissection, and anesthetic times is crucial for post-operative functional repair of the nerves [5]. A comprehensive anatomical understanding, in line with the successful practice of technical instruments and expertise in microsuturing maneuvers,

are essential for neurosurgical achievement [145]. Hence, an extensive training and repetitive practice are required to develop these skills. However, current training materials are live patients, animals (cadavers), virtual reality platforms, or prosthetics. There's a lack of training materials in medical education. In this chapter, a realistic, accessible, reliable, and standardized silicone-based composite peripheral nerve phantom to be used in the training of microsurgeons was revealed. The mechanical, structural, and tactile characterization of the model was achieved with UTM, VLM, SEM, and the microsurgery operation.

# Chapter 4

## **Skin, Axilla, Axillary Lymph Nodes, Tracheostomy, Bronchoscopy, and Vascular Models for Surgical Training**

### **4.1 Introduction**

The fabrication of synthetic tissue and organs have the potential to imitate the response of human tissues to surgical interventions [146]. Recently, simulation models are employed both in medical and theoretical trainings. The successful implementation and utilization of surgical phantoms in medical education curriculums ensure the desired outcome achievements of the faculties and training institutes [147]. Surgeons-in-training entails considerable amount of practice in order to improve their surgical skill sets and together with simulation-based training systems, the trainees learn at their own pace and experience various medical scenarios rather than incidents where the urgent response to the patients is required [148, 149]. Practicing with simulation materials offers a safe environment where failing is a part of the learning process, thanks to the unlimited repetition opportunity. Hence, there is a need for such a reliable platform to diffuse simulation-based trainings to medical curricula [150].

For training purposes, fresh cadavers can be classified as the closest media to real tissues. However, these tissue substitutes are difficult to obtain due to their price and/or unavailability. Utilization of cadavers in the training of health workers (e.g., medical doctors, nurses) is essential [151]. However, following the same trend in the donation of organs, the endowment of cadavers is also minimal [152]. Although, public campaigns to enhance altruistic donations are developed for promoting the awareness of cadaver bequest—yet, there is a need for more consistent and durable solutions [153]. Nevertheless, they are not affordable by medical schools in many countries, for instance, synthetic cadavers are priced \$30,000–\$80,000 and the cost of individual organs starts from \$300 [154]. In this study, the designed models were fabricated with these properties: i) at least 90% of the used materials have purchased from local suppliers, ii) the models were custom-made and open to immediate modifications depending on the feedback from the health professionals, and iii) the models provide realistic responses to suturing. These phantoms can be used as individual parts; yet, in the long term, a synthetic cadaver that will include these tissue parts can be built, and be employed in settings where it is difficult to attain fresh cadavers. This cost-effective and convenient solution provides trainings even in resource-limited settings, and also reduces the need for chemical/cold storage applications on the cadavers and risk of infections/molding. Thus, these attributes make the models a preferable education tool for individual practices.

In this part of the thesis, the design and fabrication of realistic, sustainable, easy-to-produce, and low-cost synthetic tissue and organ models which enable the tactile simulations in surgical skills laboratories was revealed. This tactile simulation platform will assist surgeons to improve their surgical skills and facilitate their learning process. In the framework of these purposes, i) multi layers of the skin, ii) axilla and axillary lymph nodes, iii) vascular models, iv) tracheostomy and bronchoscopy models for surgical simulations were fabricated by utilizing silicone-based elastomers with several additives and textiles. The mechanical properties were investigated through the UTM in order to confirm the resilience of the models with human tissues, for the optimized response towards suturing.

#### **4.1.1 Significance of Surgical Education Materials**

Synthetic models that act as human tissues have been produced by utilizing silicone-based composite materials. These models allow surgeons-in-training to improve their vocational and diagnostic skills as well as imitation of the surgery. In particular, the vascular models that were prepared in this study allow simulations to be performed dynamically, with interchangeable vessels, and adjustable blood flow frequency and velocity. The overall system has the potential to introduce a blood flow during the medical scenario of a vessel tear intervention.

Surgical simulation platforms include systems ranging from simple bench top and box simulators (animal models) to cadavers, where simple operations can be practiced. In box simulators, a camera and a surgical instrument are inserted through a hole, and the trainee can manipulate real tissues or synthetic materials that are inside the box [155]. Although there are differences in anatomical placements, the use of only just killed or anesthetized animals in education is often preferred; since the realistic surgical environment can be experienced due to hemorrhage during the operation, however extensive use of the animals cause major ethical issues in many countries [156, 157].

In many countries, the need of cadavers in the training of medical, dental and nursing students are not satisfied. Most of the medical students graduate without participating in the surgical practices on cadavers. There are only about twenty centers in the country that include cadavers in medical training, and many of the recently established medical faculties, cannot offer cadaver practices due to the lack of facilities [158]. Although there are public campaigns to increase cadaver donation and cadaver imports from the abroad [158], it is clear that other arrangements are needed. Alternatives to cadavers may be synthetic models; however, existing, models that the medical faculties in our country may purchase are not intended to be used by the surgeons for training in critical applications, as these models do not reflect the true sense of operation [60]. Contrarily synthetic models that are designed and manufactured to reflect human tissue and organs with i) mechanical, ii) physical and iii) cosmetic properties are alternatives to be used for educational purposes.

Overall, the employment of these advanced technology-based models in simulation labs can greatly contribute to the education of the students and patient safety. With this motive, we aimed to imitate a range of human tissue-like organs. Furthermore, in order to obtain a realistic practice environment, a vascular model with a setup that contains real-time blood flow associated with the adjustable heart pulses was fabricated. Thanks to the feedbacks and informative commentaries from surgeons, in line with the literature reviews regarding the human anatomy, we have designed our phantoms with an excellent resemblance to human tissues. This interdisciplinary research has the potential to provide an affordable and functional platform and complete the lack of these models in medical education.

In order to increase the number of successful doctors in the field, the current educational system requires new training platforms due to the live patients being used as an educational object and the lack of cadavers. One of the techniques being developed in this area is simulation-based medical education [159]. Simulation; contributes to the learning of real-life experiences, earlier with the guided accompaniment. The use of simulation in medical education is recognized over the last several decades [160]. Simulation-based medical education offers more theoretical or direct advantages over education on the live patient. Procedures learned in the clinical settings may cause stress on the student and the stress has negative effects on the ability to make clinical decisions. One of the most important causes of this stress is the mistakes that can be made on the patient or the fear of affecting the health of the patients negatively [161]. The possibility to exercise on the patient is diminished by the limited numbers of samples and hence affects the learning process inefficiently. On the other hand, the duration of on-the-patient learning method depends on the trainer and self-practice.

In the case of simulation-based medical education, the focus on the patient is distributed on to the students. The students are trained more competently by making mistakes on the simulation, proceeding at their own pace, and repeating a certain procedure without any limitations [162]. Continuous practice reduces stress on students, increases their confidence and thus increases their technical ability. Medical students who practice on simulations may learn proficiently by receiving comprehensive feedback from practical mistakes [163]. Receiving regular feedbacks during medical education improves the knowledge and skills

of trainees significantly [164]. By simulating the clinical settings similar to the reality, critical thinking, decision making and problem-solving abilities of trainees can be improved. In simulation-based medical education, active learning, the theoretical knowledge and application skills of the students are integrated. Thus, thanks to the optimized training system, the error rate is reduced practically and patient care is carried out safely [165].

The benefits of simulation-based training of health personnel are listed in many studies: i) the ability to make decisions and intervene individually and in teams successfully, in particular in the cases of emergencies, ii) to enable the experience of various emergency scenarios iv) increase the confidence of the medical personnel, iv) reduction of avoidable medical errors, v) experienced specialists and students can repeat the same scenario many times and at their own learning pace, and vi) in the long-term, drop of medical costs due to the better education [166-168]. Upon the increasing interest in medical training platforms over the last few decades, the simulation models are designed with the highest similarity to reality. These realistic tissue simulations are produced with the latest technology [169]. In the first simulation models, the anatomy of the human body is mimicked with a geometric measure [170]. The second generation simulation models are designed according to the physical interactions of each anatomical structure with each other, in addition to the anatomy geometry. In the third generation models, the physiology of the organs was also taken into consideration. The superiority of this simulation is the achievement of imitation of physical and physiological properties of the organs, in addition to the geometric resemblance to the human anatomy. Realistic tissue responses can further be developed by taking into consideration the deformability of the organs followed by the application of force during the operation (cutting, sewing, processing). Thus, simulations designed with the most similar responses during the medical processes are obtained [171].

The University of Texas and Tulane University received a positive feedback, although a small number of students have practiced the vascular knotting on a simulator. The students have successfully knotted by the application of less force. The error rates were found to be 27 % before the simulation-based practices, while this amount has been reduced by 10 % after training with a simulator [172]. These feedbacks exemplified how a simulation-based

medical education has contributed positively to the skills of trainees. Wake Forest University has also highlighted the beneficial effects of the simulation in doctor's training. In this study, anesthesia assistants, emergency medical assistants, pulmonary intensive care workers, intensive care unit nurses, and students have experienced the simulation-based training and the overall score of tracheostomy examination average was raised to 91 % from 56 % after the training [173]. These results once again emphasize the importance of simulation in medical education. According to a survey, the final year students of the medical faculties in Turkey responded only 31% of the questions about medical sciences correctly. Considering that basic medical information is the fundamental part of practical applications, that the lack of practical practice in medical faculties explains the inadequacy of assimilating this information. The results of this study led to the fact that practical applications in medical education played an important role in keeping the theoretical knowledge up to date [174-176].

In the market, a simulation model with the highest similarity to human anatomy "Adult Cric Trainer" was produced by SynDaver. The model contains cricoid cartilages and nasal passages that allow nasal intubation and surgical cricothyrotomy (Fig. 34). However, the unit price of this cricothyrotomy model is around \$ 1250 [177].



**Figure 34** ‘Adult Cric Trainer’ cricothyrotomy model produced by SynDaver [177].

The larynx model (Interventionsfähige Larynxmodell für die Laserchirurgie (IMOLA)), which allows practice microlaryngeal laser surgery in Fig. 35, is a synthetic larynx simulation produced in Germany. Although this model is similar to the larynx model produced in this thesis, it shows differences in the direction of its objectives. IMOLA microlaryngeal laser surgery has been produced to improve the surgical skills and also gives a real human tissue response [178].

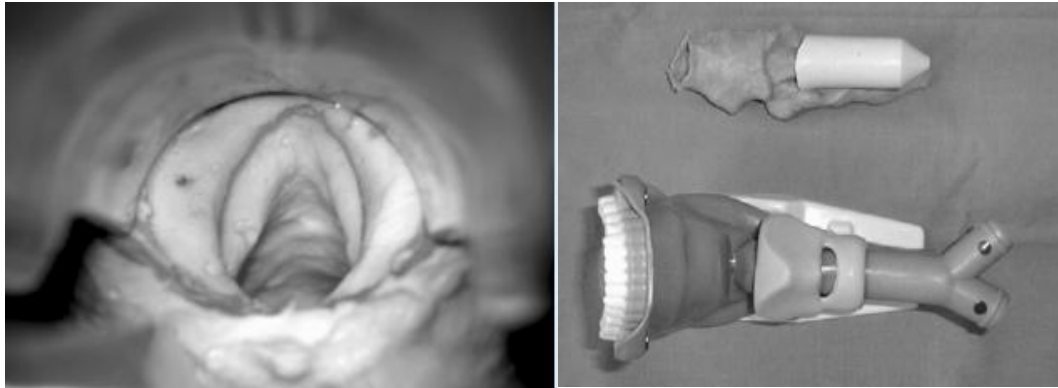


**Figure 35** IMOLA larynx model for laser microsurgery simulation [178].

The number of medical students has increased significantly, and there is substantial concern about the quality of education due to the constraints such as lack of cadaver and/or live or dead animals, the limited resources at the training centers, and the ethics about the on-patient training platforms [179-181]. The continuation of quality education in the world, where economic crises are often experienced, depends only on the low-cost, easy-to-use, and durable educational materials designed and produced in a way that is accessible by many different people or institutions. Medical departments and education and research hospitals can have the highest benefit with such designed synthetic organs as a part of this study. Training through simulation can improve the physical facilities of medical schools and hence provide a standardized education platform to these institutions [182, 183].

#### 4.1.2 Assessment of the Medical Applications and Determination of Organs to Fabricate

Tracheostomy is the surgical opening of a hole leading to the pneumatic tube. During the procedure, the patient is laid down on the back and the thyroid and cricoid cartilages are palpated. Then, a transverse incision is made about 0.5 cm below the cricoid cartilage, corresponding to the thyroid isthmus, and deepens to the platysma. When staying on the median line, the muscles can be separated easily. Infrahyoid (strap muscles) retracted from both sides to reach thyroid isthmus. The thyroid isthmus is removed from the surgical site by changing its position up or down. If the thyroid is thick enough not to allow this movement, thyroid suture is done so that thyroid isthmus is clamped on both sides and then cut off. Tracheal rings are counted and the second and third tracheal rings are opened. After the intercartilaginous membrane between the tracheal rings is incised transversally and enlarged to the extent that the cannula can pass through, the secretion in the trachea is aspirated and the tracheostomy cannulated (Fig. 36) [184-186].

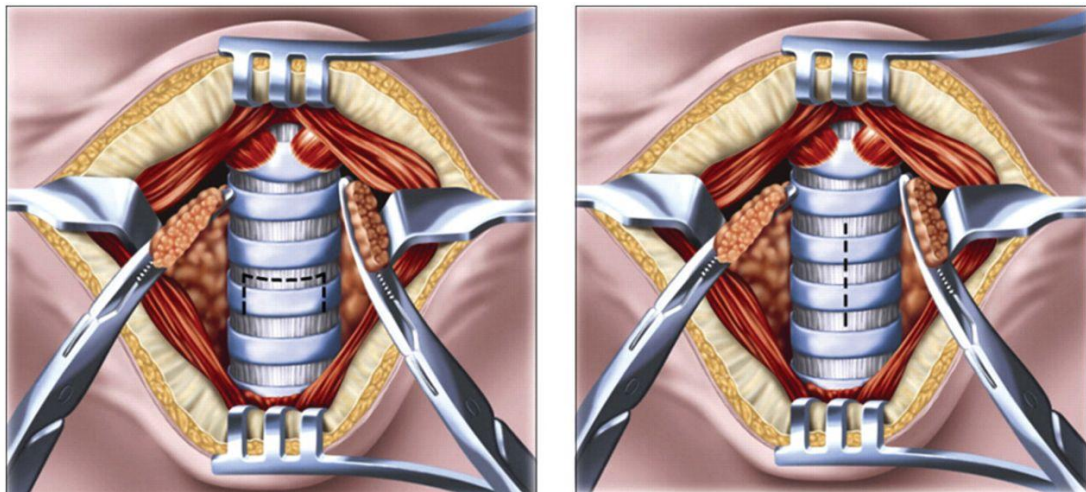


**Figure 36** A transverse and vertical incision of trachea for the tracheostomy application [184].

Endotracheal intubation is the process of placing a tube into the trachea through the mouth or nose, with the aim of securing the respiratory tract or controlling the respiration with the aid of a laryngoscope or special apparatus [187]. During the procedure, upon a slight flexion to the neck and an extension to the head of the patient, the flattening of the mouth-pharynx-larynx line is achieved. In the case of oral intubation, the laryngoscope is placed on the right side of the mouth between the teeth. The laryngoscope is placed between the root of the tongue and the epiglottis (valleculae) and is lifted up to the palate (up and forward) and pressed against the tongue to move the epiglottis to open the trachea. The intubation tube is placed right into the glottis and is pushed through the chordae vocalis to the trachea. In the case of nasal entubia, the tube is inserted into the nose perpendicularly [188]. The tube is advanced until it is seen in the oropharynx to concha attentively, and through the use of a laryngoscope, the movement of the tube near the chordae vocalis is achieved and the procedure can be seen in Fig. 37 [189].

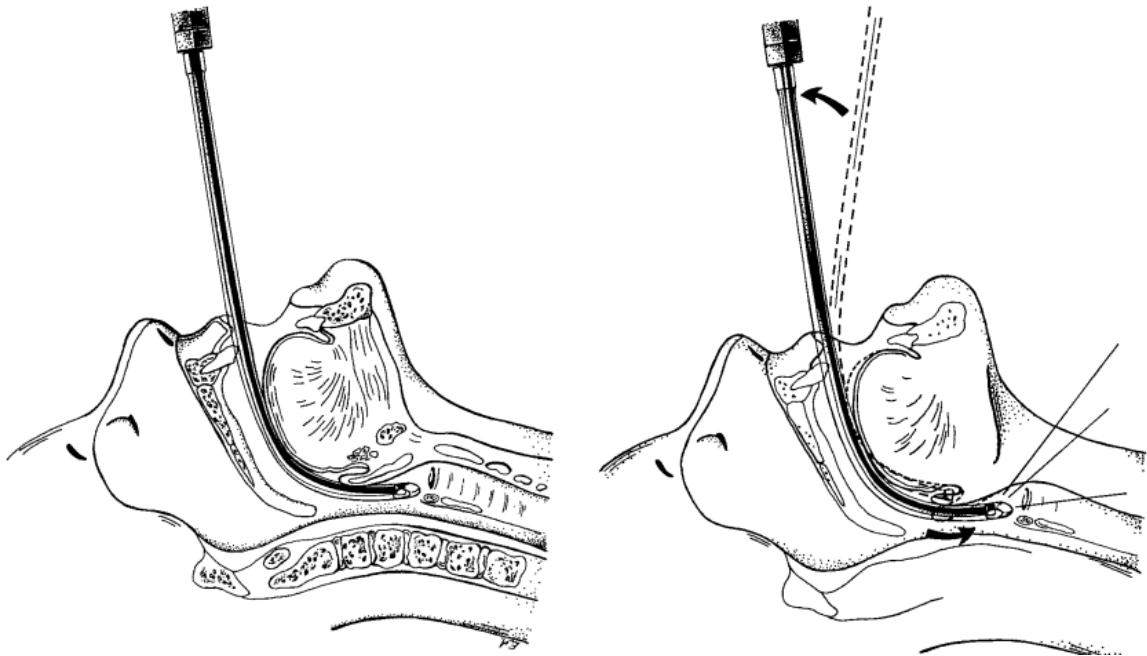


**Figure 37** Oral tracheal intubation with the aid of laryngoscope [189].

Bronchoscopy is a type of endoscopy that is used to examine the respiratory tract and lungs from the laryngeal region and to perform a number of procedures and interventions for diagnosis and treatment. During bronchoscopy, oxygen is given to the patient through the mouth. Bronchoscopy is performed when the patient is lying on the back or in a sitting position, and the bronchoscope is inserted into the trachea or to the bronchus from the mouth or the nose of the patient. In fiber optic bronchoscopes, the part that enters the bronchial tree is more incised. Through the use of this device, the bronchial tree is monitored. If the dense phlegm is overgrown in the bronchus, this phlegm obstructs the lungs from breathing and causes a pulmonary exacerbation. In order to cure this condition, bronchoscopy is performed to clear the phlegm and to aspirate these secretions that are obstructing airways [190, 191].

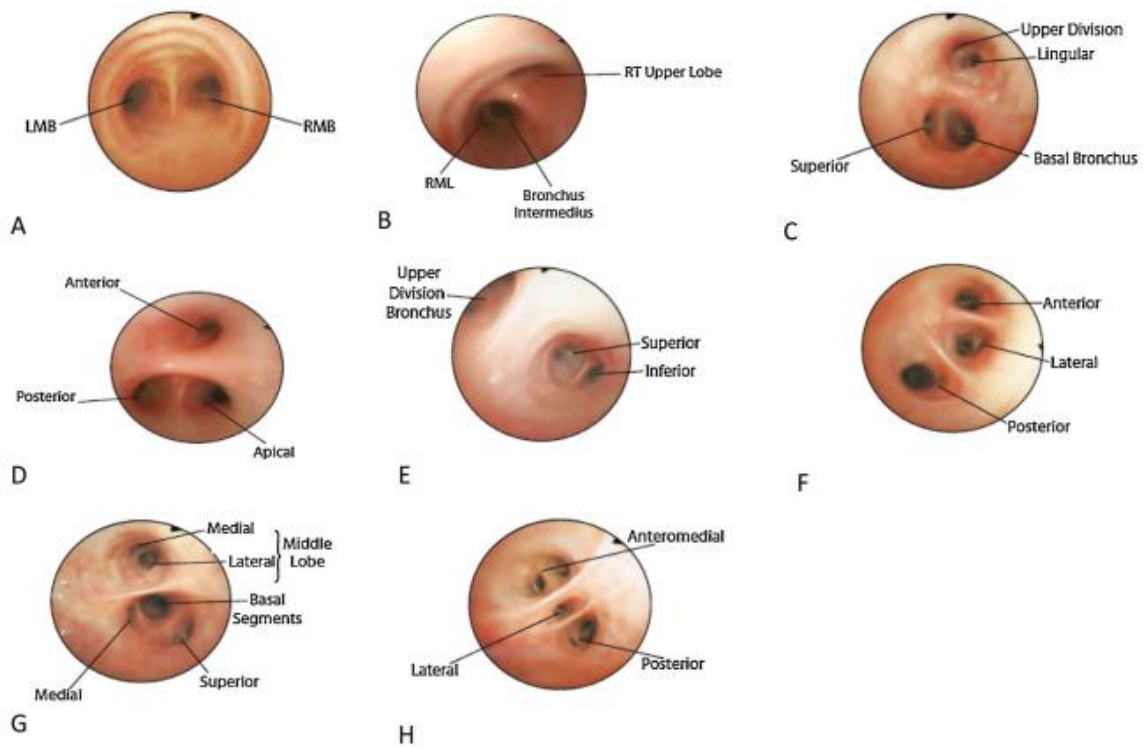


**Figure 38** The views of bronchi during bronchoscopy. a) left and right main bronchus, b) branches of right main bronchus, c) left main bronchus, d) right upper lobe, e) left upper lobe, f) right basal segments, g) right middle lobe, h) left basal segments [190].

## **4.2 Materials and Methods**

### **4.2.1 Design of the Skin Model**

Two-component silicone elastomers both liquid silicone elastomer (LSR) and room temperature vulcanizing (RTV) types were utilized in the design of the skin phantom. Silicone elastomers were combined with different additives to achieve hardness and elasticity properties of different parts of the skin. Silicone oil (50 wt %) was used as an additive in the second layer, and a textile layer was placed in between these two layers to mimic epidermis and subcutaneous fat below the epidermis. The hardness of cured silicones can be changed between 4-50 Shore hardness with these additives within the mixture. As a further contribution, skin color in the skin layer, yellow in the fat layer and red silicone paints in the muscle layer was used to obtain cosmetic properties. Unlike in microsurgery model, that contains a subcutaneous fat layer with small portions of silicone cured in a single clay mold, this suture model is a rectangular shape (20x10 cm) with a smooth texture on both sides.

### **4.2.2 Axilla and Axillary Lymph Nodes**

The model produced within the scope of the project consists of two regions, breast and the axilla. The connection between the breast tissue and the axilla was demonstrated with the addition of axillary nodes. These regions consist of skin, fat, muscle layers and lymph glands. RTV and LSR two-component silicone elastomers, woven fiber and silicone oil additive were used in the production of these tissues. In the experiments, the mold was created through the use of a medical mannequin. The arm connection was achieved with the replication of this anatomy by clay molding. Furthermore, the cast of this clay mold was produced to be used in the production of breast and axilla that was cured in the oven for 2 h, at 110 °C.

### **4.2.3 Fabrication of the Vascular Model**

Vessels were obtained by curing RTV silicone elastomer without additive around 3D-printed PLA bars with diameters of 5 and 7 mm. The bars coated with silicone by dipping method were kept in the oven for 15 minutes at 110 °C. Afterwards; the vessels were peeled from the surface of the bar in one piece and inserted into the designed system. The production of the aneurism models was achieved by the assembly of the cured silicone formulations onto the several wires that were curved with angles ranging between 40–60° with different diameters. A particular system has been developed in order to provide the blood flow. In the system, artificial blood was pulled from the reservoir by using the water pump. The blood passing through the pump was separated into four paths by a pneumatic multiplexer. This separated blood was pumped into veins that were mounted in a separate vessel with different depths and diameters. The blood passing through these vessels was reduced to a single line again with the multiplexer and returned to the chamber.

### **4.2.4 Material Selection and Design of Tracheostomy and Bronchoscopy Model**

These models were fabricated with RTV silicone elastomer without the additives, supported with fibers in order to achieve the highest similarity to thyroid and cricoid cartilages. Epiglottis and arytenoid cartilage were also produced by utilizing RTV silicone 1: 1 without additives and fibers. Moreover, the epithelial tissue that necessitates silicone oil-added RTV elastomer provided the elastic resemblance to the human tissues. The section to be cut during the tracheostomy procedure was reinforced with 10 wt % woven fiber to allow the suture. The cartilage rings were also fabricated with pristine silicone formulations since the cuts and sutures for the tracheostomy necessitate the elasticity. LSR elastomer was used to mimic the flexible tissue that covers the cartilage. LSR was preferred due to its similar elastic properties to the real tissues, in comparison to the same formulation that contains RTV silicone and the same amount of silicone oil additive. The bronchus and bronchiole were produced from the LSR elastomer with the same motive as the continuation of the ligament covering the trachea. In the preparation of inferior thyroid venules that were feeding the thyroid gland, RTV elastomer was used with the formulation of the vascular model.

## 4.3 Results and Discussions

### 4.3.1 Surgical Skin Model

2 layers skin model was developed and a muscle layer was added to the model, hence different surgical procedures could be applied on these layers. These skin, fat, and muscle layers were designed with adjusted hardness, thickness, and elasticity separately. The thickness of the skin in the human body varies according to its region. For instance, the skin of the dorsal part is about 4 mm thick, whereas the skin of the skull is about 1.5 mm thick. In the same way, the thickness of fat and muscle tissues varies due to their locations in the body [192, 193]. Based on the feedback from the consulting surgeons, the layer thicknesses of the skin model were determined to be 2 mm for the skin layer, 5 mm for the fat layer, and 3 mm for the muscle layer. These 3 layers of the designed skin model can be seen in Fig. 39. The textile between the skin and the fat layers can be observed below the epidermis part.

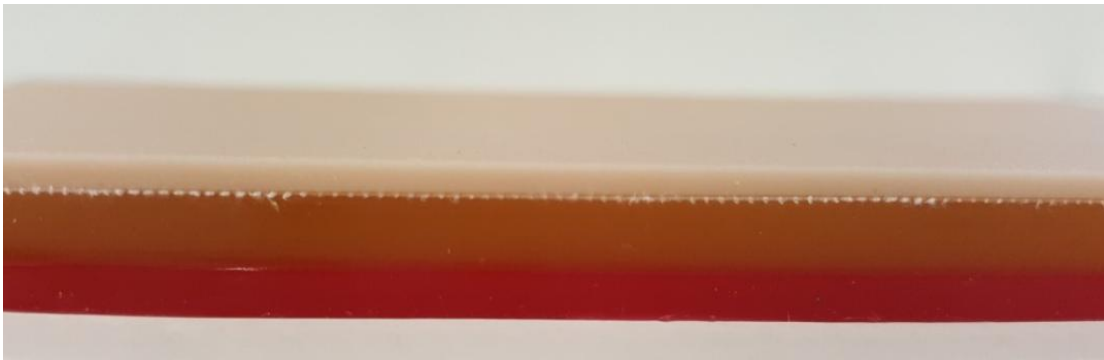


**Figure 39** The skin model with different layers: Skin, subcutaneous fat and the muscle layers from top to bottom.

The silicone oil has been added to the system at different ratios to increase the elasticity of the tissues. Among the viscosity values of the silicone oil between 0.1–100 cSt, the higher viscosity silicone oils were preferred. When the viscosity is low, a problem of silicone oil diffusion at the surface of the model has occurred. This adverse situation affected the ease of use and the durability of the model inconveniently. For this reason, the silicone formulation of the model was optimized by using silicone oils with high viscosity value. Hence, the silicone oil was only employed in the subcutaneous fat layer (between the skin and the muscle layers). However, considering the silicone oil diffusion to the outside of the model, LSR silicone elastomers with lower viscosity has been utilized. Therefore, the elimination of the silicone oil has been achieved since the cured LSR silicone resulted in the significantly higher mimicking of the skin with high elasticity (Fig. 40).



**Figure 40** Different suture techniques were applied on the designed skin model with subcutaneous fat layer and the textile in between those two layers.

Human skin can hold sutures due to its fibered structure. In order to incorporate this feature to the model, woven and nonwoven fibers were added to the silicone formulations during the fabrication of the skin layer. Unwoven fiber addition resulted in agglomerates that disrupted the homogeneous appearance and mechanical properties of the skin surface. For this reason, woven fiber has been preferred in the production process. To prevent the changes in the elasticity of the cured silicone formulation, the woven fiber that can flex in two directions was chosen. Moreover, soft-structured fibers have been used to ensure that the scalpel was not exposed to great resistance when the cut was applied to the skin.

#### **4.3.2 Axilla and Axillary Lymph Nodes**

Breast cancer is most commonly spread through the lymph nodes [194]. The lymphoid glands are in the form of beans ranging from 0.5 to 2 cm in length and are very rigid once they contain malignant tumors. The condition of the axillary lymph nodes is inspected during physical examination and then assessed by the ultrasonography. However, for the certain diagnosis, a sample from the lymph nodes should be collected and a pathology report can conclude the decision [195].



**Figure 41** The cast and clay molds prepared for the axilla model.

A fat layer was formed by pouring a mixture of polymeric expancel microspheres, RTV elastomers and silicone oil to form a porous structure inside the cast mold (Fig, 41). Particles mimicking the cancerous lymph gland that were prepared from RTV elastomer, 0.5–2 cm in size, were embedded into the fat layer. A 1 cm deep LSR elastomer was poured over the cured fat layer to fabricate the muscle layer. The resulting structure was removed from the cast and covered with woven fiber. In order to form the skin layer, the RTV elastomer with 50 wt % silicone oil additives was cured by pouring onto a pre-cured fat and muscle layers.

When the model was first prepared, it was observed that an impairment of the skin layer has developed over time. It has been determined that expancel provided the shape of the fat layer by the enhancement of volume upon heating, and the loss of function at low temperatures caused the resultant structure to shrink (Fig. 42). Since the skin layer was cured onto the fat layer and retained its initial volume after the curing process, it was shown that the skin layer has lost its stretched shape abundantly by the shrinkage the fat layer which is beneath this layer.



**Figure 42** Axilla model that consists of the breast and arm pit.

In the second design, the order of the process was changed and the production of skin and muscle layer was accomplished before the fat layer. The muscle layer was cast through the use of pristine RTV elastomer. The skin layer was prepared by the addition of 50 wt % silicone oil in order to increase the elasticity of the skin to respond the swelling fat layer

underneath. The formulation of the fat layer was prepared with the same composition and poured through the opening between the muscle and the skin and embedded in pieces made of the pristine RTV elastomer in the size of 0.5–2 cm. The obtained model was suitable for palpation of the lymph nodes and the suturing of the removed tissue that was damaged (Fig. 43).



**Figure 43** The second design of axilla model with the stretched skin layer.

### **4.3.3 Vascular Model with Blood Flow Mechanism**

The blood vessels in the human body (from the aorta to fine capillary vessels) vary in diameter and hardness due to their location in the body [193]. The veins designed in this thesis were of two different diameters and their elasticity was adjusted upon the feedbacks received from the consultant surgeons. In addition to the straight shaped and single-diameter vessels, a vein network that consists of multiple connection points and aneurism which is an abnormal balloon on the wall of an artery was simulated (Fig. 44).

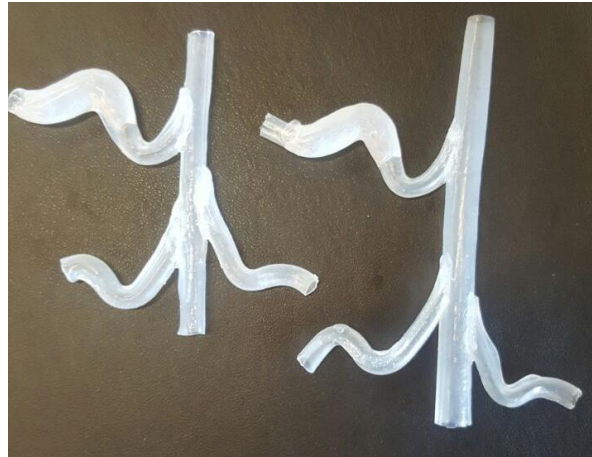


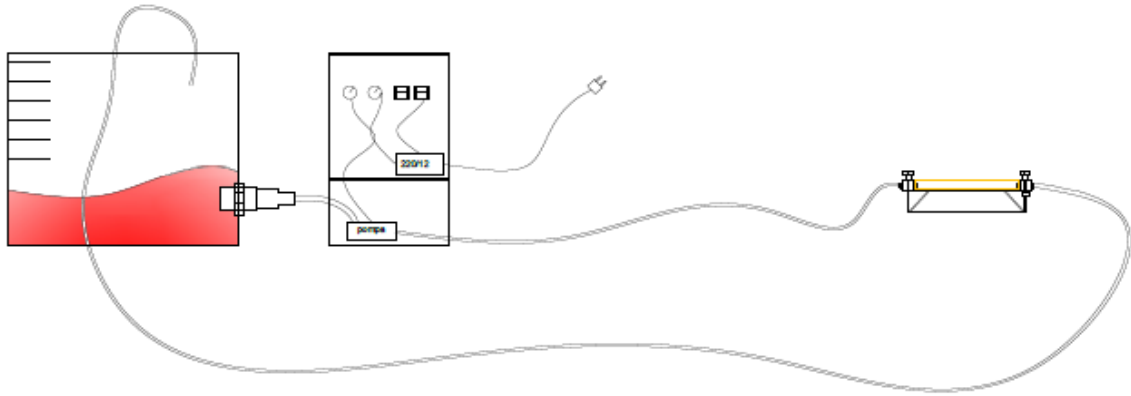
**Figure 44** Different size and diameter branched vessels for the aneurism simulation model.

One way of treating these unclog vascular sites are endovascular intervention. In this method, a long and thin plastic tube called a catheter is introduced into the problematic segment of the vein guided by an imaging camera [196]. The model was produced in such curved and branched way that the catheter can pass through these branches and be inserted into the veins once reached to the troubled region. This model provided a training platform where trainees can develop their skill-sets. The extent of the vascular passages and the angle of the junctions were tested with endovascular imaging of vessels and revised with the feedback of doctors (Fig. 45).



**Figure 45** Endovascular imaging of the aneurism model.

In the treatment of vascular injuries, the control of bleeding is significantly vital as well as preventing the clog in the veins. Therefore, the vessels with the blood flow that allows the practice of suturing techniques were also included in the vascular model (Scheme 4).



**Scheme 4** Schematic of the vascular model with blood flow mechanism.

In this system, suturing the damaged veins was simulated. The vein to be operated was blocked by the attachment of an apical clamp in order to eliminate the blood flow. The pumped blood continued to pass with a higher pressure than the other vessels. The damaged vein was sutured and the clamp was removed. The adequacy of the sutures was tested by providing the blood flow through the veins. The bypass technique can also be practiced in this model. Bridging can be achieved by suturing an external vein between the two veins where the blood flow remained. Clogged veins were cut off, and the blood flow continued through the repaired vein. Fig. 46 indicates the vascular system and the designed veins whilst the blood was passing through the veins.

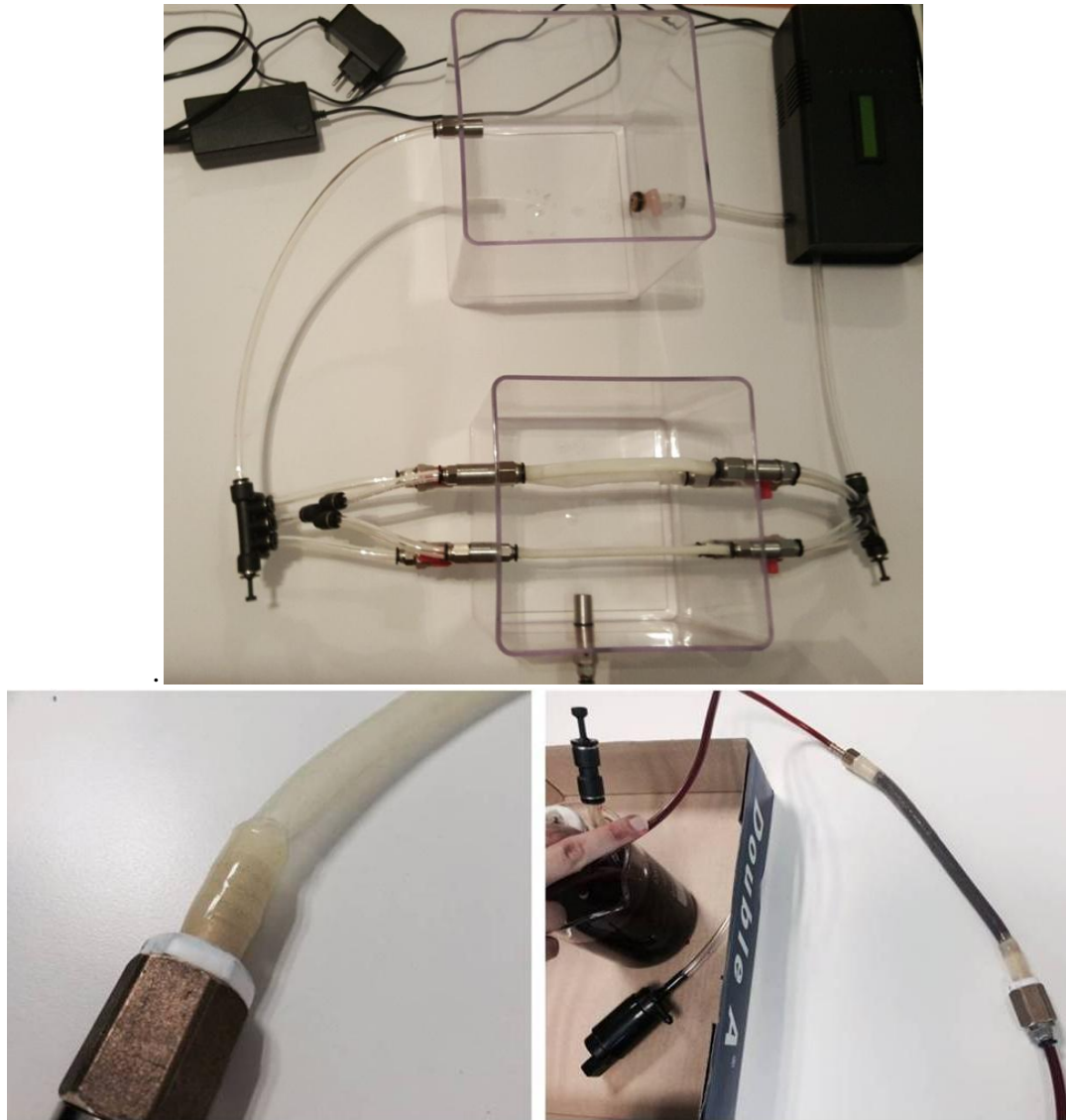


**Figure 46** The mechanism that contains fabricated veins with different diameters and a blood flow system through a water pump.

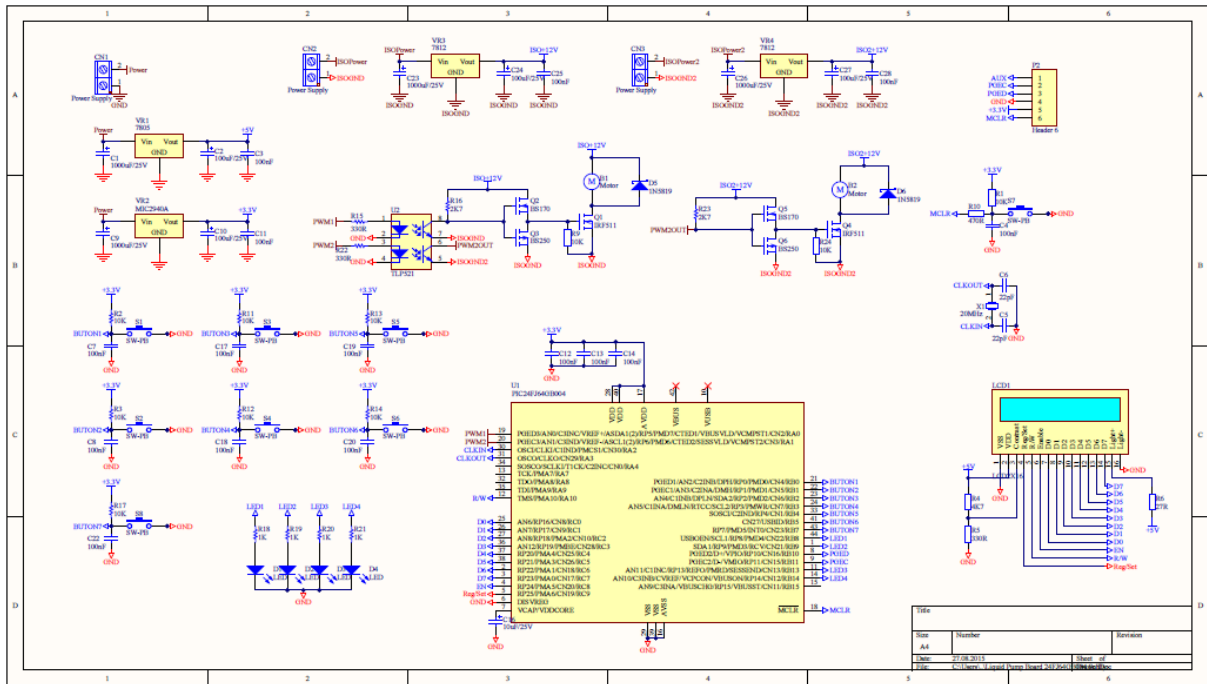
The design of the electrical circuit that allowed blood flow was achieved with a 12 V water pump to ensure the circulation of blood in the model. The flasher, used in the signal lamps, was connected to a water pump to mimic the pumping of blood from the heart at certain intervals. Furthermore, the dimmer circuit element, which adjusts the voltage of the pump, has been added to the circuit so that the blood pump rhythm and the flow of the blood can be adjusted. 220/12 V and 250 watt transformer were used as power source. Since the dimmer reduced the power of the water motor and the frequency of the flashlight at the same time, a circuit has been designed in which the dimmer and flasher can be adjusted

separately in the subsequent prototype. In this system, the engine power can be adjusted in 10 % increments. Thus, the system can change the blood pressure in the veins and obtain different blood pressure values. The engine can be adjusted separately in the on and off states which allowed to imitate the health conditions of people with different ages and medical states. The heart pumps 60–100 times per minute in adults, 100–120 times in children, and 100–140 times in babies [197]. The designed system was adjustable between 20–200 heart pulses and the time elapsed between engine run times was calculated and given in Table 2.

**Table 2** The heart pulses and the time elapsed between the two pulses is given in the table.

Heart Pulse	Time elapsed between two pulses (sec.)
20	3
40	1,5
60	1
80	0,75
100	0,6
120	0,5
140	0,428
160	0,375
180	0,333
200	0,3

With the LCD display connected to the generated circuit, the motor power and the time elapsed between two pulses (blood pumped from the motor) can be read. The schematic of the electrical circuit of the prototype is given in Scheme 5.



**Scheme 5** The schematic of the electrical circuit of the vascular mode

### 4.3.4 Tracheostomy and Bronchoscopy Model

In order to be able to comply with the tracheostomy procedure, the following structures should be included in the design of the model (Fig. 47);

- i) Thyroid and cricoid cartilages, which could be recognized from above the skin through palpation,
- ii) The thyroid gland, which can be cut and sutured from the isthmus,
- iii) Movable infrahyoids (strap muscles), which can be separated into two sides,
- iv) At least 3 tracheal cartilage rings in the continuation of the cricoid cartilage,

v) Intercartilaginous membrane between the tracheal rings that is suitable to be cut and sutured,

vi) Cutaneous and subcutaneous fat tissue that can be cut and sutured.

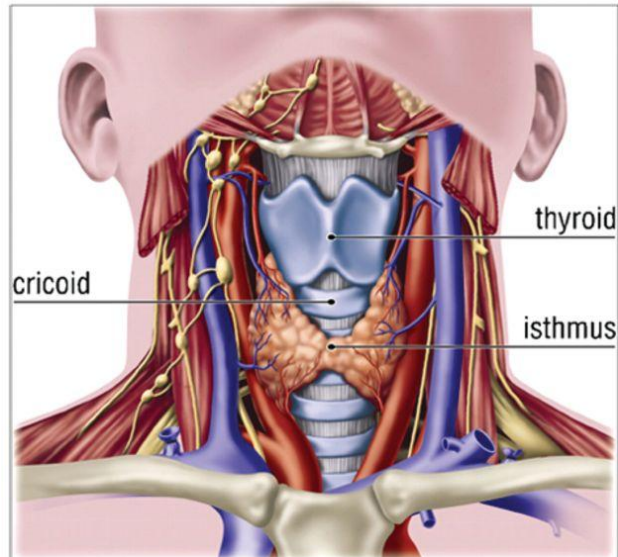


**Figure 47** The anatomy of the neck indicating the structures to be mimicked for the model [184].

In addition, the following structures have been added to the model to prepare the ground for the most common complications arising from errors during the procedure;

i) Inferior thyroid vein, which is the greatest risk of hemorrhage when the trachea is dissected from the midline,

ii) An esophagus that can be cut and sutured for the complications of tracheoesophageal fistula (a hole between the tracheal tube and the esophagus generated during the tracheal passage in the procedure).

Although surgeons generally prefer to intervene between the 2<sup>nd</sup> and 3<sup>rd</sup> tracheal cartilage rings, the applications involving the lower trachea is also possible. Hence, the model was designed to have 5 cartilage rings. Moreover, these structures in the model were also compatible with transtracheal needle ventilation (a no. 16 or thicker cannula with plastic trocar inserted through cricothyroid membrane or most palpable and nearest side of the skin

of trachea, and upon the removal of the needle, the respiration of the patient through this thick plastic trocar is achieved) and cricothyroidotomy (incision of the skin, subcutaneous and membrane which is followed by insertion of an endotracheal tube or cannula into this cricothyroid membrane, that is just above the cricothyroid cartilage and below the lower edge of the thyroid cartilage).

In order to make the model suitable for tracheal intubation within the anatomical information, it is necessary to additionally include the following:

- i) The head, which holds the oral and nasal cavities and a moving jaw,
- ii) A flexible neck,
- iii) The tongue that can stretch when pressed,
- iv) Epiglottis cartilage, which is tied to the tongue and moves when the tongue is pressed,
- v) Chordae vocalis,
- vi) Trachea.

Apart from these models, different types of structures have been added to the model in order to mimic the complications during the processes; Unilateral intubation; the excess amount of movement of the intubation tube in the main bronchus. In such a case, one lung is ventilated. To observe this condition, bronchial system and air-swellable lungs were added to the system. Another complication is the unrecognized esophageal intubation that is the most serious complication of tracheal intubation attempt. In this case, the air goes to the stomach instead of the lungs. To observe this situation, the stomach as a continuation of the esophagus was added to the model that can be inflated with air. With this motive, in order to be compatible with the bronchoscopy procedure, the model was designed with a removable bronchial tree that allowed the simulation of the adverse health conditions such as lung dysfunction and the obstruction of foreign materials.

All of the organs and tissues fabricated in the model are listed below;

- i) Cartilage derived structures; thyroid, cricoid and arytenoid cartilages, epiglottis, first 5 tracheal rings (hyaline cartilages),
- ii) Tubular organs; trachea, esophagus, bronchial tree,
- iii) Hollow structures; larynx wall, pharynx wall, lung, stomach,
- iv) Structures in the mouth; tongue and valleculae, soft and hard palate,
- v) Strap (infrahyoid) muscles,
- vi) Chordae vocalis,
- vii) Thyroid gland,
- viii) Inferior thyroid vein,
- ix) The head with mouth, and nasal cavity, and a moving neck,
- x) Skin and fat layers for the head and neck region.

The trachea is an elastic tubular organ with an average length of 11 cm and a width of 2 cm. In this model, cartilage structures of the thyroid and cricoid cartilage were prepared rigid and can be sensed with palpation from the frontal surface of the neck. Epiglottis has a flexible anatomy with respect to the cricoid cartilage. The inner surface of the trachea is covered with epithelium. There are 16–20 "C" shaped hyaline cartilages that are wrapped from the front and side. The top of the cartilage is covered with elastic tissue. The trachea is composed of ciliated epithelium, epithelial cells, muscle tissue, cartilaginous tissue, and elastic connective tissue from the inside to outside, respectively (Fig. 48) [6].

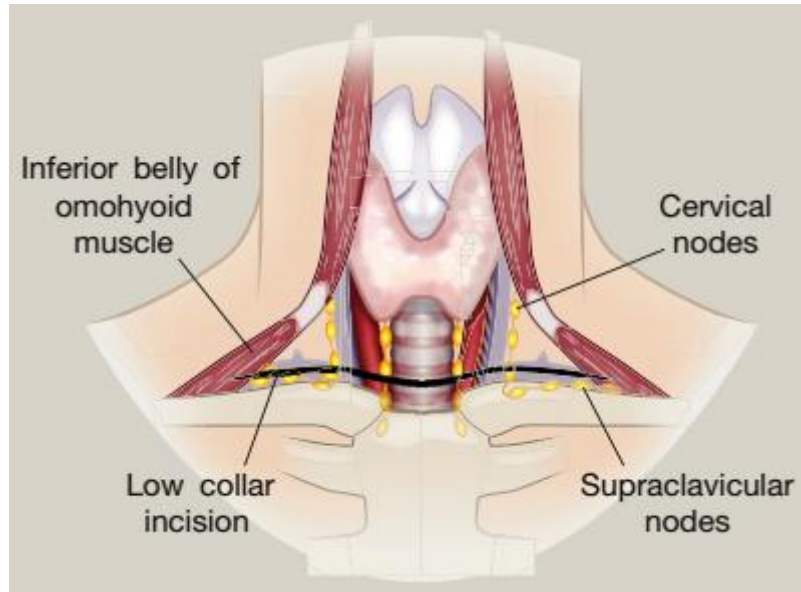


**Figure 48** The anatomy of the trachea and surrounding structures [198].

The esophagus is covered with (from inner to outer), epithelium, smooth muscle and connective tissue. The length is about 25 cm and the diameter is 2 cm (Fig. 49) [190, 193]. Silicone oil-added RTV elastomer was used in the fabrication of the model and reinforced with the woven fibers to allow re-suture in the case of tracheoesophageal fistula complication. In the nasal cavity and pharyngeal wall construction, although produced as a thin membrane, in order to preserve the shape, a high viscosity RTV elastomer was utilized.

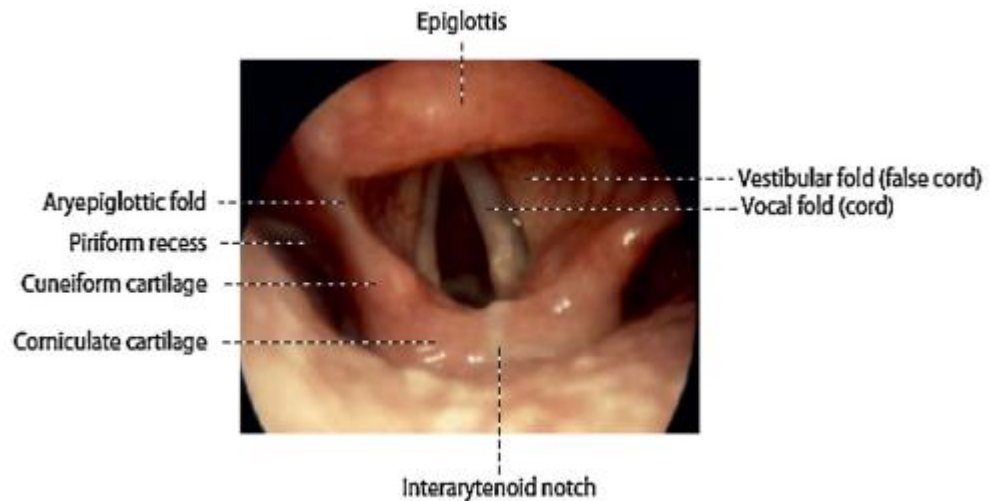


**Figure 49** The anatomy of esophagus monitored including epiglottis and cartilages that were designed within the model [190].

Although tongue has a muscular structure, it should have the elasticity to open the epiglottis flap when pressed. For this reason, RTV elastomer with 83.3 wt % silicone oil additive has been used in the fabrication. The vallecula was manufactured as a sheath that was passed on to the tongue and attached to the epiglottis to provide mechanical communication between the replaceable portion of the model and the permanent portions. It has been fabricated with pristine RTV elastomer formulation with low elasticity to effectively transmit the force applied to the tongue and the epiglottis.

Since the skull was not used in the model, hard palate is the only structure that separates the nasal cavity and the oral cavity, and it is important to preserve its shape extensively. For this reason, it was produced from pristine RTV elastomer as well. The soft palate has the higher elasticity that can be moved easily. This structure was provided by using 50 wt % silicone oil additive and RTV elastomer.

Infrahyoid (Strap) muscles are pulled on both sides during the procedure; hence their design must ensure the movement (Fig. 50) [199]. However, in some applications, doctors prefer to cut these muscles instead of moving from side to side, therefore, the model was designed with a formulation that holds the suture. The fabrication of these properties was achieved with 50 wt % silicone oil-added RTV elastomer reinforced with woven fiber.

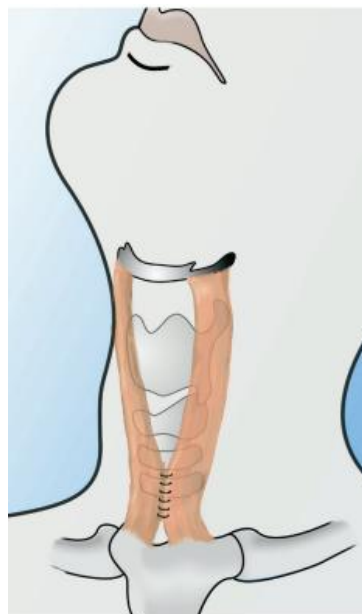


**Figure 50** The anatomy of the strap muscles [199].

The models were manufactured by using plastic anatomic models, display case manners, clay and aluminum bars in order to avoid expensive metal molds, and for the ease of access. In the production of the bronchial tree, thyroid cartilage, esophagus, and tongue anatomical models were used. The images of the anatomical can be seen in Fig. 51.



**Figure 51** The anatomical models that were utilized as a mold in the fabrication of the tracheostomy and the bronchoscopy models.

The clay molds were used for the fabrication of cricoid and arytenoid cartilage, tracheal rings, epiglottis, trachea and larynx, and thyroid gland. The pictures of the clay molds with given shapes can be seen in Fig. 53.



**Figure 52** Clay molds that were used in the production of the model.

A thyroid gland is composed of two lobes with the isthmus between them, and the structure is sensitive to the applied pressure. The thyroid gland must be moved up or down during the tracheostomy procedure, and 83.3 wt % silicone oil was used to make the model highly elastic that will allow the movement of the structure. In some cases, the thyroid gland is discontinued from isthmus, and in order to cut and suture, the structure was reinforced with 5 wt % non-woven fiber. Chordae vocalis should be flexible not to interfere with the passage of the intubation tube. For this reason, 20 wt % silicone oil-added RTV elastomer was used. The fat and skin layers of the head and neck regions were produced on the basis of the breast models with LSR elastomer, RTV elastomer and 50 wt % silicone oil. The thyroid gland was obtained by pouring RTV silicone elastomers onto the previously spread non-woven fiber to the corresponding clay mold. Consequently, a thin layer of RTV silicone elastomer was applied to imitate the membrane structure. Production of inferior thyroid veins was performed by using aluminum bars of different diameters (3–5 mm), as in the vascular model. Silicone mixtures which were applied in the liquid form around the bars were cured and then removed from the bars. Aluminum bars with small diameters were immersed in the veins formed inside the thick bars and covered with silicone and cured. Once the thin bars were removed, a number of branched veins were fabricated (Fig. 53).

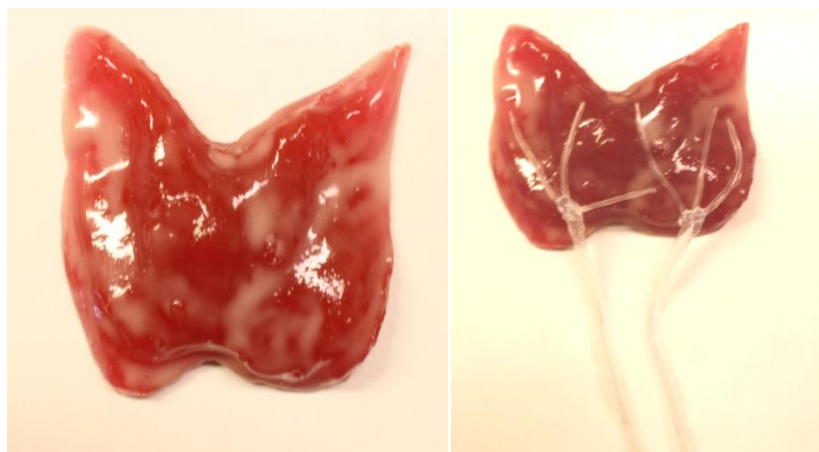


**Figure 53** Thyroid gland with inferior veins.

The anatomical pattern of the esophagus was coated with woven fiber, immersed in a silicone formulation, cured and then scraped off. The bronchial tree was constructed by immersing the anatomical model in a two-component silicone elastomer formulation and cured in the oven for 1 h at 110° (Fig. 54).

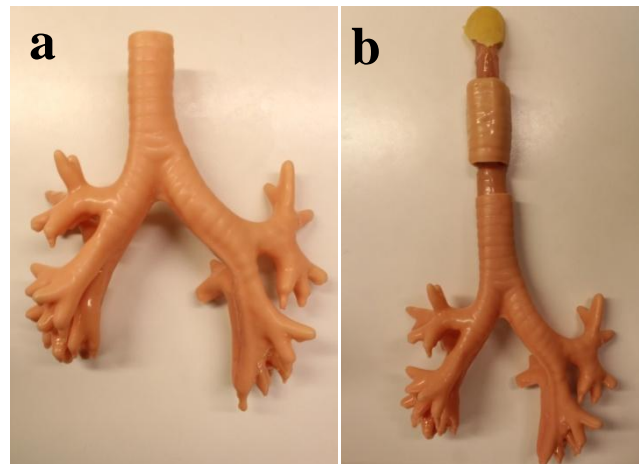


**Figure 54** a) Bronchial tree, and b) The trachea with bronchial tree and the modular parts

For the construction of the tongue, the anatomical model was coated with pristine silicone formulations. The silicone was removed after curing and used as a mold. This pristine silicone obtained in the form of a membrane was employed as a mold and a 66.6 wt % silicone oil-added RTV elastomer formulation was poured into this mold. After curing, the stiff mold was removed from the inside, and elastic tongue pattern was obtained (Fig. 55).

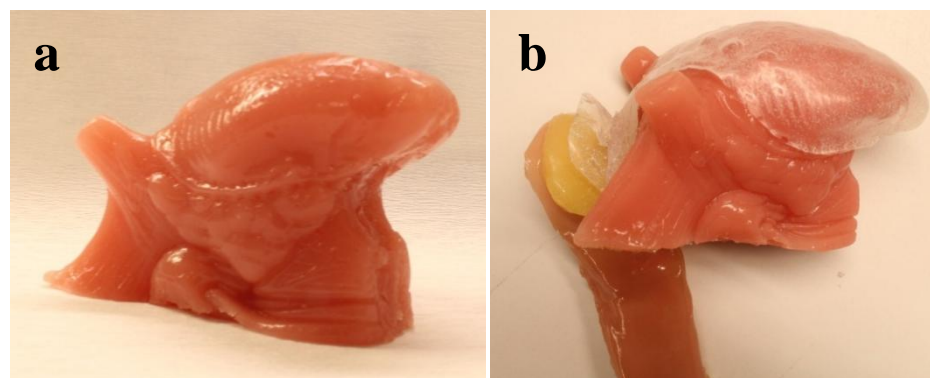


**Figure 55** a) Tongue, b) Tongue with the sheath that contains vallecula fold that allows the epiglottis movement

The cricoid and arytenoid cartilage, tracheal rings, trachea, and larynx were obtained by coating their individual clay molds with formulations of pristine silicone elastomer and 10 wt % non-woven fibers. Once cured in the oven, tracheal rings were removed from the mold and cut in a "C" shaped structure at a thickness of 4 mm. Epiglottis was formed by covering the upper front surface of the same mold with silicone in the triangular shape. The larynx and the trachea were obtained by coating the woven fiber around the clay mold and immersing it in a liquid silicone formulation and cured in the oven.

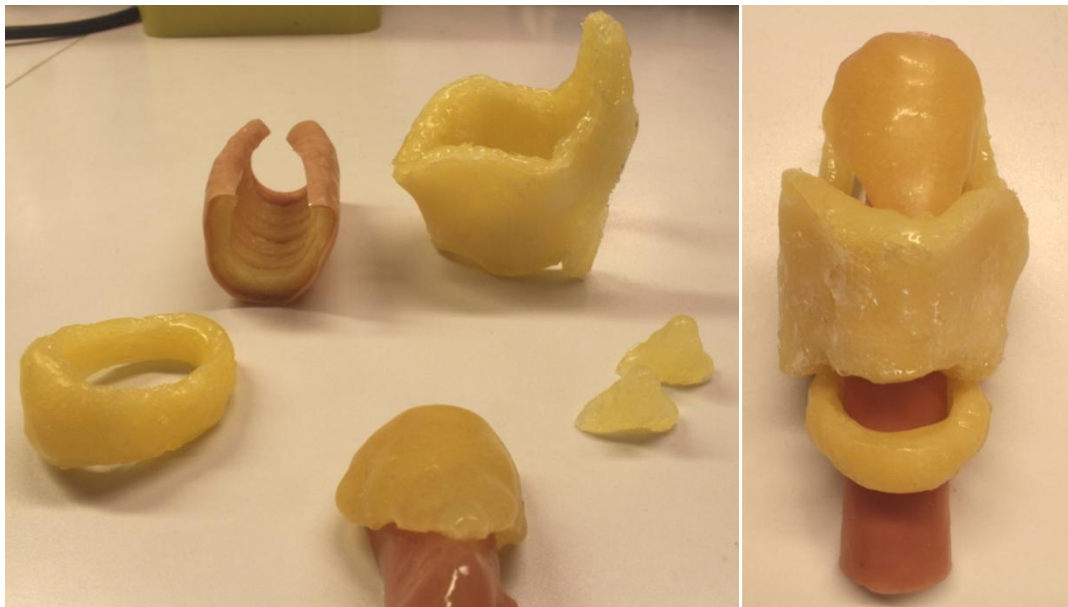


**Figure 56** Modular parts of the thyroid cartilage, cricoid cartilage, arytenoid cartilage, and tracheal rings, and their assembled image.

#### 4.4 Conclusion

Surgeons-in-training require a substantial amount of practice in order to improve their surgical skill sets and together with simulation-based training systems, the trainees learn at their own pace and experience various medical scenarios rather than incidents where the urgent response to the patients is required. Hence, there is a need for such a reliable platform to diffuse simulation-based trainings to medical curricula. In this part of the thesis, the design and fabrication of realistic, sustainable, easy-to-produce, and cost-effective synthetic tissue and organ models which enable the tactile simulations in surgical skills

laboratories was revealed. Being inspired from the anatomy of the tissues that were mimicked, and by utilizing two-component silicone elastomer formulations with silicone oil and textiles; multi-layered skin, axilla, axillary lymph nodes, vascular model with a blood flow setup, tracheostomy, and bronchoscopy models that contain the tongue, epiglottis, thyroid gland with inferior veins, tracheal rings, bronchial tree, and cricoids cartilage were fabricated. The motive for designing these structures was providing a reliable, cost-effective, and accessible surgical education platform to surgeons-in-training.

# Chapter 5

## Conclusion and Future Aspects

Formulations of two-component silicone elastomers were utilized for mimicking various human tissue and organs. The use of silicone oil and vinyl-terminated PDMS additives allowed the successful resemblance of the acoustical, mammography, surgical, and microsurgical properties. These tissue-mimicking phantoms were designed and fabricated with the motivation of providing medical training platforms to the surgeons and radiologists-in-training. In chapter two, fabricated breast models to be used in different applications were revealed in detail. An accomplishment in the design of these phantoms necessitates an extensive understanding of the anatomy of tissue and organs to be mimicked. The breast models are composed of skin, subcutaneous fat, muscle, and rib bones as well as malign tumors. The sample that contains 75 wt % thinning agent exhibited the highest similarity to acoustical properties of human breast, while the utilization of alumina to the silicone formulation simulated malign masses effectively in the ultrasonography and the mammography phantoms. The designed surgical models offer a cost-effective, easy-to-handle, and sustainable alternatives to human tissues. In addition to the allowance of the biopsy needle entry and exit, the breast models with different size and shape tumors provide a self-examination model for public education.

In chapter three, the fabrication of the peripheral nerve simulation models were discussed. The reconstructive surgery was altered with the aid of the technological advances in microsurgery. Modern microsurgical techniques endeavor to augment the preoperative planning of the intervention to the injured peripheral nerves, which in turn result in improved patient outcomes. Microsurgical skills are an essential requirement for the successful use of these techniques. Therefore, advanced education platform is vital for the training of microsurgeons. The most severe type of these peripheral nerve injuries is the fifth-degree (Seddon's neurotmesis) [138, 139] injuries, where a local response to the rigorous trauma arises. The anatomical structures that peripheral nerves composed of—endoneurium, the fascicles, Schwann cells, axons, and the epineurium are completely ruptured at this level of injury. According to the anatomical part of the nerve that has been injured, a pertinent microsuturing technique shall be achieved. The peripheral nerve simulation models that were fabricated throughout this thesis contain a fascia layer, epineurium, and the fascicles as well as the skin and the muscle layers and produced by utilizing two-component silicone elastomers with silicone oil additive and cotton fibers. In order to simulate the fifth-degree peripheral nerve injury, a cut was applied to the nerves, and these structures were repaired through the alignments of the epineurium and the fascicles by utilizing 10/0 and 8/0 sutures. Precise alignment in fascicular level with the shorter operation, dissection, and anesthetic times are crucial for post-operative functional repair of the nerves [5]. Hence, a cost-effective, easily accessible, and reliable training model was designed for microsurgeons to practice on with significant mechanical and tactile similarity.

Chapter 4 includes the fabrication of various silicone-based human body parts to be used in several medical applications (e.g. bronchoscopy, tracheostomy). Within the scope of this chapter, multi-layered skin, axilla, axillary lymph nodes, a vascular model with a blood flow setup, tracheostomy, and bronchoscopy models that contain the tongue, epiglottis, tracheal rings, thyroid gland with inferior veins, bronchial tree, and cricoids cartilage were fabricated with a tactile resemblance to human tissues. These models can be used as individual parts; yet, our long-term plan is to build a synthetic cadaver that will include these individual parts as a reliable solution to the problems related to fresh cadaver supply. These models can be combined into a traumatic thorax and abdomen models in modular

fashion. The system can allow the replacement of organs and tissues individually once they are damaged. In addition, it may be possible to repair the damaged organs with silicone-based chemicals to some extent. The user-friendly design will be considered at all times and the systems can permit individual and group use. The models will provide a medium to experience a variety of scenarios from relatively simple interventions such as hemothorax and pneumothorax to cardiopulmonary bypass.

Another future prospect is the design of a knee model that includes meniscus and bursa sacs. The knee is one of the most dynamic parts of the human body that resist to repetitive movements. The meniscus cartilages are significant anatomical structures that disperse friction in the knee joint between the tibia and the femur and these cartilages preserve the knee towards the motions, responsible for the delivery of the string load, the absorption of shock and the stabilization of joint. The outer parts of the meniscus are surrounded by blood vessels with red-like color, however, these vessels cannot reach the inner parts, and hence the color of these parts appears to be white. The outer part of the meniscus in red color can heal itself when the structure tears apart. Contrarily, the injuries of the white part require a cut off at the torn parts by the meniscectomy [200].

Additionally, bursa sacs are placed in between the bones and knee tendons that allow the movement of the knee. These sacs are filled with synovial fluid that provides the lubrication of the joint and the knee bones. The knee joint is open to the numerous pain syndromes, one of the most significant ones is bursitis of these bursa sacs [201]. The required intervention for the treatment of the inflammation in bursa sacs (i.e. bursitis) is the removal of the liquid. Hence, such phantom can be designed with self-healing materials that will allow the needle entry without any leakage. The model should also withstand the liquid pressure and expansion. Parameters such as how many times the first volume can expand upon the injection, and how much pressure it can sustain can be assessed. Therefore, again by utilizing two-component silicone elastomers with silicone oil, a knee model can be designed. The prototype of this model can be seen in Fig. 57.

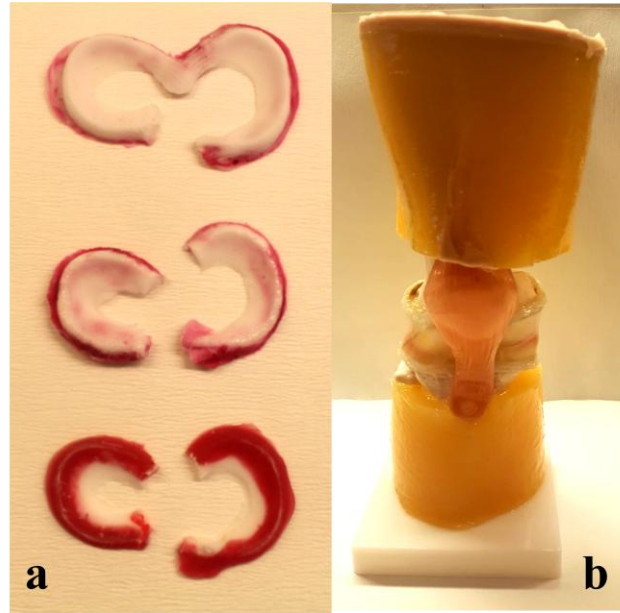


**Figure 57** The prototype of the knee model, a) meniscus structures with different colors representing the accumulation of the blood vessels, b) the knee model with the meniscus cartilages and bursa sacs combined into a single model.

With cost-controlled production and utilizing silicone and additives; it is possible to fabricate cost-effective, thus accessible models, with good quality. Hence, through effective collaboration between medical doctors and engineers, best possible training platforms can be designed for the betterment of the medical education. The participation of doctor in this thesis allows the first-hand design of phantoms with emergency scenarios, testing of these models, and receiving the feedback and input from the end-user before the fabrication of the final models. However, current training materials are live patients, animals (cadavers), virtual reality platforms, or prosthetics. There's a lack of training materials in medical education. Therefore, the designed silicone-based composite phantoms offer a realistic, accessible, reliable, and standardized training environment for radiologists and surgeons-in-training.

## BIBLIOGRAPHY

- [1] K. Zell, J. I. Sperl, M. W. Vogel, R. Niessner, and C. Haisch, "Acoustical properties of selected tissue phantom materials for ultrasound imaging," *Phys Med Biol*, vol. 52, 475-84, 2007.
- [2] M. Piper, A. W. Peled, and H. Sbitany, "Oncoplastic breast surgery: current strategies," *Gland surgery*, vol. 4, 154, 2015.
- [3] N. Bertozzi, M. Pesce, P. Santi, and E. Raposio, "Oncoplastic breast surgery: comprehensive review," *Eur Rev Med Pharmacol Sci*, vol. 21, 2572-2585, 2017.
- [4] D. Moris and M. Kontos, "Oncoplastic surgery: fashion or necessity?," *Am J Surg*, vol. 210, 199, 2015.
- [5] D. E. Kalomiri, P. N. Soucacos, and A. E. Beris, "Nerve grafting in peripheral nerve microsurgery of the upper extremity," *Microsurgery*, vol. 15, 506-511, 1994.
- [6] W. Chan, N. Niranjana, and V. Ramakrishnan, "Structured assessment of microsurgery skills in the clinical setting," *J Plast Reconstr Aesthet Surg*, vol. 63, 1329-34, 2010.
- [7] J. Gilbody, A. W. Prasthofer, K. Ho, and M. L. Costa, "The use and effectiveness of cadaveric workshops in higher surgical training: a systematic review," *Ann R Coll Surg Engl*, vol. 93, 347-352, 2011.
- [8] C. C. Hart and T. Breslin, "Advanced surgical simulation," ed: Google Patents, 2015.
- [9] R. Murniati, Sutisna, E. Wibowo, M. Rokhmat, F. Iskandar, and M. Abdullah, "Natural Rubber Nanocomposite as Human-Tissue-Mimicking Materials for Replacement Cadaver in Medical Surgical Practice," *Procedia Eng*, vol. 170, 101-107, 2017.
- [10] C. DeSantis, J. Ma, L. Bryan, and A. Jemal, "Breast cancer statistics, 2013," *CA Cancer J Clin*, vol. 64, 52-62, 2014.
- [11] J. Ferlay, I. Soerjomataram, R. Dikshit, S. Eser, C. Mathers, M. Rebelo, *et al.*, "Cancer incidence and mortality worldwide: sources, methods and major patterns in GLOBOCAN 2012," *Int J Cancer*, vol. 136, 359-86, 2015.
- [12] C. Bilgin, C. Demir, C. Nagi, and B. Yener, "Cell-Graph Mining for Breast Tissue Modeling and Classification," in *29th Annu Int Conf IEEE Eng Med Biol Soc*, 5311-5314, 2007.
- [13] V. Ozmen, S. Boylu, E. Ok, N. Z. Canturk, V. Celik, M. Kapkac, *et al.*, "Factors affecting breast cancer treatment delay in Turkey: a study from Turkish Federation of Breast Diseases Societies," *Eur J Pub Health*, vol. 25, 9-14, 2015.

- [14] F. Bray, P. McCarron, and D. M. Parkin, "The changing global patterns of female breast cancer incidence and mortality," *Breast Cancer Res*, vol. 6, 229-39, 2004.
- [15] A. Karahaliou, S. Skiadopoulou, I. Boniatis, P. Sakellaropoulos, E. Likaki, G. Panayiotakis, *et al.*, "Texture analysis of tissue surrounding microcalcifications on mammograms for breast cancer diagnosis," *Br J Radiol*, 2014.
- [16] R. F. Brem, M. J. Lenihan, J. Lieberman, and J. Torrente, "Screening Breast Ultrasound: Past, Present, and Future," *Am J Roentgenol*, vol. 204, 234-240, 2015.
- [17] C. H. Lee, D. D. Dershaw, D. Kopans, P. Evans, B. Monsees, D. Monticciolo, *et al.*, "Breast cancer screening with imaging: recommendations from the Society of Breast Imaging and the ACR on the use of mammography, breast MRI, breast ultrasound, and other technologies for the detection of clinically occult breast cancer," *J Am Coll Radiol*, vol. 7, 18-27, 2010.
- [18] T. B. Bevers, B. O. Anderson, E. Bonaccio, S. Buys, M. B. Daly, P. J. Dempsey, *et al.*, "Breast cancer screening and diagnosis," *J Natl Compr Canc Netw*, vol. 7, 1060-1096, 2009.
- [19] W. A. Berg, Z. Zhang, D. Lehrer, and *et al.*, "Detection of breast cancer with addition of annual screening ultrasound or a single screening mri to mammography in women with elevated breast cancer risk," *JAMA*, vol. 307, pp. 1394-1404, 2012.
- [20] G. M. Merry and E. B. Mendelson, "Update on Screening Breast Ultrasonography," *Radiol Clin North Am*, vol. 52, 527-537, 2014.
- [21] T. M. Kolb, J. Lichy, and J. H. Newhouse, "Comparison of the performance of screening mammography, physical examination, and breast US and evaluation of factors that influence them: an analysis of 27,825 patient evaluations," *Radiol*, vol. 225, 165-75, 2002.
- [22] T. M. Kolb, J. Lichy, and J. H. Newhouse, "Occult cancer in women with dense breasts: detection with screening US--diagnostic yield and tumor characteristics," *Radiol*, vol. 207, 191-9, 1998.
- [23] M. A. Durand and R. J. Hooley, "Implementation of Whole-Breast Screening Ultrasonography," *Radiol Clin N Am*, 55,527-539, 2017.
- [24] A. Mandava, P. R. Ravuri, and R. Konathan, "High-resolution ultrasound imaging of cutaneous lesions," *Indian J Nucl Med and Imaging*, vol. 23, 269-277, 2013.
- [25] S. Ciatto, M. Rosselli del Turco, S. Catarzi, and D. Morrone, "The contribution of ultrasonography to the differential diagnosis of breast cancer," *Neoplasma*, vol. 41, pp. 341-345, 1994.
- [26] R. J. Hooley, L. M. Scoutt, and L. E. Philpotts, "Breast Ultrasonography: State of the Art," *Radiol*, vol. 268, 642-659, 2013.

- [27] M. J. Yaffe and R. A. Jong, "Adjunctive ultrasonography in breast cancer screening," *The Lancet*, vol. 387, pp. 313-314, 2016.
- [28] K. Flobbe, P. Nelemans, A. Kessels, G. Beets, M. Von Meyenfeldt, and J. Van Engelshoven, "The role of ultrasonography as an adjunct to mammography in the detection of breast cancer: a systematic review," *Eur J Cancer*, vol. 38, 1044-1050, 2002.
- [29] P. C. Gøtzsche and K. J. Jørgensen, "Screening for breast cancer with mammography," *Cochrane Database of Syst Rev*, 6, 2013.
- [30] K. J. Nam, B.-K. Han, E. S. Ko, J. S. Choi, E. Y. Ko, D. W. Jeong, *et al.*, "Comparison of full-field digital mammography and digital breast tomosynthesis in ultrasonography-detected breast cancers," *Breast*, vol. 24, 649-655, 2015.
- [31] D. R. Holmes, W. Schooler, and R. Smith, "Oncoplastic approaches to breast conservation," *Int J Breast Cancer*, vol. 2011, 303879, 2011.
- [32] L. R. Schover, "Sexuality and body image in younger women with breast cancer," *J Nat Cancer Inst Monogr*, 177-182, 1994.
- [33] C. K. Anders, R. Johnson, J. Litton, M. Phillips, and A. Bleyer, "Breast Cancer Before Age 40 Years," *Semin Oncol*, vol. 36, 237-49, J 2009.
- [34] M. Emiroğlu, C. Karaali, İ. Sert, S. Salimoğlu, L. Uğurlu, S. Aksoy, *et al.*, "Comparison of Clinical and Pathological Differences of Breast Cancer Patients under 35 and above 55 Years of Age," *Meme Sagligi Dergisi / J Breast Health*, vol. 11, 123-127, 2015.
- [35] R. S. Sweeting, N. Klauber-Demore, M. O. Meyers, A. M. Deal, E. M. Burrows, A. A. Drobish, *et al.*, "Young women with locally advanced breast cancer who achieve breast conservation after neoadjuvant chemotherapy have a low local recurrence rate," *Am Surg*, vol. 77, 850-5, 2011.
- [36] K. B. Clough, C. Nos, R. J. Salmon, M. Soussaline, and J. C. Durand, "Conservative treatment of breast cancers by mammoplasty and irradiation: a new approach to lower quadrant tumors," *Plast Reconstr Surg*, vol. 96, pp. 363-70, 1995.
- [37] R. Masetti, A. Di Leone, G. Franceschini, S. Magno, D. Terribile, M. C. Fabbri, *et al.*, "Oncoplastic techniques in the conservative surgical treatment of breast cancer: an overview," *Breast J*, vol. 12, 174-80, 2006.
- [38] C. Urban, R. Lima, E. Schunemann, C. Spautz, I. Rabinovich, and K. Anselmi, "Oncoplastic principles in breast conserving surgery," *Breast*, vol. 20 Suppl 3, 92-5, 2011.

- [39] A. Baidam, H. Bishop, G. Boland, M. Dalglish, L. Davies, F. Fatah, *et al.*, "Oncoplastic breast surgery--a guide to good practice," *Eur J Surg Oncol*, vol. 33 Suppl 1, S1-23, 2007.
- [40] Y. Barnea, A. Inbal, D. Barsuk, T. Menes, A. Zaretski, D. Leshem, *et al.*, "Oncoplastic reduction using the vertical scar superior-medial pedicle pattern technique for immediate partial breast reconstruction," *Can J Surg*, vol. 57, 134-40, 2014.
- [41] H. M. Heneghan, R. S. Prichard, R. Lyons, P. J. Regan, J. L. Kelly, C. Malone, *et al.*, "Quality of life after immediate breast reconstruction and skin-sparing mastectomy - a comparison with patients undergoing breast conserving surgery," *Eur J Surg Oncol*, vol. 37, 937-43, 2011.
- [42] C. Urban, M. Rietjens, and J. Hurley, "Oncoplastic and Reconstructive Surgery: Qualifications, Limits, and Mentoring," in *Oncoplastic and Reconstructive Breast Surg*, 441-445, 2013.
- [43] N. Houssami, L. Irwig, and S. Ciatto, "Radiological surveillance of interval breast cancers in screening programmes," *Lancet Oncol*, vol. 7, 259-265, 2006.
- [44] J. Sutcliffe, R. L. Hardman, N. C. Dornbluth, and K. A. Kist, "A Novel Technique for Teaching Challenging Ultrasound-Guided Breast Procedures to Radiology Residents," *J Ultrasound Med*, vol. 32, 1845-1854, 2013.
- [45] T. S. Desser, "Simulation-Based Training: The Next Revolution in Radiology Education?," *J Am Coll Radiol*, vol. 4, 816-824, 11, 2007.
- [46] Y. H. Kim, "Ultrasound Phantoms to Protect Patients from Novices," *Korean J Pain*, vol. 29, 73-77, 2016.
- [47] A. Sekhar, M. R. Sun, and B. Siewert, "A Tissue Phantom Model for Training Residents in Ultrasound-guided Liver Biopsy," *Acad Radiol*, vol. 21, 902-908, 7, 2014.
- [48] W. Xia, D. Piras, M. Heijblom, W. Steenbergen, T. G. van Leeuwen, and S. Manohar, "Poly(vinyl alcohol) gels as photoacoustic breast phantoms revisited," *J Biomed Opt*, vol. 16, p. 075002, 2011.
- [49] E. L. Madsen, M. A. Hobson, H. Shi, T. Varghese, and G. R. Frank, "Tissue-mimicking agar/gelatin materials for use in heterogeneous elastography phantoms," *Phys Med Biol*, vol. 50, pp. 5597-5618, 2005.
- [50] A. I. Farrer, H. Odéen, J. de Bever, B. Coats, D. L. Parker, A. Payne, *et al.*, "Characterization and evaluation of tissue-mimicking gelatin phantoms for use with MRgFUS," *J Ther Ultrasound*, vol. 3, 9, 2015.

- [51] L. M. Cannon, A. J. Fagan, and J. E. Browne, "Novel tissue mimicking materials for high-frequency breast ultrasound phantoms," *Ultrasound Med Biol*, vol. 37, pp. 122-35, 2011.
- [52] C. Li, J. Allen, T. Alliston, and L. A. Pruitt, "The Use of Polyacrylamide Gels for Mechanical Calibration of Cartilage – A Combined Nanoindentation and Unconfined Compression Study," *J Mech Behav Biomed Mater*, vol. 4, 1540-1547, 2011.
- [53] A. Iravani, J. Mueller, and A.-M. Yousefi, "Producing homogeneous cryogel phantoms for medical imaging: a finite-element approach," *J Biomater Sci Polym Ed*, vol. 25, pp. 181-202, 2014.
- [54] J. A. Rogers and G. Balooch, "Biomedical materials: A restorative synthetic skin," *Nat Mater*, vol. 15, pp. 828-829, 08, 2016.
- [55] P. D. Costantino, "Synthetic biomaterials for soft-tissue augmentation and replacement in the head and neck," *Otolaryngol Clin North Am*, vol. 27, pp. 223-262, 1994.
- [56] P. A. L. S. Martins, R. M. Natal Jorge, and A. J. M. Ferreira, "A Comparative Study of Several Material Models for Prediction of Hyperelastic Properties: Application to Silicone-Rubber and Soft Tissues," *Strain*, vol. 42, 135-147, 2006.
- [57] Gerben E. Breimer, Vivek Bodani, Thomas Looi, and James M. Drake, "Design and evaluation of a new synthetic brain simulator for endoscopic third ventriculostomy," *J Neurosurg Pediatr*, vol. 15, pp. 82-88, 2015.
- [58] I. M. de Carvalho, R. L. Q. Basto, A. F. C. Infantosi, M. A. von Krüger, and W. C. A. Pereira, "Breast ultrasound imaging phantom to mimic malign lesion characteristics," *Phys Procedia*, vol. 3, 421-426, 2010.
- [59] T. N. Trotta, J. A. Trotta, and S. Lowe, "Ultrasound phantom models, materials, and methods," ed: Google Patents, 2016.
- [60] A. P. Sarvazyan and V. Egorov, "Human tissue phantoms and methods for manufacturing thereof," ed: Google Patents, 2008.
- [61] M. S. A. E. Gordon, "Simulator for Body Organs," GB Patent, 1999.
- [62] O. J. M. J.D. Wilkins, "Ultrasound Training Mannequin," US 2008/0293029 A1, 2008.
- [63] B. A. M. Ault, "Medical Training Methods And Devices," US 2009/0142741 A1, 2009.
- [64] R. A. Jesinger, "Breast Anatomy for the Interventionalist," *Tech Vasc Interv Radiol*, vol. 17, 3-9, 2014.

- [65] D. Da Costa, A. Taddese, M. L. Cure, D. Gerson, R. Poppiti, Jr., and L. E. Esserman, "Common and unusual diseases of the nipple-areolar complex," *Radiographics*, vol. 27 Suppl 1, pp. S65-77, 2007.
- [66] H. Y. An, K. S. Kim, I. K. Yu, K. W. Kim, and H. H. Kim, "Image presentation. The nipple-areolar complex: a pictorial review of common and uncommon conditions," *J Ultrasound Med*, vol. 29, 949-62, 2010.
- [67] S. Rummel, M. T. Hueman, N. Costantino, C. D. Shriver, and R. E. Ellsworth, "Tumour location within the breast: Does tumour site have prognostic ability?," *Ecancermedicalscience*, vol. 9, 552, 2015.
- [68] G. S. Kino, *Acoustic waves : devices, imaging, and analog signal processing*. Englewood Cliffs: Prentice-Hall, 1987.
- [69] P. N. T. Wells and H.-D. Liang, "Medical ultrasound: imaging of soft tissue strain and elasticity," *J R Soc Interface*, vol. 8, 1521-1549, 2011.
- [70] S. A. Goss, R. L. Johnston, and F. Dunn, "Comprehensive compilation of empirical ultrasonic properties of mammalian tissues," *JASA*, vol. 64, pp. 423-457, 1978.
- [71] G. L. Lamb, "The attenuation of waves in a dispersive medium," *J Geophys Res*, vol. 67, 5273-5277, 1962.
- [72] G. Arpino, V. J. Bardou, G. M. Clark, and R. M. Elledge, "Infiltrating lobular carcinoma of the breast: tumor characteristics and clinical outcome," *Breast Cancer Res*, vol. 6, 149, 2004.
- [73] P. S. F. S. Fitzal, P., in *Oncoplastic Breast Surg*, ed, 2010.
- [74] R. Matkowski, B. Szynglarewicz, P. Kasprzak, J. Forgacz, R. Skalik, M. Zietek, *et al.*, "Batwing mastopexy as oncoplastic surgical approach to periareolar tumors in upper quadrants," *Tumori*, vol. 98, 421-7, 2012.
- [75] M. Rezai, S. Kraemer, R. Kimmig, and P. Kern, "Breast conservative surgery and local recurrence," *Breast*, vol. 24, Supplement 2, S100-S107, 2015.
- [76] M. Rezai, S. Strauss, R. Kimmig, and P. Kern, "Risk-reducing, conservative mastectomy-analysis of surgical outcome and quality of life in 272 implant-based reconstructions using TiLoop((R)) Bra versus autologous corial flaps," *Gland Surg*, vol. 5, pp. 1-8, Feb 2016.
- [77] Erdem *et al.*, "Knowledge, Attitudes, and Behaviors about Breast Self-Examination and Mammography among Female Primary Healthcare Workers in Diyarbakir, Turkey," *BioMed Research International*, vol. 2016, 6, 2016.

- [78] B. O. Anderson, C.-H. Yip, S. D. Ramsey, R. Bengoa, S. Braun, M. Fitch, *et al.*, "Breast Cancer in Limited-Resource Countries: Health Care Systems and Public Policy," *Breast J*, vol. 12, S54-S69, 2006.
- [79] W. Z. Ray and S. E. Mackinnon, "Clinical Outcomes Following Median to Radial Nerve Transfers," *J Hand Surg*, vol. 36, 201-208.
- [80] G. Said and C. Krarup, *Peripheral nerve disorders : handbook of clinical neurology*: Oxford : Elsevier, 2013.
- [81] Y. Hirasawa and K. Sakakida, "Sports and peripheral nerve injury," *Am J Sports Med*, vol. 11, pp. 420-6, 1983.
- [82] M. T. Houdek and A. Y. Shin, "Management and Complications of Traumatic Peripheral Nerve Injuries," *Hand Clin*, vol. 31, 151-163, 2015.
- [83] A. E. Barr and M. F. Barbe, "Pathophysiological Tissue Changes Associated With Repetitive Movement: A Review of the Evidence," *Phys ther*, vol. 82, 173-187, 2002.
- [84] S. Carp, *Peripheral Nerve Injury An Anatomical and Physiological Approach for Physical Therapy Intervention*: FA Davis, 2015.
- [85] C. B. Novak, D. J. Anastakis, D. E. Beaton, S. E. Mackinnon, and J. Katz, "Relationships among pain disability, pain intensity, illness intrusiveness, and upper extremity disability in patients with traumatic peripheral nerve injury," *J Hand Surg Am*, vol. 35, pp. 1633-9, 2010.
- [86] D. M. Wojtkiewicz, J. Saunders, L. Domeshek, C. B. Novak, V. Kaskutas, and S. E. Mackinnon, "Social impact of peripheral nerve injuries," *Hand (New York, N.Y.)*, vol. 10, 161-167, 2015.
- [87] D. M. Guse and S. L. Moran, "Outcomes of the surgical treatment of peripheral neuromas of the hand and forearm: a 25-year comparative outcome study," *Ann Plast Surg*, vol. 71, 654-8, 2013.
- [88] W. Y. Chan, P. Matteucci, and S. J. Southern, "Validation of microsurgical models in microsurgery training and competence: a review," *Microsurg*, vol. 27, pp. 494-9, 2007.
- [89] E. Veznedaroglu, *Controversies in Vascular Neurosurgery*: Springer, 2016.
- [90] T. W. Rutner, V. B. Ziccardi, and M. N. Janal, "Long-term outcome assessment for lingual nerve microsurgery," *J Oral Maxillofac Surg*, vol. 63, 1145-9, 1998.
- [91] A. Chhabra, S. Ahlawat, A. Belzberg, and G. Andreseik, "Peripheral nerve injury grading simplified on MR neurography: As referenced to Seddon and Sunderland classifications," *Indian J Radiol Imaging*, vol. 24, 217-224, 2014.

- [92] H. Seddon, "A classification of nerve injuries," *Br Med J*, vol. 2, 237, 1942.
- [93] S. Sunderland, "A classification of peripheral nerve injuries producing loss of function.," *Brain*, vol. 74, 491, 1951.
- [94] J. M. Brown, A. Yee, and S. E. Mackinnon, "Distal median to ulnar nerve transfers to restore ulnar motor and sensory function within the hand: technical nuances," *Neurosurg*, vol. 65, 966-77; 2009.
- [95] H. Sadideen, A. Alvand, M. Saadeddin, and R. Kneebone, "Surgical experts: Born or made?," *Inter J Surg*, vol. 11, 773-778, 2013.
- [96] N. E. McAmis, D. A. Prospero, J. Standeven, W. Z. Ray, Z. Zohny, and J. R. Engsborg, "Development of a method to compare microsurgery techniques across different levels of surgical experience," *Interdiscip Neurosurg*, vol. 10, 52-56, 2017.
- [97] B. Kerr and J. P. O'Leary, "The training of the surgeon: Dr. Halsted's greatest legacy," *Am Surg*, vol. 65, 1101-2, 1999.
- [98] V. G. Ilie, V. I. Ilie, C. Dobreanu, N. Ghetu, S. Luchian, and D. Pieptu, "Training of microsurgical skills on nonliving models," *Microsurg*, vol. 28, 571-577, 2008.
- [99] K. Steffens, E. Koob, and G. Hong, "Training in basic microsurgical techniques without experiments involving animals," *Arch Orthop Trauma Surg*, vol. 111, 198-203, 1992.
- [100] M. Goldstein, "Use of fresh human placenta for microsurgical training," *J Microsurg*, vol. 1, 70-1, 1979.
- [101] A. Govila and D. Sharma, "Microsurgical practice on avulsed skin," *Br J Plast Surg*, vol. 43, 250-1, 1990.
- [102] S. P. Fanua, J. Kim, and S. E. F. Wilgis, "Alternative model for teaching microsurgery," *Microsurg*, vol. 21, 379-382, 2001.
- [103] S. M. Nam, H. S. Shin, Y. B. Kim, E. S. Park, and C. Y. Choi, "Microsurgical training with porcine thigh infusion model," *J Reconstr Microsurgery*, vol. 29, 303-306, 2013.
- [104] D. A. Lannon, J.-A. Atkins, and P. E. M. Butler, "Non-vital, prosthetic, and virtual reality models of microsurgical training," *Microsurg*, vol. 21, 389-393, 2001.
- [105] M. Singh, N. Ziolkowski, S. Ramachandran, S. R. Myers, and A. M. Ghanem, "Development of a Five-Day Basic Microsurgery Simulation Training Course: A Cost Analysis," *Arch Plast Surg*, vol. 41, 213-217, 2014.
- [106] E. Evgeniou, H. Walker, and S. Gujral, "The Role of Simulation in Microsurgical Training," *J Surg Educ*, 2017.

- [107] K. E. Korber and B. A. Kraemer, "Use of small-caliber polytetrafluoroethylene (gore-tex ®) grafts in microsurgical training," *Microsurg*, vol. 10, 113-115, 1989.
- [108] S. Ramasastry, K. Narayanan, and M. F. Angel, "A simple and inexpensive device for microvascular training," *Ann Plast Surg*, vol. 14, 462-4, 1985.
- [109] A. L. James Kolenchery Rappel, "Apparatus, method and system for microsurgical suture training," US Patent, 2012.
- [110] J. Braga-Silva, "The Use of Silicone Tubing In the Late Repair of the Median and Ulnar Nerves in the Forearm," *J Hand Surg*, vol. 24, 703-706, 1999.
- [111] D. P. Goossens, S. M. Gruel, and V. K. Rao, "A survey of microsurgery training in the United States," *Microsurg*, vol. 11, 2-4, 1990.
- [112] V. Chiono and C. Tonda-Turo, "Trends in the design of nerve guidance channels in peripheral nerve tissue engineering," *Prog Neurobiol*, vol. 131, 87-104, 2015.
- [113] P. J. Driscoll, M. A. Glasby, and G. M. Lawson, "An in vivo study of peripheral nerves in continuity: biomechanical and physiological responses to elongation," *J Orthop Res*, vol. 20, 370-375, 2002.
- [114] M. Nordin and V. H. Frankel, *Basic biomechanics of the musculoskeletal system*: Lippincott Williams & Wilkins, 2001.
- [115] J. K. Mai and G. Paxinos, *The human nervous system*: Academic Press, 2011.
- [116] Y. He, G.-h. Xue, and J.-z. Fu, "Fabrication of low cost soft tissue prostheses with the desktop 3D printer," *Sci Rep*, vol. 4, 6973, 2014.
- [117] Smooth-On, ed, 2017.
- [118] A. Mehta, P. S. Li, and M. Goldstein, "Male infertility microsurgical training," *Translational Andrology and Urology*, vol. 3, pp. 134-141, 2014.
- [119] M. Hosnuter, Z. Tosun, and N. Savaci, "A nonanimal model for microsurgical training with adventitial stripping," *Plast Reconstr Surg*, vol. 106, 958-9, 2000.
- [120] S. Sunderland, "The anatomic foundation of peripheral nerve repair techniques," *Orthop Clin North Am*, vol. 12, 245-66, 1981.
- [121] H. Millesi, G. Zoch, and R. Reihnsner, "Mechanical properties of peripheral nerves," *Clin Orthop Relat Res*, 76-83, 1995.
- [122] G. Mattana, P. Cosseddu, B. Fraboni, G. G. Malliaras, J. P. Hinestroza, and A. Bonfiglio, "Organic electronics on natural cotton fibres," *Org Electron*, vol. 12, 2033-2039, 2011.

- [123] A. P. Fantilli, S. Sicardi, and F. Dotti, "The use of wool as fiber-reinforcement in cement-based mortar," *Constr Build Mater*, vol. 139, 562-569, 2017.
- [124] G. H. Borschel, K. F. Kia, W. M. Kuzon, Jr., and R. G. Dennis, "Mechanical properties of acellular peripheral nerve," *J Surg Res*, vol. 114, 133-9, Oct 2003.
- [125] G. Liu, Q. Zhang, Y. Jin, and Z. Gao, "Stress and strain analysis on the anastomosis site sutured with either epineurial or perineurial sutures after simulation of sciatic nerve injury," *Neural RegenRes*, vol. 7, 2299-2304, 2012.
- [126] X. Ma, Z. Yang, X. Li, J. Ma, Y. Zhang, H. Guo, *et al.*, "[A study on biomechanical properties of chemically extracted acellular peripheral nerve]," *Zhongguo Xiu Fu Chong Jian Wai Ke Za Zhi*, vol. 24, 1293-7, 2010.
- [127] L. C. T. Serpe, E. B. d. Las Casas, A. C. M. M. Toyofuku, and L. A. González-Torres, "A bilinear elastic constitutive model applied for midpalatal suture behavior during rapid maxillary expansion," *Res Biomed Eng*, vol. 31, 319-327, 2015.
- [128] P. Su, Y. Yang, and L. Huang, "Biomechanical simulation of needle insertion into cornea based on distortion energy failure criterion," *Acta Bioeng Biomech*, vol. 18, 2016.
- [129] J. Noble, C. A. Munro, V. S. Prasad, and R. Midha, "Analysis of upper and lower extremity peripheral nerve injuries in a population of patients with multiple injuries," *J Trauma*, vol. 45, 116-22, Jul 1998.
- [130] R. Birch and A. R. Raji, "Repair of median and ulnar nerves. Primary suture is best," *J Bone Joint Surg Br*, vol. 73, 154-7, Jan 1991.
- [131] R. M. G. Menorca, T. S. Fussell, and J. C. Elfar, "Peripheral Nerve Trauma: Mechanisms of Injury and Recovery," *Hand clinics*, vol. 29, 317-330, 2013.
- [132] D. Grinsell and C. P. Keating, "Peripheral Nerve Reconstruction after Injury: A Review of Clinical and Experimental Therapies," *BioMed Res Inter*, vol. 2014, 13, 2014.
- [133] S. D. Dodds and A. Halim, "Advances in nerve repair and reconstruction," *CurrOrthop Pract*, vol. 24, 529-535, 2013.
- [134] Kutluay Uluç, Gregory C. Kujoth, and Mustafa K. Başkaya, "Operating microscopes: past, present, and future," *Neurosurg Focus*, vol. 27, E4, 2009.
- [135] R. T. e. Silva, T. F. S. Barros, J. T. de Carvalho, A. A. Ribeiro, A. F. Pires, and T. H. Wei, "Comparative Study Of Microanastomosis With Distinct 10-0 Nylon Sutures In Rats," *Acta Ortop Brasileira*, vol. 24, 35-38, 2016.
- [136] L. Rasulić, "Introduction: Facing the Challenges of Peripheral Nerve Surgery in the 21<sup>st</sup> Century," *World Neurosurg*, vol. 84, p. 596.

- [137] G. F. Pratt, W. M. Rozen, D. Chubb, I. S. Whitaker, D. Grinsell, M. W. Ashton, *et al.*, "Modern adjuncts and technologies in microsurgery: An historical and evidence-based review," *Microsurg*, vol. 30, 657-666, 2010.
- [138] A. B. Dagum, "Peripheral nerve regeneration, repair, and grafting," *Journal of Hand Ther*, vol. 11, 111-117, 1998.
- [139] B. Katirji, "Case 12," in *Electromyography in Clinical Practice (Second Edition)*, ed Philadelphia: Mosby, 2007, 189-197.
- [140] W. W. Campbell, "Evaluation and management of peripheral nerve injury," *Clin Neurophys*, vol. 119, 1951-1965, 2008.
- [141] M. Ravikanth, P. Soujanya, K. Manjunath, T. R. Saraswathi, and C. R. Ramachandran, "Heterogeneity of fibroblasts," *Journal of Oral and Maxillofacial Pathology : JOMFP*, vol. 15, 247-250, 2011.
- [142] Mark G. Burnett and Eric L. Zager, "Pathophysiology of peripheral nerve injury: a brief review," *Neurosurg Focus*, vol. 16, 1-7, 2004.
- [143] C. Thorne, K. C. Chung, A. Gosain, G. C. Guntner, and B. J. Mehrara, *Grabb and Smith's Plastic Surgery*: Wolters Kluwer/Lippincott Williams & Wilkins Health, 2014.
- [144] H. Millesi, "Peripheral nerve repair: terminology, questions, and facts," *J Reconstr Microsurg*, vol. 2, 21-31, 1985.
- [145] M. Bayramiçli, H. Şirinoğlu, and D. Yalçın, "A basic experimental model for end-to-end anastomosis of vessels with diameter discrepancy," *Microsurg.*, vol. 34, 333-334, 2014.
- [146] C. Mandrycky, Z. Wang, K. Kim, and D.-H. Kim, "3D bioprinting for engineering complex tissues," *Biotechnol Adv*, vol. 34, 422-434, 2016.
- [147] P. A. Thomas, *Curriculum development for medical education: a six-step approach*: JHU Press, 2015.
- [148] L. M. Sutherland, P. F. Middleton, A. Anthony, J. Hamdorf, P. Cregan, D. Scott, *et al.*, "Surgical simulation: a systematic review," *AnnSurg*, vol. 243, 291, 2006.
- [149] M. McDonald, S. Lochhead, R. Chopra, and M. J. Bronskill, "Multi-modality tissue-mimicking phantom for thermal therapy," *Phys Med Biol*, vol. 49, 2767, 2004.
- [150] A.-K. Brascher, J. A. Blunk, K. Bauer, R. Feldmann Jr, and J. Benrath, "Comprehensive curriculum for phantom-based training of ultrasound-guided intercostal nerve and stellate ganglion blocks," *Pain Med*, vol. 15, 1647-1656, 2014.

- [151] D. J. Anastakis, G. Regehr, R. K. Reznick, M. Cusimano, J. Murnaghan, M. Brown, *et al.*, "Assessment of technical skills transfer from the bench training model to the human model," *Am J Surg*, vol. 177, 167-170, 1999.
- [152] L. A. Siminoff, R. M. Arnold, and J. Hewlett, "The process of organ donation and its effect on consent," *Clin Transplant*, vol. 15, 39-47, 2001.
- [153] B. W. Turney, "Anatomy in a modern medical curriculum," *AnnRoyal Coll Surg Eng*, vol. 89, 104-107, 2007.
- [154] G. S. Becker and J. J. Elias, "Introducing incentives in the market for live and cadaveric organ donations," *J Econ Perspect*, vol. 21, 3-24, 2007.
- [155] A. H. Al-Elq, "Simulation-based medical teaching and learning," *J Famil Community Med*, vol. 17, 35-40, 2010.
- [156] J. Balcombe, "Medical training using simulation: Toward fewer animals and safer patients," 2004.
- [157] D. Solanki, "Unnecessary and cruel use of animals for medical undergraduate training in India," *J Pharmacol Pharmacother*, vol. 1, 59, 2010.
- [158] Ü. t. S. Şehirli, E. n. Saka, and Ö. Sarikaya, "Attitudes of Turkish anatomists toward cadaver donation," *Clin Anat*, vol. 17, 677-681, 2004.
- [159] W. C. McGaghie, S. B. Issenberg, E. R. Petrusa, and R. J. Scalese, "A critical review of simulation-based medical education research: 2003–2009," *Med Educ*, vol. 44, 50-63, 2010.
- [160] K. R. Rosen, "The history of medical simulation," *J Critic Care*, vol. 23, 157-166, 2008.
- [161] R. H. Fletcher, S. W. Fletcher, and G. S. Fletcher, *Clinical epidemiology: the essentials*: Lippincott Williams & Wilkins, 2012.
- [162] J. Torkington, S. Smith, B. Rees, and A. Darzi, "The role of simulation in surgical training," *Ann Royal Coll Surg Eng*, vol. 82, 88, 2000.
- [163] A. Nabavi and J. Schipper, "Simulation in surgical training," *HNO*, vol. 65, pp. 7-12, 2017.
- [164] B. Özkalp and Ü. Saygılı, "The Effectiveness of Similitor Usage in the Paramedic Education," *Procedia Soc Behav Sci*, vol. 174, pp. 3150-3153, 2015.
- [165] A. Ziv, S. Ben-David, and M. Ziv, "Simulation based medical education: an opportunity to learn from errors," *Med Teacher*, vol. 27, 193-199, 2005.
- [166] I. Balasundaram, R. Aggarwal, and L. A. Darzi, "Development of a training curriculum for microsurgery," *Brit Oral Maxillofac Surg*, vol. 48, 598-606, 2010.

- [167] J. Fitzgerald, C. Giddings, G. Khera, and C. Marron, "Improving the future of surgical training and education: consensus recommendations from the Association of Surgeons in Training," *Int J Surg*, vol. 10, 389-392, 2012.
- [168] J. Milburn, G. Khera, S. Hornby, P. Malone, and J. Fitzgerald, "Introduction, availability and role of simulation in surgical education and training: review of current evidence and recommendations from the Association of Surgeons in Training," *Int J Surg*, vol. 10, pp. 393-398, 2012.
- [169] A. G. Gallagher, E. M. Ritter, H. Champion, G. Higgins, M. P. Fried, G. Moses, *et al.*, "Virtual reality simulation for the operating room: proficiency-based training as a paradigm shift in surgical skills training," *AnnSurg*, vol. 241, 364, 2005.
- [170] A. T. Stotter, A. Becket, J. Hansen, I. Capperauld, and H. Dudley, "Simulation in surgical training using freeze dried material," *BritJ Surg*, vol. 73, pp. 52-54, 1986.
- [171] A. R. Faulkner, A. C. Bourgeois, Y. C. Bradley, and A. S. Pasciak, "A robust and inexpensive phantom for fluoroscopically guided lumbar puncture training," *Simul Healthcare*, vol. 10, 54-58, 2015.
- [172] J. L. Hsu, J. R. Korndorffer, and K. M. Brown, "Force feedback vessel ligation simulator in knot-tying proficiency training," *Am J Surg*, vol. 211, 411-415, 2016.
- [173] L. H. Dorton, C. R. Lintzenich, and A. K. Evans, "Simulation model for tracheotomy education for primary health-care providers," *Ann Otol, Rhinol Laryngol*, vol. 123, pp. 11-18, 2014.
- [174] E. Göçgeldi, H. İstanbulluoğlu, M. Uçar, H. Yaren, S. Ceylan, and N. Koçak, "Tıp fakültesi 5. ve 6. sınıf öğrencilerinin tıp eğitimleri süresince pratik uygulama yapabilme durumunun araştırılması," *Gulhane Med J*, vol. 53, 2011.
- [175] L. S. Shulman, "Theory, practice, and the education of professionals," *Element School J*, vol. 98, 511-526, 1998.
- [176] Y. Akvardar, Y. Demiral, G. Ergor, and A. Ergor, "Substance use among medical students and physicians in a medical school in Turkey," *Soc Psychiatry Psychiatr Epidemiol*, vol. 39, 502-506, 2004.
- [177] *Adult Cric Trainer*.
- [178] N. Stasche, T. Quirrenbach, M. Bärmann, M. Krebs, M. Harrass, and K. Friedrich, "IMOLA—ein interventionsfähiges LarynxmodellIMOLA—a new larynx model for surgical training," *HNO*, vol. 53, 869-875, 2005.
- [179] A. Donabedian, "Evaluating the quality of medical care," *Milbank Memorial Fund*, vol. 44, 166-206, 1966.

- [180] J. Eden, D. M. Berwick, and G. R. Wilensky, *Graduate medical education that meets the nation's health needs*: National Academies Press Washington, DC, 2014.
- [181] R. M. Middleton, A. Alvand, P. G. Roberts, C. Hargrove, G. Kirby, and J. L. Rees, "Simulation-based training platforms for arthroscopy: A randomized comparison of virtual reality learning to benchtop learning," *Arthroscopy*, vol. 33, 996-1003, 2017.
- [182] N. Multak, K. Newell, S. Spear, R. J. Scalese, and S. B. Issenberg, "A multi-institutional study using simulation to teach cardiopulmonary physical examination and diagnosis skills to physician assistant students," *J Physician Assist Educ*, vol. 26, 70-76, 2015.
- [183] I. Eardley, Y. Reisman, S. Goldstein, A. Kramer, J. Dean, and E. Coleman, "Existing and future educational needs in graduate and postgraduate education," *J Sex Med*, vol. 14, 475-485, 2017.
- [184] P. De Leyn, L. Bedert, M. Delcroix, P. Depuydt, G. Lauwers, Y. Sokolov, *et al.*, "Tracheotomy: clinical review and guidelines☆," *Eur J Cardio-Thorac Surg*, vol. 32, 412-421, 2007.
- [185] N. H. Cheung and L. M. Napolitano, "Tracheostomy: Epidemiology, Indications, Timing, Technique, and Outcomes," *Respir Care*, vol. 59, 895-919, 2014.
- [186] C. B. Taylor and R. A. Otto, "Open Tracheostomy Procedure," *Adjuncts for Care of the Surgical Patient, An Issue of Atlas of the Oral & Maxillofacial Surgery Clinics 23-2, E-Book*, vol. 23, p. 117, 2016.
- [187] K. McCluskey and M. Stephens, "Alternative techniques for tracheal intubation," *Anaesth Intensive Care Med*, vol. 18, 163-167, 2017.
- [188] H. Dharmarajan, Y.-C. C. Liu, H. K. Hippard, and B. Chandy, "Difficult airway intubation simulation using Bonfils fiberscope and rigid fiberscope for surgical training," *Int J Pediatr Otorhinolaryngol*, vol. 105, pp. 171-175, 2018.
- [189] L. Davis, S. D. Cook-Sather, and M. S. Schreiner, "Lighted Stylet Tracheal Intubation: A Review," *Anesth Analge*, vol. 90, 745-756, 2000.
- [190] A. Soni, S. Badatya, M. Modi, and S. Saluja, "Neonatal bronchoscopy – A review," *Current Med Res Practice*, vol. 6, pp. 192-201, 2016.
- [191] P. J. Reynisson, H. O. Leira, T. N. Hernes, E. F. Hofstad, M. Scali, H. Sorger, *et al.*, "Navigated bronchoscopy: a technical review," *J Bronchol Intervent Pulmonol*, vol. 21, 242-264, 2014.
- [192] A. Sharma, L. R. Zakka, and M. C. Mihm Jr, "Anatomy of the human skin and wound healing," in *Bioengineering In Wound Healing: A Systems Approach*, ed: World Scientific, 27-57, 2017.

- [193] F. H. Netter, *Atlas of Human Anatomy E-Book*: Elsevier Health Sciences, 2017.
- [194] E. Wagenblast, M. Soto, S. Gutiérrez-Ángel, C. A. Hartl, A. L. Gable, A. R. Maceli, *et al.*, "A model of breast cancer heterogeneity reveals vascular mimicry as a driver of metastasis," *Nature*, vol. 520, 358, 2015.
- [195] R.-C. Ji, "Lymph Nodes and Cancer Metastasis: New Perspectives on the Role of Intranodal Lymphatic Sinuses," *Int J Mol Sci*, vol. 18, 51, 2017.
- [196] A. K. Thukkani and S. Kinlay, "Endovascular intervention for peripheral artery disease," *Circul Res*, vol. 116, 1599-1613, 2015.
- [197] K. M. Berg, W. K. Berg, and F. K. Graham, "Infant heart rate response as a function of stimulus and state," *Psychophysiol*, vol. 8, 30-44, 1971.
- [198] M. Charlesworth and A. Ashworth, "Anaesthesia for surgery of the trachea and main bronchi," *Anaesth Intensive Care Med*, vol. 18, 614-619, 2017.
- [199] T. T. Tollefson, A. Rafii, and J. D. Kriet, "Tracheostomy scar revision," *Oper Tech Otolayngol Head Neck Surg*, vol. 19, pp. 128-131, 2008.
- [200] M. Á. Saavedra, J. E. Navarro-Zarza, P. Villaseñor-Ovies, J. J. Canoso, A. Vargas, K. Chiapas-Gasca, *et al.*, "Clinical Anatomy of the Knee," *Reumatología Clín*, vol. 8, pp. 39-45, 2012.
- [201] S. D. Waldman, "CHAPTER 191 - Bursitis Syndromes of the Knee," in *Pain Rev*, ed Philadelphia: W.B. Saunders, 318-322, 2009.

## **CURRICULUM VITAE**

**Name:** Burçin

**Surname:** Gül

**Maiden Name:** Üstbaş

**Address:** Sabancı University, Orta Mah., Üniversite Cad., No:7, Orhanlı, Tuzla, Istanbul, 34956, TURKEY

**Mobile:** +90 555 3283452

**Email:** burcinustbas@sabanciuniv.edu

### ***Areas of Research Interest***

Biomaterials, silicone-based materials, simulation phantoms, composite materials, product design, product engineering.

### ***Education***

#### **Sabancı University, Istanbul, Turkey, (2014 – 2018)**

- PhD – Materials Science & Engineering

#### **University of Sheffield, Sheffield, United Kingdom, (2010 – 2012)**

- MSc – Bionanotechnology – Materials Science & Engineering (GPA: 2:1 Upper 2nd Class Honours)

#### **Istanbul University, Istanbul, Turkey, (2005 – 2009)**

- BS – Biology, Faculty of Science (GPA: 78.67/100)

#### **Anadolu University, Eskisehir, Turkey, (2007 – 2009)**

- 2nd BS – Public Relations, Dept. of Economical and Administrative Programs

## ***Professional Experience***

**Research Assistant**, Dept. of Biomedical Science, University of Sheffield, UK, *October 2012 – 2013*

*Project:* Scavenger Receptor B Expression in Carcinoma: A Potential Therapeutic Target for Nanoparticle Mediated Drug Delivery (**Yorkshire Cancer Research (YCR) Funded 1 Year Project**)

*Supervisors:* Dr. Irene Canton (Dept. of Biomedical Science) and Prof. Steve Armes (Dept. of Chemistry) *Responsibilities:* Preparation and physical characterization of polymeric nanoparticles with enhanced surface topologies via UV-Spectrophotometer, DLS, TEM, GPC column, RP-HPLC and analyzing uptake kinetics of these nanoparticles in 30 different cancer cell lines via FACS, CLSM. Also set-up a new Tissue Culture lab, working with 30 different human cell lines.

Attended YCR Annual Meeting, June 2013, Harrogate, UK.

**Graduate Research Project**, Dept. of Biomedical Science, University of Sheffield, UK, *October 2010 – 2011* *Project:* Screening and Qualitative Analysis of Nanopolymersomes Targeting Transcytosis across Blood-Brain- Barrier (BBB).

*Supervisors:* Prof. Giuseppe Battaglia and Dr. Irene Canton

*Responsibilities:* Design, fabrication and physical characterization of polymeric nanoparticles (Polymersomes) with a linking strategy for a targeting motif that allows drug delivery across BBB via transcytosis.

**Graduate Research Trainee**, Molecular Biology and Genetics Laboratory, Istanbul Kultur University, Turkey, *November 2009 – June 2010*

*Project:* Investigating the effects of the anti-cancer drugs (Roscovitin and Purvalanol) on the apoptosis mechanisms of the human breast and prostate cancer cell lines.

*Supervisor:* Prof. Narcin Palavan-Unsal, Assoc. Prof. Dr. E. Damla Arisan

*Responsibilities:* Cell culture techniques, dose and time dependent experiment designs and advanced data analysis.

**Undergraduate Research Trainee**, DETAE, Research Institute of Experimental Medicine, Dept. of Molecular Medicine, Istanbul University, Turkey, *July – September 2007*

*Supervisor:* Prof. Dr. Turgay Isbir

*Responsibilities:* Training on molecular biology techniques such as DNA isolation from blood or tissues, PCR.

### ***Lab Skills***

***Physical characterisation of nanoparticles:*** UV-Spectrophotometer, Dynamic Light Scattering (DLS), Transmission Electron Microscopy (TEM), Scanning Electron Microscopy (SEM), Gel Permeation Chromatography (GPC) column and Reversed Phase High Pressure Liquid Chromatography (RP-HPLC).

***Cell culture techniques:*** Traditional monolayer cell culture techniques, Cell Death ELISA assays, MTT cell viability assays. 3D cell culture set-ups (multicell tumour spheroids (MCTS) culture and a 3D blood-brain-barrier tissue culture model). Immunocytochemistry and immunohistochemistry (MCTS tissue), Traditional Optical Microscopy of tissue culture samples and morphological analysis, high content bio-imaging and analysis by Epi-Fluorescence Microscopy using the BD Pathway 855 Imaging Systems and Confocal Laser Scanning Microscope (CLSM).

***Molecular Biology techniques:*** DNA Laddering, RNA- cDNA isolations, RT-PCR.

***Medium and high-content techniques:*** High-content Fluorescence Activated Cell Sorting (FACS) and medium content semi-automatic Western Blot Simon (Protein Simple, UK).

**Computer Skills:** Matlab, Image J (Java-based image processing program), Linux.

**Language Skills:** Turkish (native), English (advanced), German (beginner).

## Publications

1. Burcin Ustbas, Deniz Kilic, Dilan Arslan, Mehmet Bayramicli, and Ozge Akbulut. *Silicone-based peripheral nerve microsurgery simulation phantoms for medical training*. Submitted to Microsurgery, 2018.
2. Burcin Ustbas, Deniz Kilic, Ayhan Bozkurt, Mustafa Erkin Aribal, and Ozge Akbulut. *Silicone-based Composite Materials Simulate Breast Tissue to be used as Ultrasonography Training Phantoms*. Submitted to Ultrasonics, 2017. (Under review)
3. Deniz Kilic, Burcin Ustbas, Ece Polen Budak, Hande Eyisoğlu, Cem Yılmaz, Barkin Eldem, and Ozge Akbulut. *Silicone-based Composites as Surgical Breast Models for Oncoplasty Training*. Procedia Eng., 2016.
4. Guven Z. P., Ustbas B., Harkness K. M., Coskun H., Joshi C. P., Besong T. M., Stellacci F., Bakr O. M., and Akbulut O. *Synthesis and characterization of mixed ligand chiral nanoclusters*. Dalton transactions, 2016.
5. Gokay Avcı, Omid Akhlaghi Baghoojari, Burcin Ustbas, Ceren Ozbay, Yusuf Z. Menciloglu, and Ozge Akbulut. *A PCE-based rheology modifier allows machining of solid cast green bodies of alumina*. Ceramics International, 2016.
6. *Abdullah M. Alswieleh, Nan Cheng, Irene Canton, Burcin Ustbas, Xuan Xue, Vincent Ladmiral, Sijing Xia, Robert E. Ducker, Osama El Zubir, Michael L. Cartron, C. Neil Hunter, Graham J. Leggett, and Steven P. Armes. Zwitterionic Poly(amino acid methacrylate) Brushes*. Journal of American Chemical Society, 2014.
7. B. Ustbas, S. P. Armes and I. Canton. Galactosylated block copolymers: a versatile nano-based tool for effective intracellular drug delivery? Therapeutic Delivery. 2014 (Invited Editorial)
8. *Madsen J., Canton I., Warren N. J., Themistou E., Blanz A., Ustbas B., Tian X., Pearson R., Battaglia G., Lewis A. L. & Armes S. P.* Nile Blue-based nanosized pH sensors for simultaneous far-red and near-infrared live bioimaging. Journal of American Chemical Society, 2013.
9. “Synthetic Polymeric Nanoparticles for Biological Applications” presented in the Synthetic Biology Annual Meeting, July 2013, Sheffield, UK.
10. “Peptide-functionalized Polymersomes Targeting Blood-Brain-Barrier by Transcytosis” presented in the TechConnect World Nanotech Conference and Expo, 2011, US.

## **Social Activities & Membership**

International Istinye Rotary Club Member (International Committee President – 2008)  
2002 – present.

## **Honors & Awards**

Falling Walls Lab 2017 winner PhD project in Turkey, attended the Falling Walls Lab  
November 2017, Berlin.

National Graduate Studies Scholarship, *The Scientific and Technological Research Council  
of Turkey (TUBITAK)*.

Full Scholarship for PhD, *Sabanci University*, 2014 –2018.